Physics – Uspekhi **43** (9) 863 – 900 (2000)

REVIEWS OF TOPICAL PROBLEMS PACS numbers: 47.27.Ak, 47.27.Eq, **92.10.–c**, **92.90.+x**

Quasi-two-dimensional turbulence

S D Danilov, D Gurarie

DOI: 10.1070/PU2000v043n09ABEH000782

Contents

Abstract. We review the results of numerical and experimental studies in quasi-two-dimensional (Q2D) turbulence. We demonstrate that theoretical energy spectra with slopes $-5/3$ and -3 (Kraichnan – Batchelor – Leith) can be observed only for a special set of external parameters. The bottom drag, beta effect, finite Rossby – Obukhov radius or vertical stratification, which distinguish geophysical Q2D turbulence from its purely 2D counterpart, determine the organization of a Q2D flow on a large scale. Since the spectral energy flux in 2D turbulence is directed upscale, the bottom friction takes on a special role. In the absence of bottom drag the energy condenses on the largest resolvable scale and flow equilibration is not attained.

1. Introduction

Strong rotation or a magnetic field (for electro-conducting fluids) confine fluid motion to a plane, and there are numerous examples of this kind in the natural world and technology. When the driving force significantly exceeds the critical value for stability, the fluid acquires a large number of excited spatial and temporal modes, and we can treat such systems as two-dimensional turbulence.

S D Danilov A M Obukhov Institute of Atmospheric Physics, Russian Academy of Sciences, Pyzhevskiĭ per. 3, 109017 Moscow, Russian Federation, Tel. (7-095) 951 84 80
E-mail: danilov@omega.ifaran.ru
D Gurarie Math. Department, Case Western Reserve University, Cleveland, OH 44106-7044, USA
E-mail: dxg5@po.cwru.edu

Received 22 May 2000, revised 20 June 2000
Uspekhi Fizicheskikh Nauk **170** (9) 921 – 968 (2000)
Translated by D Gurarie; edited by A V Getling

Under geophysical conditions rapid Earth rotation makes large-scale motions of the atmosphere and ocean nearly two-dimensional, with a broad spectrum of temporal/spatial scales; thus, 2D-turbulence is important in the case of geofluids.

Here we shall review 2D turbulence from the stand point of geophysical fluid dynamics, and distinguish between a strictly two-dimensional one (governed by the 2D Navier – Stokes equation), and a quasi-two-dimensional one, where the fluid motion is approximately two-dimensional, but is influenced by additional factors (beta-effect, finiteness of the Rossby – Obukhov radius, stratification), that lead to new features and phenomena (discussed below).

Strictly two-dimensional turbulence is an idealization, since natural flows could sustain two-dimensionality only for a limited range of scales, before other physical (environmental) factors intervene. Nevertheless, understanding the simplest two-dimensional case could give a good grasp of more complicated systems.

A Kolmogorov type theory was formulated for 2D turbulence in papers [1 – 4] and became widely accepted, particularly the notion of inverse cascade, which carries energy from the source up to large scales (small wave-numbers), in the opposite way to the direct (downscale) cascade of 3D turbulence.

Large-scale geophysical flows, though approximately two-dimensional, are not governed by equations of strictly 2D fluid dynamics. The gradient of the planetary vorticity (latitudinal change of the Coriolis vector), called the beta-effect, gives rise to anisotropic Rossby waves. The inclination of isopicnal (ocean) or isentropic (atmosphere) surfaces is responsible for the presence of the available potential energy of the fluid. There are important dissipative factors, such as bottom friction, radiative cooling, or orography, which could

drive the system to a statistical equilibrium. Lastly, at very large scales of motion, the horizontal compressibility, or finiteness of the Rossby – Obukhov deformation radius, becomes important. It can screen the upscale energy fluxes. For the meaning and significance of all these factors we refer to standard geophysical texts, e.g. Refs [5 – 7].

Such additional factors would typically set up external scales of the system, which arrest the upscale energy flux, and limit the typical size of the energy-carrying eddies. We shall review them in Sections 4 – 6.

The foremost of the extended 2D-theories is due to Rhines [8], who suggested the external (arrest) scale of geostrophic turbulence, based on the beta-effect. Bottom friction can play a similar role and create its own arrest scale [9 – 11], so does the combination of beta-effect and bottom friction [12]. If one adds baroclinic effects, the resulting integral scales would involve a complex interplay of several factors [13 – 15]. Here the problem of parametrization of the external scale (in terms of the basic inputs) becomes more intricate (Section 5).

We start with a brief overview of the standard phenomenology and known results for strictly two-dimensional turbulence. This classical subject was discussed in a number of review articles and monographs, e.g. Refs [16 – 21]. So we do not attempt to present a complete survey and the historic development of the subject, but rather focus on the aspects relevant to more realistic quasi-two-dimensional fluids. We shall also survey some less known recent results and developments in the two-dimensional case, which challenge the conventional view of universality of two-dimensional turbulence.

2. Strictly two-dimensional turbulence

2.1 Energy spectra

Two-dimensional incompressible flows are described by the vorticity equation

$$\partial_t \zeta + [\psi, \zeta] = D + F. \tag{1}$$

Here ψ designates the stream-field, whose velocity components are

$$u_x = -\frac{\partial \psi}{\partial y}, \qquad u_y = \frac{\partial \psi}{\partial x},$$

and $\zeta = \Delta\psi$ is the vorticity, F the forcing, and D the dissipation. The latter usually contains a viscous term, $D = \nu\Delta\zeta$, with a kinematic viscosity coefficient ν (Newtonian fluid), but may include other dissipative factors. Differential equation (1) should be augmented with proper boundary conditions.

In the absence of forcing-dissipation dynamic equation (1) conserves two integrals: kinetic energy

$$E = \frac{1}{2}\int (u_x^2 + u_y^2)\,\mathrm{d}x\,\mathrm{d}y = -\frac{1}{2}\int \psi\zeta\,\mathrm{d}x\,\mathrm{d}y$$

(assuming a uniform fluid density of 1 and appropriate boundary conditions), and enstrophy

$$\Omega = \frac{1}{2}\int \zeta^2\,\mathrm{d}x\,\mathrm{d}y.$$

Furthermore, Lagrangian conservation of vorticity (1) gives rise to an infinite set of conserved integrals (moments, or isolevel areas, of vorticity in the xy-plane), called Casimirs.

If the forcing and dissipation scales are spectrally separated, two conserved integrals give rise to two inertial intervals — the energy and enstrophy ranges [1 – 3]. The basic principle of the 2D-cascade theory states that the energy should go up to large scales, while enstrophy moves in the opposite direction. A simple spectral argument, used repeatedly (see e.g. monographs [6, 22]), amounts to estimating the wave-number 'centroids' k_1, k_2 of the isotropic energy and enstrophy spectra

$$k_1 = \frac{\int_0^\infty kE(k)\,\mathrm{d}k}{\int_0^\infty E(k)\,\mathrm{d}k}, \qquad k_2 = \frac{\int_0^\infty k^3E(k)\,\mathrm{d}k}{\int_0^\infty k^2E(k)\,\mathrm{d}k}.$$

Using the conservation laws of energy and enstrophy along with the Cauchy inequality, one easily estimates

$$k_1 \leqslant k^*, \qquad k_2 \geqslant k^* = \left(\frac{\Omega}{E}\right)^{1/2}$$

in terms of the total energy E and enstrophy Ω.

Another important assumption is the spectral localness of the cascades, meaning that the energy or enstrophy flux at a given wave-number k should depend only on k, the local energy density $E(k)$, and the local straining rate. Thus, using simple dimensional arguments, one could get the following isotropic energy spectra in two inertial intervals: in the enstrophy range

$$E(k) \sim C_1\eta^{2/3}k^{-3}$$

and in the energy range

$$E(k) \sim C_2\varepsilon^{2/3}k^{-5/3}.$$

Here η and ε represent the constant dissipation rates of enstrophy and energy, which should be equal to their fluxes in their inertial intervals or to their production rates by the source. Figure 1 gives a schematic view of the stationary spectrum of 2D turbulence.

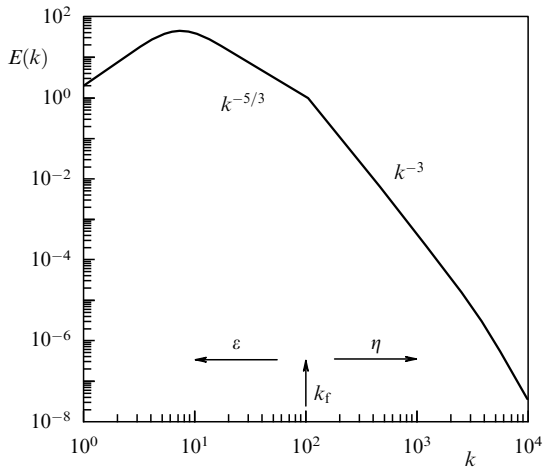

Figure 1. Schematic view of the kinetic energy spectrum of 2D turbulence. k_f is the forcing wave-number. On the right is the enstrophy interval characterized by the enstrophy flux η, which transforms into the enstrophy dissipation range at large $k_d = (\eta/\nu^3)^{1/6}$. On the left is the energy interval characterized by the energy flux ε.

It should be noted that any rigorous derivation of enstrophy and energy spectra requires some closure hypothesis on the third moments of random velocity (energy/enstrophy spectral transfers), in terms of its second moments (cf. Ref. [25]), and the localness narrows the possible class of such closures.

In the energy-range, the spectrum is local because the main contribution to the rate of strain at a given k

$$s_k = \left(\int_0^k (k')^2 E(k')\, \mathrm{d}k' \right)^{1/2}$$

comes from the upper limit of integration, $k' \approx k$.

The -3 spectrum on the enstrophy side clearly violates the localness, since each spectral octave gives an equal contribution to s, and the enstrophy flux, estimated to be $Z_k = s_k k \Omega(k)$ ($\Omega(k) = k^2 E(k)$ being the enstrophy spectrum), has a logarithmic divergence. Precisely, picking the lower limit of the s_k-integral, at the low end of the enstrophy range k_1 (e.g. near the source), we get $Z_k \sim \ln(k/k_1)$, i.e. a logarithmic growth.

Kraichnan suggested a logarithmic correction to the -3 spectrum, $E(k) \propto k^{-3}(\ln(k/k_1))^{-1/3}$, which resolved the divergence problem but did not make the enstrophy spectrum local (it depends on some external parameter k_1). The -3 slope serves as a critical borderline separating local and non-local spectra. Dropping the assumption of localness, one could get an infinite number of 'non-local' spectra with no obvious selection criteria. [This refers to 'universal selection criteria'; as we shall see, real (physical) turbulence or simulated turbulence exhibit a high degree of non-locality.]

The upscale energy flux in the 2D turbulence without large-scale dissipation creates another problem. Here one should expect the energy to accumulate at the largest available scales (in a finite-size system), and grow unbound, unless some dissipation mechanism could arrest this process and bring the system to a quasi-stationary regime [26, 27].

No such mechanism is required for decaying turbulence [4], since the energy is practically conserved (in the limit of zero viscosity), while the enstrophy decays. To show it, we remove the source from equation (1), multiply it by the stream-field ψ and integrate over space, to get the energy decay law

$$\frac{\partial E}{\partial t} = -2\nu\Omega = -\varepsilon\,,$$

and a similar enstrophy decay law

$$\frac{\partial \Omega}{\partial t} = -\nu \overline{|\nabla\zeta|^2}$$

(the bar denotes area averaging). As the enstrophy decays, the r.h.s. of the energy equation remains bound, hence negligibly small in the limit of zero viscosity. So one could consider the energy practically constant.

In such a limiting regime Batchelor postulated the energy spectrum of the decaying turbulence to evolve according to the law

$$E(k,t) = E^{3/2} t f(E^{1/2} k t)\,,$$

defined in terms of a single parameter — the total (nearly conserved) energy E — and the dimensionless function f (of the only possible dimensionless combination of E, k and t). By the same argument we could get the decay law for the total enstrophy

$$\Omega \propto t^{-2}\,.$$

Once again, the dimensional arguments would give a slope of -3 for the energy spectrum of the decaying turbulence at large k.

Unlike the 3D case, we have only very limited experimental verification of the 2D turbulence laws. One could simulate it (to some extent) in the laboratory environment, but only within a limited range of scales (see Section 6.2). Therefore, the bulk of 2D-turbulence results were obtained in numerical simulations, with somewhat tenuous and speculative links to experiments and observation.

There are also analytic theories [19, 28, 29], advanced in the 60s and 70s and based on certain closure assumptions. Their premises, however, are also hard to verify experimentally or numerically. We shall not discuss them here.

In the next section we shall review the alternative language of structure functions, widely used in the description and study of turbulence. We recall that Kolmogorov cast his original theory in this language, and later (Obukhov) it was converted into the more common 'spectral language'. Structure functions proved useful in the analysis of experimental results [30, 31], and in the study of intermittency [27, 32, 33].

2.2 Structure functions

The cornerstone of the Kolmogorov theory in the 3D case is the $4/5$ law for the third-order structure function, which links it to the dissipation rate of the kinetic energy [36]

$$\langle \delta u_L \delta u_L \delta u_L \rangle = -\frac{4}{5}\,\varepsilon r\,. \tag{2}$$

Here $\delta\mathbf{u} = \mathbf{u}' - \mathbf{u}$ denotes the difference of velocities between $\mathbf{x}$ and $\mathbf{x}'$ separated by $\mathbf{r}$, angular brackets mean ensemble averaging over realizations, and subscript L (T) denotes the longitudinal (transverse) components of velocity relative to $\mathbf{r}$.

The derivation of the $4/5$ law can be found in many publications, e.g. in Refs [34, 35]. It corresponds, in the Fourier formulation, to a positive energy flux in the inertial interval [35] and is exact for homogeneous, isotropic turbulence.

A similar relation holds for 2D-turbulence. We shall derive it here, following Ref. [31] (it was also reported in some earlier works, see, for example, Ref. [30]). The velocity of a 2D incompressible fluid obeys the Navier–Stokes equation

$$\partial_t \mathbf{u} + (\mathbf{u}\nabla)\mathbf{u} = -\frac{1}{\rho}\,\nabla p + \nu\nabla^2\mathbf{u} + \mathbf{f}\,, \tag{3}$$

with driving force $\mathbf{f}$. To derive the two-point correlator $\langle \mathbf{u}(\mathbf{x})\mathbf{u}'(\mathbf{x}') \rangle$, we sum the $\mathbf{u}$-equation multiplied by $\mathbf{u}'$ with the $\mathbf{u}'$-equation multiplied by $\mathbf{u}$, which yields after a few simple transformations (similar to those for the 3D case [34, 35])

$$\partial_t \langle \mathbf{u}\mathbf{u}' \rangle = \frac{1}{2}\,\nabla \langle \delta\mathbf{u}\delta\mathbf{u} \cdot \delta\mathbf{u} \rangle + 2\nu\nabla^2 \langle \mathbf{u}\mathbf{u}' \rangle + \langle \mathbf{u}\mathbf{f}' \rangle + \langle \mathbf{f}\mathbf{u}' \rangle\,. \tag{4}$$

Here all correlators depend on t and the space separation $\mathbf{r}$. Applying the Laplacian, we transform it into the evolution

equation for the vorticity-correlator for $\zeta = (\nabla \times \mathbf{u})_z$,

$$-\partial_t \langle \zeta \zeta' \rangle = \frac{1}{2} \nabla^2 \big(\nabla \langle \delta\mathbf{u} \delta\mathbf{u} \cdot \delta\mathbf{u} \rangle \big) + 2\nu \nabla^4 \langle \mathbf{u}\mathbf{u}' \rangle + \nabla^2 \langle \mathbf{u}\mathbf{f}' \rangle + \nabla^2 \langle \mathbf{f}\mathbf{u}' \rangle \,. \quad (5)$$

When two space points $\mathbf{x}$, $\mathbf{x}'$ collapse to a single $\mathbf{x}$, we obtain the enstrophy equation, for $\Omega = \langle \zeta\zeta \rangle / 2$

$$\partial_t \Omega = -\eta + Q \,, \qquad \eta = \nu \langle \nabla\zeta \cdot \nabla\zeta \rangle \,, \qquad Q = -\nabla^2 \langle \mathbf{u} \cdot \mathbf{f} \rangle, \quad (6)$$

with the enstrophy dissipation rate η, and production rate Q.

The two rates must be equal in a stationary regime. Subtracting twice the enstrophy equation (6) from the vorticity correlation (5), dropping the time derivative and inverting the Laplacian (in view of homogeneity), we get [31]

$$\nabla \langle \delta\mathbf{u} \delta\mathbf{u} \cdot \delta\mathbf{u} \rangle = (\eta - Q) r^2 + 4P - 2\langle \mathbf{u}\mathbf{f}' \rangle - 2\langle \mathbf{f}\mathbf{u}' \rangle - 2\nu \langle \delta\zeta \delta\zeta \rangle \,. \quad (7)$$

Here $P = \langle \mathbf{u}\mathbf{f} \rangle$ measures the rate of energy production. The first term on the r.h.s. is zero in the stationary state, but we leave it here in the general form.

If forcing is confined to scale l_f, smaller than the outer scale, but much larger than dissipation scale l_d, then we approximate

$$-Qr^2 + 4P \approx 2\langle \mathbf{u}\mathbf{f}' \rangle + 2\langle \mathbf{f}\mathbf{u}' \rangle$$

on the r.h.s. of Eqn (7) in the intermediate range $l_\mathrm{d} \ll r \ll l_\mathrm{f}$ (since the l.h.s. gives the first two terms of Taylor expansion of the r.h.s.).

Taking into account that $\eta r^2 \gg 2\nu \langle \delta\zeta\delta\zeta \rangle$ in this range, we get

$$\nabla \langle \delta\mathbf{u} \delta\mathbf{u} \cdot \delta\mathbf{u} \rangle = \eta r^2 \,, \quad (8)$$

whence follows

$$\langle \delta u_L \delta u_L \delta u_L \rangle = \langle \delta u_T \delta u_T \delta u_L \rangle = \frac{1}{8} \eta r^3 \,. \quad (9)$$

Thus in the *enstrophy interval*, $l_\mathrm{d} \ll r \ll l_\mathrm{f}$, the third-order structure function is proportional to the enstrophy dissipation rate η (or production rate Q).

On the other side of the source $l_\mathrm{f} \ll r$, we can drop all terms of (7) but P, hence the structure function becomes

$$\langle \delta u_L \delta u_L \delta u_L \rangle = 3 \langle \delta u_T \delta u_T \delta u_L \rangle = \frac{3}{2} Pr \quad (10)$$

in the energy interval.

Notice the opposite sign in the r.h.s. of (10), compared to the 3D case (2), which reflects the opposite sense of the energy cascade. Let us remark, however, that the energy interval in 2D feels (practically) no viscous dissipation. So equation (10) should be understood as quasi-stationary, and valid until the energy reaches the gravest modes of the system. The existence of such a quasi-stationary flow was confirmed by numerical experiments [27].

Another interpretation would require going beyond the strict 2D turbulence and imposing an artificial large-scale dissipation, that would bring the system to a stationary state. If the large-scale dissipation resides far above the forcing scale, one can still get relation (10) by augmenting (4) with the large-scale friction term. But the role of P is now played by the energy dissipation rate. The third-order structure function is most important, since it is proportional to the energy/enstrophy flux with an explicitly computed coefficient.

Let us note that the Kolmogorov similarity hypothesis [37] could be formulated for structure functions of any order. For longitudinal functions in the energy range it takes on the form

$$\langle \delta u_L^n \rangle \sim (Pr)^{\zeta_n} \,, \qquad \zeta_n = \frac{n}{3} \,, \quad (11)$$

which follows from the dimensional analysis, assuming local, homogeneous and isotropic turbulence. Such structure functions depend only on the energy flux and separation r. Without localness the coefficient should be a function of the ratios r/l_f, r/l_ext, so the system would remember its outer (external) scales, via nonlocal transfers.

Second-order structure functions ($n = 2$) of 2D turbulence in the enstrophy interval were studied in papers [31, 38]. Based on dimensional arguments one should expect

$$\langle \delta u_L^2 \rangle \sim \eta^{2/3} r^2 f\left(\frac{r}{l_\mathrm{d}}\right) ,$$

with some dimensionless function $f(r/l_\mathrm{d})$, where l_d is the viscous dissipation scale. The latter in the 2D case depends on the enstrophy dissipation rate η as

$$l_\mathrm{d} = (\nu \eta^{-1/3})^{1/2} \,.$$

Since the ratio r/l_d is large in the enstrophy interval, one may like to replace f by its limiting value at infinity. But the -3 spectrum precludes the existence of such a limit, since $f(z) \approx \ln z$ at large z. Paper [31] argued that the observed departures of the computer simulated spectra from -3 could be attributed to such an inconsistency in f.

The second-order correlation function is related to the energy spectrum

$$E(k) = \pi k \, \widehat{\langle \mathbf{u}\mathbf{u}' \rangle} \,, \quad (12)$$

via the Fourier ('hat') transform

$$\widehat{\langle \mathbf{u}\mathbf{u}' \rangle} = \frac{1}{(2\pi)^2} \int \langle \mathbf{u}\mathbf{u}' \rangle \exp(-\mathrm{i}\mathbf{k}\mathbf{r}) \, \mathrm{d}\mathbf{r} \,. \quad (13)$$

Hence one can derive the relation between spectra and structure functions taking into account that

$$\langle \mathbf{u}\mathbf{u}' \rangle = \langle \mathbf{u}\mathbf{u} \rangle - \frac{1}{2} \langle \delta\mathbf{u} \delta\mathbf{u}' \rangle \,.$$

Then one can easily show that the 2/3 law for structure functions (in the energy range) corresponds to a $-5/3$ law in the Fourier representation.

For nonlocal spectra in the enstrophy range there is no direct relation between spectra and structure functions [38]. In that case everything depends on the infrared cutoff of the inertial interval, and all such nonlocal spectra would give structure functions with an r^2-dependence. We shall come back to the topic of the structure function in 2D-turbulence later on.

3. Non-universality in two-dimensional turbulence

Equation (1) for a double-periodic flat domain is usually solved by pseudo-spectral methods, though earlier works used finite-difference schemes, e.g. Refs [9, 39, 40]. Another commonly used geometry, the sphere, exploits spherical harmonics.

In a flat geometry, one expands the vorticity (and related fields) in a Fourier series (integral) with coefficients

$$\zeta_{\mathbf{k}} = \frac{1}{4\pi^2}\int \zeta \exp(-\mathrm{i}\mathbf{k}\mathbf{x})\,\mathrm{d}\mathbf{x}$$

labeled by 2D wave vectors $\mathbf{k} = (k_x, k_y)$. The infinite Fourier expansion is further truncated to a finite grid, hence its **x**-representation is discretized accordingly, and the Fourier integrals turn into (finite) sums. Thus we take a coordinate rectangle $2\pi \times 2\pi$ with N grid points along each axis, and vary the wave numbers in the range $[-N/2, N/2]$.

In the Fourier representation (discrete or continuous) equation (1) takes on the form

$$\frac{\mathrm{d}}{\mathrm{d}t}\,\zeta_{\mathbf{k}} + J_{\mathbf{k}} = D_{\mathbf{k}} + F_{\mathbf{k}}\,. \tag{14}$$

Here $J_{\mathbf{k}}$ denotes the **k**th Fourier mode of the Jacobian $J(\psi, \zeta)$, which in spectral methods is implemented via fast Fourier transform (going back and forth between the **k** and **x**-spaces, and replacing convolutions with products). It has a Fourier expansion

$$J_{\mathbf{k}} = \sum_{\mathbf{p},\,\mathbf{q}} a_{\mathbf{kpq}}\psi^*_{\mathbf{p}}\psi^*_{\mathbf{q}}\,, \tag{15}$$

with structure coefficients

$$a_{\mathbf{kpq}} = \frac{1}{2}(q^2 - p^2)(p_x q_y - p_y q_x)\delta_{\mathbf{k}+\mathbf{p}+\mathbf{q}=0}\,,$$

where ψ^* denotes complex conjugation.

Forced 2D turbulence can attain a statistically stationary state, if the energy and enstrophy injected by a source are balanced by the dissipation. Though standard viscosity could in principal dissipate sufficient enstrophy, in numerical simulations one often uses steeper hyper-viscous dissipation, $D = (-1)^{n+1}\nu_n\Delta^n\zeta$, $n > 0$. It has the advantage that the inertial (enstrophy) interval may be pushed to higher k without increasing the computational grid.

A number of papers have studied the effect of short-wave dissipation on the spectral laws in the enstrophy interval and on other turbulent statistics (see Refs [41, 42]). They all conclude that there is some hyper-viscosity-type effect on spectral slopes or inertial intervals, but it is not significant. Moreover, the qualitative change, if any, could be understood through changes in the effective Reynolds number, for given forcing and spectral resolution.

As we mentioned, to arrest the inverse cascade of forced 2D turbulence and prevent infinite energy accumulation at low k, one needs an artificial infra-red dissipation, absent in strictly two-dimensional fluids. Numerically, it could be obtained in several ways. One could impose Rayleigh friction on the lowest modes of the system (see, e.g., Refs [41, 43]) — a procedure easily implemented in the pseudo-spectral code. Another scale-dependent dissipation, called hypo-friction, is defined via negative powers of the Laplacian, $(-\Delta)^{-n}$ (see, e.g., Refs [44–46]). Some papers avoid the problem of large-scale dissipation altogether by studying non-stationary (quasi-stationary) turbulence [26, 27, 47].

Following Lilly [9], the forcing term is typically modeled by a random Markov process, localized within a narrow spectral band. Paper [41] suggests the following finite-difference scheme in time steps n:

$$F_{\mathbf{k},\,n+1} = A_{\mathbf{k}}(1 - r^2)^{1/2}\exp(\mathrm{i}\theta) + rF_{\mathbf{k},\,n}\,.$$

Here $A_{\mathbf{k}}$ is the dimensionless amplitude, the parameter r defines the time correlation radius, and θ, the random phase uniformly distributed over $[0, 2\pi]$. Other authors [44, 48, 49] use a Gaussian white noise process as the source.

The space resolution of 64^2 in early works (e.g. Ref. [39]) was lately pushed to 4096^2 (see Refs [28, 48, 50]). But so far most papers dealing with the statistical properties of 2D turbulence have a typical resolution of 256 or 512 grid points.

Figure 2 illustrates the vorticity distribution and spectra for stationary (a, b) and decaying (c, d) turbulence, simulated on a 256^2 grid. For stationary turbulence the source is located in the range $k \in [58, 62]$, while the decaying turbulence has an initial spectrum confined near wave number 45.

The stationary turbulence exhibits strong localized vortices, whose size remains close to the forcing scale (Fig. 2a). No clearly identified structures appear at the energy peak scale (Fig. 2b). But the stream-field (not shown) exhibits elongated circulation zones, whose size may exceed the forcing scale many times and come close to the energy peak.

In these simulations the stationary turbulence was equilibrated by Rayleigh friction $-\lambda\zeta$ with $\lambda = 0.03$. The forcing was of uniform amplitude in the spectral band $k \in [58, 62]$ and developed (for a chosen time-step) an energy flux of 0.0009. The spectral slope comes close to $-5/3$ on the left of k_{f} and is steeper than the expected -3 on the right of k_{f}.

The decaying turbulence evolves into well developed and broad vortices, whose life spans over many eddy turnover periods. While the turbulent energy changes slowly during the decay phase, the enstrophy drops significantly. The spectral slope for large k grows steeper than -3 after some initial phase. The initial energy in the above experiment was 1. The vorticity field in Fig. 2c is shown at the dimensionless time

$$t_v = \int_0^t \Omega(t')^{1/2}\,\mathrm{d}t' = 124\,.$$

This time measures the number of eddy turnovers. The spectra of Fig. 2d show the shift of the spectral peak at times $t_v = 0.5, 40, 70, 124$, during the evolution.

3.1 Forced stationary turbulence: enstrophy range

In most works the observed enstrophy spectra are steeper than the theoretically predicted k^{-3}. Though some early papers reported a theoretical value for the spectral slope, their spectral resolution and the Reynolds number were too low. A brief overview of the early results can be found in monograph [22].

Subsequent work [41, 51, 52] reported significant departures from the -3 law (steepening) for the stationary 2D turbulence. Such steep spectra should be nonlocal, so the system would feel the width of the enstrophy range resolution and retain the memory of forcing-dissipation.

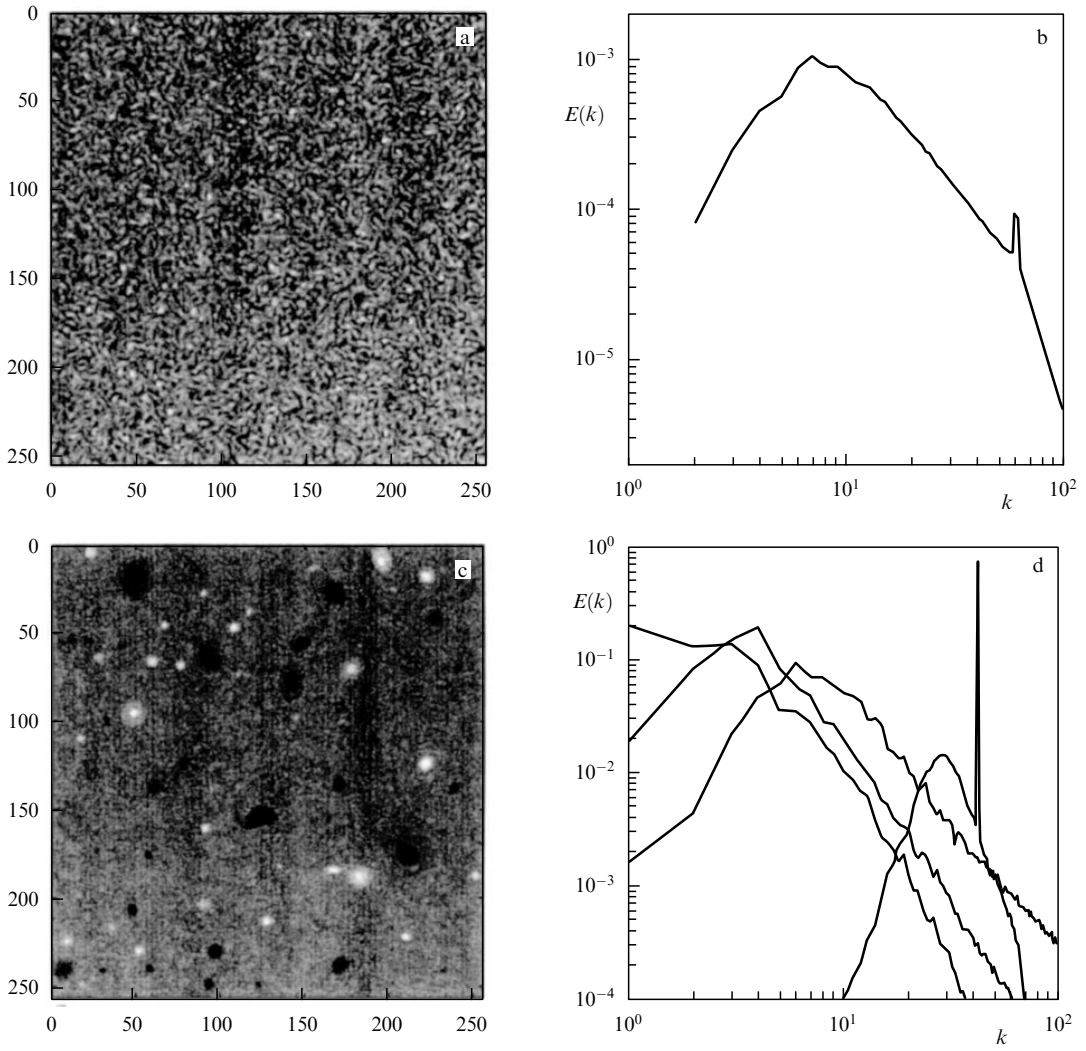

Figure 2. Vorticity and energy spectra in stationary (a, b) and decaying (c, d) turbulence. (a) Realization of vorticity field at the quasistationary stage of evolution, (b) time-averaged energy spectrum, forced at wave numbers $k \in [58, 62]$ and stabilized by the bottom friction; (c) Realization of vorticity field at the late stage of the decay process, $t_v = 124$; (d) Evolution of the energy spectrum during the decay phase ($t_v \approx 0.5, 40, 70, 124$). The initial spectral peak at $k \approx 45$, and initial energy equals 1.

In the language of triad-interactions $(\mathbf{k}, \mathbf{p}, \mathbf{q})$, 'localness' means that the principal contribution to the k-mode comes from nearby $p \sim q \sim k$. So one needs to study the effect of nonlinear triad interactions on energy and enstrophy transfers.

Papers [25, 43, 48, 53] set up such a task and found large contributions to the enstrophy transfer into the k-mode coming from elongated (nonlocal) triads with two legs in the enstrophy interval and one short leg near the energy peak. We shall briefly describe this following paper [43].

To get the energy balance for the $\mathbf{k}$ Fourier mode, $E_\mathbf{k} = -(1/2)\psi^*_\mathbf{k}\zeta_\mathbf{k}$, we multiply relation (14) by $\psi^*_\mathbf{k}$, and write

$$\frac{\mathrm{d}}{\mathrm{d}t} E_\mathbf{k} = T_\mathbf{k} + \mathcal{F}_\mathbf{k} + \mathcal{D}_\mathbf{k} , \tag{16}$$

Here $\mathcal{F}_\mathbf{k} = -\mathcal{R}(\psi^*_\mathbf{k} F_\mathbf{k})$, $\mathcal{D}_\mathbf{k} = -\mathcal{R}(\psi^*_\mathbf{k} D_\mathbf{k})$, $\mathcal{R}$ denotes the real part and

$$T_\mathbf{k} = \sum_{\mathbf{p},\mathbf{q}} T_\mathbf{kpq} , \qquad T_\mathbf{kpq} = \mathcal{R}(a_\mathbf{kpq}\psi_\mathbf{k}\psi_\mathbf{p}\psi_\mathbf{q}) , \tag{17}$$

denotes the total transfer to the $\mathbf{k}$th mode. A positive T corresponds to an incoming energy flux; a negative T, to an outgoing flux. Each $T_\mathbf{kpq}$ measures the energy transfer to k due to $\mathbf{p}, \mathbf{q}$-interaction.

The enstrophy transfer is obtained by multiplying T by k^2,

$$S_\mathbf{kpq} = k^2 T_\mathbf{kpq} , \qquad S_\mathbf{k} = k^2 T_\mathbf{k} .$$

Figure 3 reproduces Fig. 2a of paper [43]. It shows enstrophy transfers S_{kp} obtained by averaging $S_\mathbf{kpq}$ over all $\mathbf{q}$ and over all directions of $\mathbf{k}$ and $\mathbf{p}$. The numerical resolution was 512^2 with the forcing range at $10-14$. The wave-number $k = 70$ in the plot of the transfer function lies within the enstrophy interval. The solid line shows time-averaged transfer; the dotted lines show standard deviations from the mean.

The authors, Maltrud and Vallis, made several observations. First, they noted that the enstrophy transfers look almost local in the p-variable, as the main contribution to S_{kp} comes from $p \approx k$ (which automatically implies small q). Furthermore, the shape and amplitude of the transfer function remained almost constant as k varied (we do not show this here). Finally, the area under the curve S_{kp} was approximately zero, which means vanishing net transport to

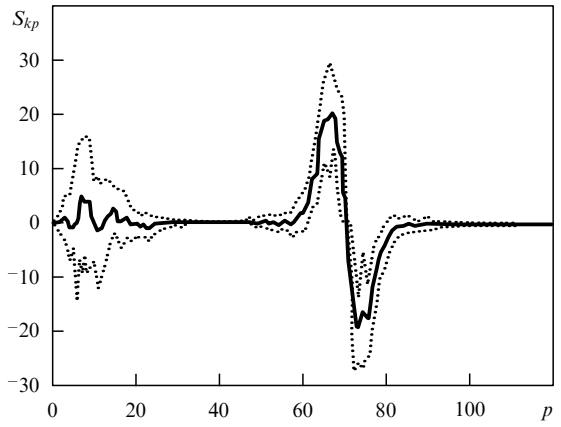

Figure 3. Average enstrophy transfer S_{kp} (sum over all **q** and the directions of **p** and **k**) as a function of p, for $k = 70$ (solid line), and standard deviations (dotted lines) [43].

the wave number k, as expected in the inertial interval. Thus the principal enstrophy exchange proceeds between close wave numbers p, k, but a short leg **q** should complement the triad.

Paper [43] illustrates the triad structure through the map of

$$S_{\mathbf{kp}} = \sum_{\mathbf{q}} S_{\mathbf{kpq}}$$

(for a fixed **k**) in the **p**-plane. It clearly exhibits the principal contribution to $S_{\mathbf{kp}}$ coming from the wave modes $\mathbf{p} \approx -\mathbf{k}$. Our Fig. 4, similar to Fig. 4b of Ref. [43], shows the input of various S_{kpq} (obtained from $S_{\mathbf{kpq}}$ by averaging over all triangles p, q, k with fixed q and $p < k$) for 3 different values: $k = 50$ (solid), 70 (short dashed), and 90 (long dashed). The total flux to k is zero in the equilibrium state, and the range $p < k$ corresponds to positive flux (cf. Fig. 3). Figure 4 also shows that the largest contribution to the flux comes from q below the forcing range, near the energy peak (numerical experiments [43] have the forcing confined to the range of 10−14 located on the right to the peak of the histogram in Fig. 4).

The authors conclude that the nonlinear interactions responsible for enstrophy transfer are highly nonlocal, and

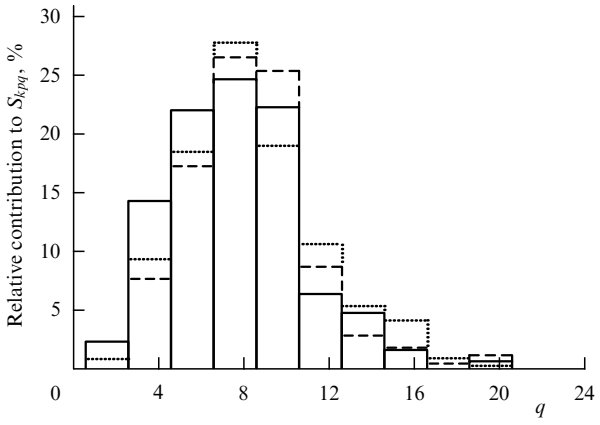

Figure 4. Histogram of relative contributions of all $p < k$ to the enstrophy transfer S_{kpq} for $k = 50$ (solid), 70 (short dashed), 90 (long dashed) [43].

low modes in the vicinity of the energy peak can play an active role in the enstrophy range. The principal transfers still look mostly local, confined to close wave-numbers, while small modes k serve mainly to catalyze the transport of enstrophy.

Since the transfer is symmetric with respect to **p**, **q** triads, $q \sim k \gg p$ can also give a significant input, reflected in Fig. 3, for small p. Those are precisely the energy peak values corresponding to $q \sim k$.

In the physical space, the non-universal behavior of the forced two-dimensional turbulence is associated with the appearance of coherent structures — vortices on the forcing scale. A typical realization of the vorticity field is shown in Fig. 1a of paper [41], and in our lower resolution experiments, Fig. 2a. The reader should not confuse the coherent structures of forced turbulence with the coherent vortices of decaying turbulence (McWilliams [54]). Unlike the decaying turbulence, typical vortices in the forced stationary case do not grow in size far above the forcing scale (with some exceptions discussed in Ref. [44], and examined below).

Maltrud and Vallis [41] observed that vortex production could be suppressed under special conditions, like strong frictional dissipation on the forcing scale. The presence of strong vortices makes turbulence intermittent and nonlocal, as they strain small eddies and strongly influence the transfer (cascade) of enstrophy in their vicinity to ever decreasing scales.

Paper [25] proposed a conceptually simple model of coherent structures in physical space and their spectral characteristics based on the ensemble of elliptic vortex patches in the mean-field background. If the vorticity level ζ is sufficiently high, such a vortex patch can survive under the conditions of a mean shear, defined via the symmetric part of the rate-of-strain tensor:

$$s^2 = -\det\left(\frac{\partial u_i}{\partial x_j} + \frac{\partial u_j}{\partial x_i}\right).$$

(the antisymmetric part gives the vorticity).

For ζ less than a critical value (for a given shear) the vortex is strained, and its width (perpendicular to the straining direction) goes down exponentially in time (we recall that a uniform elliptic vortex patch is unstable to the shear strain s, provided $s/\zeta > \gamma \approx 0.15$).

Each vortex patch is subject to the mean straining field, formed by the background, and the vortices around it. Since the vortex intensity typically decreases with its size, only large vortices can survive, while smaller ones should be strained and dissipated.

Thus we draw a dividing line between strong vortices and the background, so the enstrophy range would contain two spectral intervals, separated by a transition zone. The large vortices (in the enstrophy range) have a long life span, and effectively block, or curtail, the direct energy cascade to small scales [55, 56]. Hence, one gets steep spectral slopes in the enstrophy range, well below the theoretical prediction.

This also means that the main contribution to shear strain comes from 'large vortex patches', while the small scale background field is carried over, as a passive tracer. The theory predicts a spectral slope of −1 for passive tracers (see, e.g., Ref. [57]). Hence, we could expect the enstrophy spectrum to be nearly k^{-1} for large k (corresponding to −3 energy slope).

This similarity between the enstrophy and passive scalar cascades was already noted by Kraichnan [2]. He also

noted the dominant role of large scales in the enstrophy cascade.

The theory [25], based on the spectral parameter α — the reciprocal of the vortex size — predicts enstrophy spectra α^{-1} for both the coherent vortices and the background flow, but with different amplitudes, and a sharp transition between the two regions. The k^{-1}-spectrum in the 'coherent zone', due to the α^{-1}-distribution of vortex sizes, is masked by a steeper k^{-2}-spectrum, due to the vortex shape. Since in real numerical simulations coherent vortices occupy only a small fraction of the spectral range (near the source), the true enstrophy spectrum is steeper than -1.

The theoretical model of Ref. [25] shows qualitative agreement with the numerical simulations described therein, as well as the numerical results of Ref. [48]. The latter show the enstrophy slope -1 (and the corresponding energy slope -3) to be an asymptotic limit obtained by taking the Reynolds number large enough. Low spectral resolution can practically eliminate the k^{-1} range. Numerical simulations [48] estimate the Kraichnan–Batchelor constant C_1 in the k^{-3} enstrophy range to be somewhere between 1.5 and 1.7.

To estimate the contribution of coherent vortices, paper [25] introduced a parameter equal to the ratio of the enstrophy flux η to the product of the enstrophy at the forcing scale by the mean shear. For small values of this parameter the system maintains a low enstrophy flux, so the bulk of enstrophy is concentrated in coherent vortices. Hence, one can expect strong intermittency and a departure from the -3 law (the limit of small η corresponds to the decaying turbulence). The specific value of this parameter depends on the details of the forcing, dissipation and resolution.

Paper [58] utilizes flow scale separation into large-scale and small-scale components. The latter moves as a passive tracer and could be modeled by wave packets — quasiparticles in the external large-scale velocity field. This method allows one to increase the space resolution in the enstrophy range, though the separation into large-scale and small-scale components is somewhat arbitrary, given the continuous spectrum of scales in the well developed turbulence. In some ways, the basic ideas of Ref. [48] are similar to those of Ref. [25], that we have just outlined.

To conclude this section we reiterate the main points: the interactions and transfers in the enstrophy range are highly nonlocal, with one (short) leg of the triad lying near the energy peak. This agrees with the physical space view of the enstrophy cascade: straining of small scale structures by large vortices at the forcing scale. Clearly, such systems should carry information about the source, down the spectrum [43], and thus invalidate the idea of the inertial interval.

The ideal k^{-3} spectrum can be obtained in the limit of large k, at sufficiently high resolution and high Reynolds number. It corresponds to the 'passive scalar' dynamics of small scales, driven by large eddies. The contribution of small scales to the mean shear grows logarithmically with k (for spectra with -3 slope), and can become the dominant factor in the asymptotic limit $k \to \infty$. In that case one can get a logarithmic correction to k^{-3} [48], predicted by Kraichnan in Ref. [2].

We should however note that experiments [48], as well as [25, 43], were carried out for hyperviscous dissipation. Regular viscosity should have a similar effect, but would require a much higher cut-off k, hence the higher resolution. Indeed, recent work [59] combined theoretical analysis and numeric experiments on a 4096^2 grid, to show that the energy spectrum approaches

$$E(k) = C_1 \eta^{2/3} k^{-3} \left(\frac{k}{k_\mathrm{d}}\right)^{-\delta} \left[\ln\left(\frac{k}{k_\mathrm{f}}\right)\right]^{-(2-\delta)/(6-\delta)},$$

where $k_\mathrm{d} = (\nu^3/\eta)^{-1/6}$ and k_f are the dissipation and forcing wave-numbers, and δ a small parameter slowly decreasing with increasing Reynolds number. For the maximal Reynolds number explored in Ref. [59],

$$\mathrm{Re} = \frac{u_0}{\nu k_\mathrm{f}} = 9.2 \times 10^4, \qquad k_\mathrm{d} = 414, \qquad \delta = 0.355$$

and the departure from the logarithmic spectra [2] is quite significant.

However, the numerical experiments by Lindborg [60] at the same resolution as in Ref. [59] showed no departure from -3. He also claimed that the logarithmic corrections of Ref. [2] are redundant. We have no explanation of the discrepancy between [59] and [60], except possibly different regimes of forcing, and the somewhat broader forcing interval in Ref. [60].

3.2 Forced stationary turbulence: energy range

Most numerical experiments on turbulent spectra in the inertial energy range came close to the theoretical $k^{-5/3}$ law (see, for instance, Refs [41, 55, 61]), but different authors report different values of the Kolmogorov constant C_2, ranging from 5.8 to 7.0.

The nonlinear triad interactions in the energy interval were analyzed in paper [43], discussed in the previous section. It showed that the triad interactions of the energy range are also nonlocal, as in the enstrophy range considered above. The energy transfer function T_{kp} for k in the energy range looks similar to the enstrophy range S_{kp} (Fig. 3), with extrema near $p \approx k$. Energy comes to the k mode from the interval $p < k$ and, conversely, is transferred to p for $p > k$. This suggests the energy-range transfer to be directed toward larger k, in apparent contradiction to the idea of 'inverse cascade'. The contradiction, however, could be resolved by balancing the contributions of various spectral components to the energy flux past k, whereby large (direct) local transfers cancel each other, and yield a positive net balance into small k.

The histogram of relative contributions of wave-numbers q, obtained by summing transfers T_{kpq} over all $p > k$ (for k in the energy interval), shows the dominant role of small q, at the energy peak. Unlike a similar histogram for the enstrophy transfer (see Fig. 4), this histogram reveals a significant flux coming from large q. While small q imply $k \sim p$, i.e. an energy transfer to small scales, the large ones $q \sim p \gg k$ do the opposite, and give an overall negative cumulative energy flux.

Analysis of Ref. [43] found the elongated triads with one (long) leg in (or above) the forcing range k_f to carry the bulk of the energy transfer. This implies highly nonlocal processes in the inverse cascade that proceed directly from the source to the energy peak-range. According to Ref. [43] vortex merging should play an important role here, but the details of such a vortex dynamics have not yet been explored. The prevalence of nonlocal transfers put into question the universality of the $-5/3$ spectrum observed in many numerical studies and calls for further validation and explanation of it.

Our discussion of stationary turbulence does not apply directly to the non-stationary case. Indeed, paper [27] showed

the principal energy carrying triads to be local in the absence of infrared dissipation. The localness here means that the flux across k comes primarily from triads whose p, q legs obey the inequality

$$k < p\,,\ q \leqslant 4k\,.$$

To establish such estimates one needs high resolution simulations.

Borue's paper [44] cast further doubt on the standard notion of universality and cascade in the energy range. He used a 512^2 spectral resolution with the source at $k \in [100-102]$, and a yet higher 1024^2 spectral resolution with two sources at $k \in [250-252]$, or at $[350-352]$. The long-wave modes were dissipated by hypo-friction expressed via the operator

$$D_{\mathbf{k}} = -\nu_i k^{-16}\zeta_{\mathbf{k}}\,.$$

He ran his numerics over a sufficiently long time interval to bring the system to a statistically stationary state, and observed $k^{-5/3}$ energy spectra during intermediate stages. In the long run, however, they evolved much steeper slopes close to -3. (The departure from a $-5/3$ slope may not look too surprising, as nonlocal triads in the energy range should make energy spectrum sensitive to the flow organization in physical space and the infrared dissipation mechanism.)

The change of the slope was accompanied by the growth of coherent vortices of various sizes and intensities. Borue proceeded by dividing the vorticity field into a background and a (strong) vortex component (using $\zeta > 2\zeta_{\rm rms}$ criteria for vortices). He found the classical $k^{-5/3}$ energy spectrum for the background field, while the vortex component carried 80% of the energy and had much steeper slopes. Moreover, the statistical distribution of strong vortices by their size and intensity was consistent with the -3 spectral slope. Thus Borue found strong vortices to be the prime reason for the departure from the conventional phenomenology.

Borue also claimed the energy cascade to proceed mostly through vortex merging, whereby large vortices absorb smaller ones, but he didn't elaborate this nonlinear process, nor produced direct evidence. Strong vortices appear after long integration, when local vorticity fluctuations grow sufficiently high and intense to sustain the background shear strain. For a relatively short integration time, and strong infrared and ultraviolet dissipation, vorticity extrema would remain small, and keep the spectrum close to $k^{-5/3}$, as observed in other works.

Paper [44] did not discuss the specific role of long wave (hypo-frictional) dissipation in the formation of strong vortices, but speculated that such phenomena should arise for any infrared dissipation law, including Rayleigh friction, $D = -\lambda\zeta$, given sufficient spectral resolution.

Paper [44] raised many questions on the structure of nonlinear interactions and the universality of 2D turbulence, and vortex growth processes. Subsequent works [26], [27], and more recently [62] brought some clarity in this issue. The former two study forced 2D turbulence in the absence of infrared dissipation, with resolution ranging from 512^2 to 2048^2. As long as the energy spectrum does not reach the gravest modes of the system in its 'upscale climb', the spectral slope remains close to $-5/3$, no coherent vortices appear, and the normalized even structure functions of the velocity field remain nearly Gaussian.

As soon as the cascade reaches box-size scales, the vorticity field starts to condense into two strong vortices, and its energy spectrum develops a steep non-universal slope. The velocity structure functions also depart from the Gaussian state at large scales. Paper [62] attributes these features to termination of the inverse cascade at the lowest modes, and claims that uninhibited cascade should proceed according to theoretical predictions (while conceptually possible, such a scenario is unrealistic for finite physical systems).

Long-wave dissipation arrests the inverse cascade and thus can lead to large deviations from the classical $k^{-5/3}$ spectrum. Such a spectrum, strictly speaking, requires some special arrest mechanism to sustain it. This mechanism should absorb the energy flux from k above some small cut-off value k_{ls}, without producing backscatter into large k. Paper [62] suggests the large scale dissipation coefficient,

$$\nu_{ls}(k_{ls}|k) = -\frac{S_k(k_{ls}|k)}{2k^2\Omega_k}\,, \tag{18}$$

where the summation in S_k is implemented over all triads $\mathbf{k}, \mathbf{p}, \mathbf{q}$, satisfying

$$|k-p| < q < k+p\,, \qquad p, q < k_{ls}\,.$$

Here the enstrophy transfer function S_k is computed, using the quasi-normal approximation (QNM), with relaxation times of triple correlators (need for QNM) derived via renormalization group methods. This yields

$$\nu_{ls}(k_{ls}|k) = 0.0974\varepsilon^{2/3}k_{ls}^{-4/3}F\left(\frac{k}{k_{ls}}\right), \tag{19}$$

where the dimensionless function F obeys $F(1) = 1$, and

$$F(x) \approx x^{-2.58}\,,$$

for large x (in the sense of least square approximation). Formula (19) corresponds to a (scale-dependent) hypo-frictional law,

$$\lambda \propto \left(\frac{k}{k_{ls}}\right)^{-0.58},$$

which is much shallower than Borue's law k^{-16} of Ref. [44].

Paper [62] runs simulations on 1024^2-grid, with a forcing scale $k \in [215, 222]$, and high order hyperviscosity $\propto k^{14}$ in the enstrophy range. It describes three experiments. The first one has no long-wave friction, but all wave numbers below $k = 8$ are quenched (made zero at each computational step). Formally, it corresponds to a step-wise hypo-friction: $\lambda = \infty$, for $k < 8$, and zero, for $k > 8$. The second one uses hypo-friction $D_{\mathbf{k}} \propto k^{-10}\zeta_{\mathbf{k}}$, and the third one the friction (19), with $k_{ls} = 8$, and the same cut-off of modes below $k = 8$ as in the first case.

Figure 5a taken from Ref. [62] shows a Kolmogorov constant

$$C_2 = E(k)k^{5/3}\varepsilon^{-2/3}$$

(and the compensated spectra) in all three cases. The last case comes closest to the theoretical predictions, while the hypo-frictional case features the largest departure.

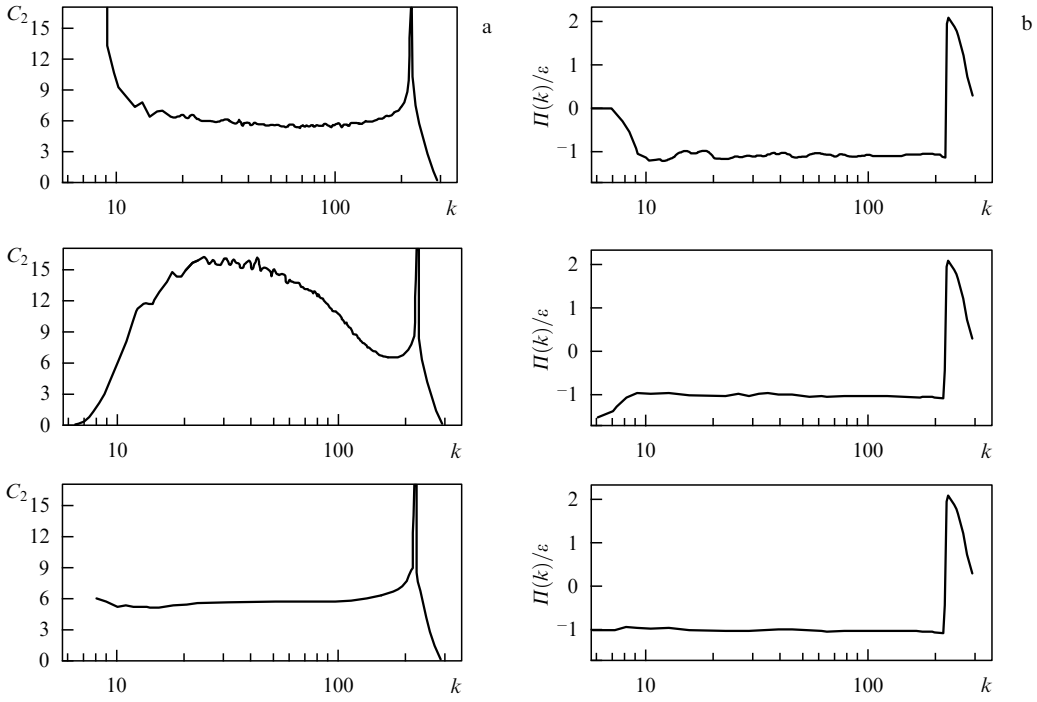

Figure 5. (a) Kolmogorov constant as function of the wave-number in 3 experiments with different long-wave dissipation: modes $k \leqslant 8$ made zero on each time step (upper plot); hypo-friction, described in the text (center plot); friction (19) (lower plot); (b) Normalized energy fluxes for the same experiments [62].

The former two cases take a long time to saturate energy, and the figure shows an intermediate stage. In the second case, Ref. [62] reports the formation and growth of strong vortices, completely absent in the third case. Figure 5b shows normalized energy fluxes in all 3 cases. All three have a sufficiently long inertial interval, however the hypo-frictional turbulence exhibits a local increase of the energy flux at small k (it must be local, since the flux goes to zero as $k \to 0$).

Paper [62] has thus demonstrated that the departure from the Kolmogorov law (due to strong coherent vortices) depends on the type of frictional dissipation. Large hypo-friction (high negative power of the Laplacian) suppresses low modes, but becomes negligible above a certain wave number k_i. The limiting case removes friction above some integral scale k_i, and completely suppresses all modes below k_i. It leads, according to Ref. [27], to energy condensation at the lowest allowed modes, or 'crystallization' of the flow into a quasi-regular vortex lattice with step π/k_i. In the hypo-frictional case, one could estimate k_i by comparing time scales: eddy-turnover $\left(\varepsilon k_i^2\right)^{-1/3}$ with 'hypo-frictional' k_i^{2n}/ν_{-n}. For large power n, it has only a weak dependence on the energy flux (or dissipation rate).

When the inverse cascade reaches the integral scale of the system, the energy condensation should modify its spectra, as one could expect, based on nonlocal transfers (above), and should change the flow organization at the energy carrying modes. But the precise role of the frictional dissipation in such an organization remains unclear.

The classical $k^{-5/3}$ spectrum would persist in dissipation-free problems, during intermediate stages, when the cascade has not reached the minimal wave numbers [27]. Here the field is close to Gaussian, and strong vortices are absent. Yakhot [63] suggested a theory to explain such behavior of non-stationary turbulence in terms of the two-point characteristic function

$$Z = \left\langle \exp(\mathbf{l}\delta\mathbf{u}) \right\rangle$$

(angular brackets denote ensemble average). For transverse velocity differences (in the direction $\mathbf{l}$ perpendicular to $\mathbf{r} = \mathbf{x} - \mathbf{x}'$) he showed Z to obey the Langevin-type equation with a random Gaussian source. Longitudinal structure functions were shown to deviate from the Gaussian values, but the deviations are too small to be measurable.

If the infrared dissipation arrests the inverse energy cascade 'softly' (like Rayleigh friction), the stationary spectra can remain close to $k^{-5/3}$ in some range of wave numbers. But the exponents ζ_p of structure functions

$$\langle \delta u^p \rangle \sim r^{\zeta_p}$$

can depart noticeably from their Kolmogorov values, as found in Ref. [32]. This is usually attributed to intermittency. The authors of Ref. [32] claim that in this case, the natural assumption is the extended self-similarity

$$\langle \delta u^p \rangle \sim \langle \delta v^s \rangle r^{\zeta_p/\zeta_s}$$

(see also Ref. [33]). Exponent $s = 3$ plays a special role, since the third moment is proportional to the energy dissipation rate. While absolute exponents can vary with r, the relative ones (for the low order structure functions) may remain constant and this is indeed observed in Ref. [32, 33]. We shall return to this issue in Section 6.2 (laboratory experiments), and here just mention that non-universal inverse cascade due to infrared dissipation, would make the conclusion of Refs [32, 33] on noticeable intermittency in the inverse cascade non-universal, as well.

The high resolution numerics of Ref. [64] corroborate this remark. It studied odd structure functions in the

energy range on a 2048^2 grid with a linear friction law. The friction coefficient was chosen to arrest the inverse cascade before it reaches the box size. The energy spectra give an almost ideal $-5/3$ slope over two decades. The increments of longitudinal velocity components (their PDFs) show a small but discernible asymmetry. The symmetrized PDF is nearly Gaussian, and the compensated third order structure function for streamwise velocity (multiplied by $1/r\varepsilon$) has a $3/2$ plateau region, consistent with the Kolmogorov law.

The paper also computes the 5th and 7th structure functions of the longitudinal velocity. They both have intervals that obey the Kolmogorov scaling

$$\langle \delta u_L^n \rangle = C^{(n)} (\varepsilon r)^{n/3}$$

with coefficients $C^{(5)} \approx 130$, and $C^{(7)} \approx 14000$. Such behavior of structure functions suggests a small intermittency level within experimental error. Of course, linear friction creates a non-uniform energy flux, inconsistent with the basic premise of the Kolmogorov theory. The authors claim their flux to be 'nearly constant' over a decade, but one could clearly see its variation over the plateau region, which far exceeds the variation of the third structure function.

3.3 Decaying turbulence

Many papers on 2D-turbulence in the past have studied the decaying case, as it seems more natural and requires no large-scale dissipation. McWilliams [54] has shown decaying turbulence to evolve into long-lived coherent vortices, which persist for many turnover periods. The first examples of coherent vortices in decaying turbulence appeared in the early papers [65, 66], but McWilliams demonstrated this phenomena in different systems and for various initial conditions. Fig. 2c shows a typical vorticity field of decaying turbulence.

Paper [54] takes an initial spectrum with a slope of -3 at large k, and resolves the system on a 256^2 grid. As the system evolves its spectrum steepens to -5, and the enstrophy transfer drops to zero. But the vorticity kurtosis shoots from the initial Gaussian value of 3 to several dozen. Vortices form at intermediate scales (between the initial state and the box size).

The vortices can slow down the cascade processes [56], since they carry the bulk of enstrophy, but do not stretch and filament one another. Paper [67] made a systematic study of decaying turbulence and its spectra in an attempt to reconcile the multitude of reported spectral slopes. It uses a high resolution 1024-grid and long time integration of the initial Gaussian field of zero mean, and the energy spectrum

$$E_0(k) \sim k \left[1 + \left(\frac{k}{k_0} \right)^{\gamma+1} \right]^{-1}$$

for $k_0 = 6$, and $\gamma = 6$.

The initial evolution creates vortex filaments via stretching by the large-scale velocity field. They carry over small-scale eddies as passive tracers, hence developing a slope -3 in the enstrophy range. At the next stage large coherent vortices evolve from the local vorticity extrema, and start breaking down into smaller size vortices. Due to two different mechanisms of vortex formation, no universal distribution of vortices by size and intensity appears, as evident in their spectra.

The energy spectra have an interval of steep slope at small k, and a shallower (closer to -3) interval in the small vortices range. The total energy remains nearly constant during the evolution, while the enstrophy declining does not, however, drop to zero. Indeed, large-scale stable vortices lock up a sizable fraction of enstrophy, and will not let it cascade to small scales.

The main conclusion of Ref. [67] is that the -3 spectrum could appear only at an intermediate stage of the process. Large vortices destroy scale invariance and steepen the low-mode spectra. Besides, the paper claims the resulting spectral shape to depend strongly on the initial state of the system. In particular, an initially steep spectrum produces π/k_0-size vortices that dominate the future evolution of the system. Shallower initial spectra, like the -3 of Refs [54, 68], give a broad spectrum of vortex sizes. Paper [67] sets the borderline initial slope for the two patterns somewhere between -3 and -6.

The appearance of coherent vortices in the decaying turbulence allows them to be studied as statistical vortex ensembles [68–72]. To that end one needs to select coherent vortices from the small-scale turbulent background. The simplest selection rule identifies regions of vorticity field that exceed a prescribed threshold (in terms of rms vorticity). Another census analyzes the determinant of the velocity gradient and seeks regions where it takes negative values. Paper [68] claims that the two methods give similar results.

The vortex distribution by radius in Ref. [68] obeys the law

$$P(R) \sim R^{-\alpha}$$

with $\alpha \approx 1.9$. The observed vortices are self-similar,

$$\zeta(r) = \zeta_0 f\left(\frac{r}{R} \right)$$

with nearly fixed ζ_0 and a vortex profile f.

The initial -3 spectrum (at 512 - resolution) evolves to $k^{-4.3}$. The authors estimate the vortex contribution to the energy spectrum to have a slope of $-6 + \alpha$, depending on the vortex size distribution. That yields an energy slope of -4.1, close to the observed value. At the final stages of evolution the dynamics of coherent vortices can be well approximated by point vortices.

Paper [69] studies the characteristics of 2D vortices, particularly their time evolution. It takes an initial state with the energy spectrum

$$E(k) = \frac{k^6}{(k + 2k_0)^{18}} ,$$

on a 450^2 grid. The vortices are selected by comparison with the 'ideal' vortex profile. Their number decays in time, as

$$N_v \sim t^{-0.71} .$$

The maximal vorticity decreases, but its mean absolute value over all vortices remains nearly constant. The mean vortex size grows as $t^{0.2}$, and the mean separation as $t^{0.4}$. The vortices maintain a nearly Gaussian profile, but unlike [68] this profile is not universal. The difference between the two cases could be attributed to different initial conditions. Finally, the enstrophy decreases as $t^{-0.4}$, in stark contrast to Ref. [4].

The prominent role of vortices in the decaying turbulence motivated the development of vortex models [70 – 72]. They assume that vortices behave like point vortices, at large separations, and each is determined by two parameters — the vortex radius and (uniform) vorticity level. When two vortices collide, that is come within a distance $1.7(R_1 + R_2)$ of their radii, they merge into a single vortex of radius $\left(R_1^4 + R_2^4\right)^{1/4}$. Such collisions conserve energy and decrease enstrophy, and thus can account for the enstrophy loss due to vortex straining and filamentation in real systems.

Different initial conditions in Refs [70 – 72], however, lead to divergent results. Thus [71] has vortex sizes distributed initially according to the R^{-3} law, which corresponds to the -3 spectrum of numerical simulations [68]. The terminal size-distribution comes close to R^{-2}, which gives a -4 energy slope (close to -4.1 of Ref. [68]). The number of vortices decays as $t^{-0.6}$, which differs from the $t^{-0.7}$ law of Ref. [69], the $t^{-0.75}$ law of Ref. [70], and the $t^{-0.72}$ law of Ref. [72].

The point-vortex dynamics of Refs [70, 72] provide scaling laws for the vortex number, size distribution, distance distribution, and enstrophy, which agree with the pseudospectral results of Ref. [69]. Based on the numeric results of Ref. [69], particularly the conservation of average vorticity amplitude (over all vortices), the authors of Ref. [70] proposed a hypothesis for decaying turbulence, consistent with the numerics.

Except energy conservation, as in the Batchelor theory (Section 2.1), they postulated the conservation of vorticity extrema. The latter follows naturally, when one views decay turbulence as the process of vortex merging. The enstrophy decay is confined to the vortex periphery (caused by filamentation), but it does not affect vortex cores. Assuming the conservation of vortex extrema ζ_{ext}, one could introduce the time and length parameters

$$l = \frac{\sqrt{E}}{\zeta_{\text{ext}}}\,, \qquad \tau = \frac{1}{\zeta_{\text{ext}}}\,.$$

Assuming further a power decay law for the number of vortices N_v with an exponent ξ, and writing the energy and enstrophy (confined in vortex cores) as

$$E \sim N_v R^4 \zeta_{\text{ext}}^2\,, \qquad \Omega \sim N_v R^2 \zeta_{\text{ext}}^2\,,$$

one gets the mean vortex size to grow as

$$l\left(\frac{t}{\tau}\right)^{\zeta/4}$$

(energy conservation), while the distance between vortices grows as

$$l\left(\frac{t}{\tau}\right)^{\zeta/2}\,,$$

and the enstrophy of the entire flow decays as

$$\Omega(t) \sim \tau^{-2}\left(\frac{t}{\tau}\right)^{-\zeta/2}\,.$$

Such conclusions also agree with the numerical studies.

The proposed scaling differs from the classical Batchelor results, as well as the selective decay theory (see for instance Ref. [7]). The latter postulates that turbulent decay should minimize enstrophy, subject to the energy constraint [75]. This theory was applied to describe late stages of turbulent decay in papers [73, 74] and others. Paper [75] shows selective decay to predict higher decay rates than numerical simulations, as it fails to account for the role of coherent vortex structures in slowing the decay process.

Dritschel [76] questioned the validity and utility of pseudospectral methods for turbulence dominated by vortices. He argued that pseudospectral methods introduce significant numerical dissipation on the vortex periphery, thus giving a wrong description of vortex mergers and the resulting filamentation [77]. Paper [78] demonstrated that thin filaments on the periphery, subjected to strong hyperviscous dissipation, bring about a sharp increase of the overall dissipation rate of vorticity. Furthermore, the hyperviscosity could cause undue oscillations of iso-contours on the periphery of vortex cores.

He proposed an alternative method of contour dynamics, augmented by so-called surgery. It allows in principle a higher spatial resolution than pseudospectral methods and, hence, a broader spectral range. Paper [76] does it for the spherical geometry. The initial state of the system consists of 200 vortices of uniform vorticity distribution (and zero total vorticity). The vortices are distributed according to their area A, $n(A) \sim A^{-p}$, with exponent p.

The dissipation scale (which cuts off fine structures) corresponds to resolution 7000 in pseudospectral methods. The paper finds that the vortex size distribution is not self-similar, and steepens as the system evolves. The corresponding energy spectra vary from nearly k^{-5} at large scales to k^{-3} at small ones. It also finds that some other characteristics, like the growth rate of vortex sizes for large vortices and the decay rate of enstrophy, are markedly different from the pseudospectral results. The reason for such a departure, however, is not only the overall decrease of dissipation, as claimed by the author, but may include other factors, such as sharp boundaries of the vortex patches, in the contour dynamics.

Let us stress that the entire decay process is due to the enstrophy dissipation at short wavelengths. Without such dissipation, the system would relax to a statistical equilibrium state with an equipartition energy spectrum k^{-1} (see, for instance, Ref. [29]). One could expect the numerical dissipation to be equally important. Indeed, the key process of large scale condensation (vortex merger) is largely determined by small-scale dissipation.

The criticism of pseudospectral methods in Ref. [76] is based on the notion of a well identified (sharp) vortex boundary, while pseudospectral methods operate with smooth fields, without jumps. It is not clear to what extent vortex patches could represent smooth fields. On the other hand the different behavior of 'pseudospectral' decaying turbulence from that of contour dynamics could be interpreted as a difference in initial conditions, in the spirit of Ref. [67].

Recent papers [50, 79, 80] describe the dependence of the decay characteristics on the enstrophy dissipation mechanism. The former considers the temporal evolution of the vorticity PDF in the decaying turbulence. According to the Batchelor theory it scales as

$$p(\zeta) = t f(\zeta t)\,.$$

Numerical results show this relation to hold approximately near the distribution peak, but not on its tails. Paper [79]

shows a sharp decline of $p(\zeta)$ at large ζ, so it becomes practically zero at $|\zeta| > \zeta_m(t)$. The PDF tails have a power decay law

$$p(\zeta) \sim \frac{c}{|\zeta t|^{1+q_c}},$$

with universal constants c, q_c determined from the numerics (such universality is consistent with Ref. [80]). Clearly, the time evolution of the moments of vorticity $|\zeta|^q$ should depend on q. For q less than q_c the main contribution to the q-moment comes from PDF near zero, and yields a power decay t^{-q}, according to the Batchelor prediction. For $q > q_c$ we get

$$\langle |\zeta|^q \rangle \sim (q - q_c)^{-1} \zeta_m^{q-q_c} t^{-q_c},$$

independent of q, as claimed in Ref. [70]. The latter statement, however, proves not accurate. Indeed, the numerics of Ref. [79] claim the true dependence to be

$$\langle |\zeta|^q \rangle \sim t^{-a_q}$$

with $a_q \approx 0.4$ in the hyperviscous case $-\nu_8 \Delta^8 \zeta$, and $a_q \approx 0.2 + 0.5q$ for the regular Newtonian viscosity $\nu\Delta$. The latter agrees with the universality of values c, q_c, given that a finite Reynolds number would make ζ_m a power function of time. This implies that the decay exponents are also functions of the Reynolds number.

Paper [50] simulates decaying turbulence with Newtonian viscosity on a 4096 grid, which allows resolution of the enstrophy cascade, while keeping the energy peak away from the outer (integral) scale of the system. It studies the dependence of the energy and enstrophy decay laws on the Reynolds number, determined by the initial spectrum,

$$\mathrm{Re} = \frac{E}{\Omega^{1/2}\nu},$$

and shows the existence of a critical value Re_c, so that, beginning with the Reynolds number $\mathrm{Re}(0) < \mathrm{Re}_c$, the decay proceeds with the Reynolds number decreasing with time. For $\mathrm{Re}(0) = \mathrm{Re}_c$, this number approaches a value Re_c' constant during the decay. In this case the theoretical consideration in Ref. [50] predicts that the energy decays as t^{-1}, while the enstrophy exhibits a t^{-2} decay. Indeed, for the critical value of $\mathrm{Re}(0)$ one could expect a self-similar decay process with the energy spectrum

$$E(k,t) = u^2 l \hat{E}(kl), \qquad u^2(t) = \langle u^2(t) \rangle, \qquad l(t) = \frac{u(t)}{\langle \zeta^2 \rangle^{1/2}}.$$

In that case the decay exponents could be derived in the following way: assuming

$$\langle u^2 \rangle = bt^n, \qquad \langle \zeta^2 \rangle = ct^m,$$

and constant Reynolds number $\mathrm{Re} = \mathrm{Re}_c'$, one gets $n = m/2$, while the evolution equation

$$\frac{\partial \langle u^2 \rangle}{\partial t} = -2\nu \langle \zeta^2 \rangle$$

yields the relation $nb = -2\nu c$. This immediately implies $n = 1$, $m = 2$ and the coefficients

$$b = \nu \frac{\mathrm{Re}_c'^2}{2}, \qquad c = \frac{\mathrm{Re}_c'^2}{4}.$$

If $\mathrm{Re}(0) > \mathrm{Re}_c$ the Reynolds number grows during the decay process, but the decay does not proceed in a self-similar way. The energy and enstrophy decay depend on the Reynolds number, but for sufficiently large values (> 1000) the energy remains nearly constant, while enstrophy decays as $t^{-0.8}$. The decay rate increases for low Re, and the case $t^{-1.2}$ [79] falls in this category. Unlike the decay laws, the energy spectra are almost self-similar, but their slope is steeper than -3.

Careful numerical experiments (4096 resolution, averaged over 64 realizations) and theoretical analysis [80] clarify and extend the previous results of Refs [79, 50]. They make a distinction between complete and incomplete self-similarity of the decaying turbulence. Complete self-similarity requires, besides a self-similar spectrum, a constant ratio of length scales l and

$$\mu = \frac{\langle \zeta^2 \rangle^{1/2}}{\langle (\nabla \zeta)^2 \rangle^{1/2}}.$$

The former should be thought of as the external scale; the latter, as the internal (dissipation) scale. According to Ref. [80] complete self-similarity yields the enstrophy decay law t^{-1} in the limit of large Reynolds numbers. In that case viscosity explicitly enters the decay law.

Partial self-similarity could be restored by neglecting viscosity for the wave numbers where the energy spectrum remains self-similar. This yields the Batchelor t^{-2} enstrophy decay law.

Numerical experiments [80] suggest the improved enstrophy decay law $t^{-0.9}$. It is close to $t^{-0.8}$ obtained in Ref. [50] and to the theoretical prediction.

Similar considerations for hyperviscous decay turbulence yield a $t^{-1/n}$ law, where n is the power of the Laplacian. Numerical results of Ref. [80] for the largest Reynolds number 8192 and biharmonic viscosity ($n = 2$) show the exponent in the enstrophy decay to reach the minimal value -0.8 and approach the limiting value -0.66 at time

$$\tau = \int_0^t \langle \zeta^2 \rangle^{1/2} \, \mathrm{d}t = 70.$$

This should be compared with theoretical value 0.5. The exponent -0.4 for $n = 8$ [79] differs significantly from the theoretical estimate $1/n = 0.125$.

Computed PDFs confirm the basic conclusions of Ref. [79] on the tails. The assumption of complete self-similar decay [80] predicts $q_c = 1$ for normal viscosity, and $q_c = 0.5$ for biharmonic viscosity. This is confirmed by numerical simulations in Ref. [80] carried out for decaying turbulence with the initial Reynolds numbers $\mathrm{Re}(0) = 1024$ and 8192 respectively. That disproves, however, the universality hypothesis of Ref. [79] where the value $q_c = 0.4$ was indicated for both viscous and hyperviscous decay. Additionally, Ref. [80] shows that complete self-similarity is consistent with [79] if the parameter $\zeta_m(t)$ of Ref. [79] is a function of the viscosity coefficient, the ratio of the inner and outer length scales, and the energy.

Thus one should not expect the statistics of coherent vortices to be universal. They should rather depend on the type of viscous dissipation and the Reynolds number (if the latter is not too large).

4. Quasi-two-dimensional turbulence

4.1 Rotation, bottom friction, beta-effect

A layer of incompressible fluid of depth H, and zero forcing-dissipation conserves the so-called potential vorticity (PV)

$$\omega = \frac{\zeta + f}{H}\,, \tag{20}$$

where $\zeta = \Delta\psi$ is the relative vorticity. The simplest way to derive it is using rotating shallow water equations

$$\partial_t \mathbf{v} + (\mathbf{v}\nabla)\mathbf{v} + f\mathbf{e}_z \times \mathbf{v} + g\nabla h = 0\,,$$

$$\partial_t H + \operatorname{div}(H\mathbf{v}) = 0\,, \tag{21}$$

where $\mathbf{e}_z$ is a vertical unit vector, f the (local) Coriolis parameter — twice the angular speed of rotation, $\mathbf{v}$ is the horizontal velocity, H the total fluid depth, g the acceleration due to gravity, and h the elevation. Applying curl to the first equation and eliminating $\operatorname{div}\mathbf{v}$ via the second one gives the evolution equation for the relative vorticity. Combining it with the second equation leads to the conservation law

$$D_t\omega = 0\,, \qquad D_t = \partial_t + (\mathbf{v}\nabla)\,. \tag{22}$$

Large-scale atmospheric motions are slow compared to the Earth's rotation, hence they have a small Rossby number

$$\mathrm{Ro} = \frac{U}{Lf} \ll 1\,,$$

where U and L are typical velocity and length scales. A small Rossby number means that the Coriolis acceleration exceeds the local one, so the flow is geostrophically balanced

$$f\mathbf{e}_z \times \mathbf{v} + g\nabla h \approx 0\,,$$

and hence can be described by the geostrophic stream function

$$\psi = \frac{gh}{f}\,.$$

The geostrophic balance is a purely diagnostic relation, without dynamic content.

To get the dynamic evolution, one needs to go to the first order terms in small Rossby number, the so called quasigeostrophic approximation. The simplest derivation exploits the PV conservation law (22). We write its denominator as

$$H = H_0 + h - h_\mathrm{b}\,,$$

where h_b is the bottom profile, and H_0 the mean depth, and assume the ratios h/H_0, h_b/H_0 to be of the order of the Rossby number. Hence in the first order approximation, the quasigeostrophic PV

$$\omega_q = \zeta + f - \frac{\psi}{L_0^2} + \frac{fh_\mathrm{b}}{H_0} = \omega H_0 + O(\mathrm{Ro}^2)\,. \tag{23}$$

where $L_0 = (gH_0)^{1/2}/f$ is the Rossby – Obukhov deformation radius. Then the PV conservation law (22) implies the quasigeostrophic equation

$$D_t\,\omega_q = 0\,,$$

or

$$\frac{\partial}{\partial t}\left(\zeta - \frac{\psi}{L_0^2}\right) + \left[\psi, \zeta + f - \frac{\psi}{L_0^2} + f\frac{h_\mathrm{b}}{H_0}\right] = 0\,. \tag{24}$$

In general, one should also include the sources and dissipation in the r.h.s of equation (24). The principal dissipation comes from a thin Ekman boundary layer over the rigid bottom, where the velocity profile changes from zero on the boundary to the geostrophic value inside the fluid layer. The net effect of the Ekman layer on the mean flow should be an extra dissipation term $-\lambda\zeta$ in the r.h.s. of (24), with coefficient $\lambda = \nu/(H_0\delta_E)$. Here ν denotes the kinematic viscosity, or turbulent viscosity of the large-scale (atmospheric) motions, and $\delta_E = (2\nu/f)^{1/2}$ the thickness of the Ekman layer.

The Ekman dissipation exceeds the horizontal dissipation $\nu\Delta\zeta$ on scales above

$$H_S = (H_0\delta_E)^{1/2}$$

— the thickness of the Proudman – Stewartson layer. According to Ref. [81] the motions on scales below H_S are 3-dimensional, and the Ekman friction prevails and should be included on all scales, where the motion is two-dimensional.

For scales below the Rossby – Obukhov radius, one can drop the term proportional to L_0^{-2}, and we shall do this in the next two sections.

If furthermore, $h_\mathrm{b} = 0$, and $f = \mathrm{const}$, equation (24) coincides with the vorticity equation for a 2D incompressible fluid. In what follows we shall use mostly quasigeostrophic PV, called simply PV.

The quasi-2D flows in the atmosphere and ocean have a local Coriolis parameter varying with latitude. For a limited zonal band we could approximate it by a linear function of the latitudinal (South – North) coordinate y, $f = f_0 + \beta y$. This is conventionally called the *beta-plane approximation* (or beta-effect).

The beta-effect could significantly change the dynamics of the system, due to the y-dependence of f and, hence, of the PV content of a fluid parcel. The Lagrangian conservation property of PV means that any latitudinal displacement of a parcel (North or South) will result in a deficit or excess of PV compared to the background. The corresponding displacement waves should propagate westward. They are known as *Rossby waves*, and the substitution of the standard (monochromatic) Fourier mode

$$\psi = A\exp(-\mathrm{i}\omega t + \mathrm{i}k_x x + \mathrm{i}k_y y)$$

in the linearized equation (24) yields the Rossby dispersion relation

$$\omega = -\frac{\beta k_x}{k^2}\,. \tag{25}$$

Rossby waves play a fundamental role in large-scale (atmospheric) circulation, but our main focus is the beta-effect in the 2D turbulence.

4.2 Bottom friction

As we already mentioned, 2D turbulence can attain a stationary state when its energy is properly dissipated at small k and the natural dissipation mechanism is linear (bottom) drag $D_\lambda = -\lambda\zeta$. In the geophysical context it

appears as Ekman friction, determined by the physical parameters of the system [5, 82].

The linear drag (also called *Rayleigh friction*) affects equally all scales of motion, hence it invalidates the idea of a dissipationless inertial interval. The energy spectrum attains its maximum at some intermediate value k_m between the forcing scale and the integral scale, and the relevant problem here is to parametrize the arrest scale, where the energy flux comes to a halt.

Lilly [9] was the first to study the role of friction in the inverse cascade. He introduced the scale

$$L_D = \frac{(2E)^{3/2}}{\varepsilon} = \frac{(2E)^{1/2}}{\lambda},$$

where E is the mean kinetic energy of the flow (per unit mass), and ε its dissipation rate due to the bottom friction. According to Lilly the energy peak is estimated to be reached at $35L_D^{-1}$, which corresponds to $L_{\max} = (2\pi/35)L_D \sim 0.5E^{3/2}/\varepsilon$ and agrees with Lilly's numerics at resolution 64^2 (maximal wave-number 32, and forcing at $k_f = 8$).

Lilly also suggested modifying the energy and enstrophy spectra taking into account the variable energy flux. He writes the integral relation

$$E(k) = \alpha\left[2\int_0^k \lambda E(k)\,\mathrm{d}k\right]^{2/3} k^{-5/3},$$

and derives the modified energy spectrum

$$E(k) = \alpha^3 k^{-5/3}\left[\lambda(k_c^{-2/3} - k^{-2/3})\right]^2$$

in terms of the small (cut-off) wave-number k_c that terminates the spectrum. Although Lilly's formula gives a smooth transition from $k^{-5/3}$ to 0 at small k, such a form is not unique (or universal). Indeed, a better way to account for friction would be parameterizing variable flux in the energy balance equation rather than substituting a variable dissipation rate in the $-5/3$ law.

Bottom friction was also considered in Ref. [83], which parametrized the arrest scale in terms of the energy dissipation rate

$$L_D = \left(\frac{\varepsilon}{\lambda^3}\right)^{1/2}. \tag{26}$$

Estimating ε as $E\lambda$, one gets the above Lilly parametrization (to a factor of order unity). Many other authors discussed the role of bottom friction in the inverse cascade (see, for instance, Refs [84, 85]). Manin [10] came with an estimate similar to (26), but from a different perspective — the stability analysis of quasi-2D flows with bottom friction.

Relation (26) can be cast in terms of the Reynolds number based on forcing and bottom friction. To this end we render equation (1) dimensionless, and write $D = -\lambda\zeta + D_u$, as the sum of frictional plus short-wave (ultraviolet) dissipation. Introducing the time scale $1/\lambda$, the vorticity scale λ, the forcing length scale l and the amplitude F_0, we write (1) as

$$\partial_{t'}\zeta' + [\psi', \zeta'] = -\zeta' + \frac{D_u}{\lambda^2} + \mathrm{Re}_\lambda F', \tag{27}$$

where primes denote dimensionless quantities, and $\mathrm{Re}_\lambda = F_0/\lambda^2$ the requisite forcing–friction Reynolds number. This yields the arrest scale

$$L_D \sim l\,\mathrm{Re}_\lambda^{3/4}$$

and, hence, the dependence of the energy carrying scale L_D on forcing.

Clearly, one could construct outer scales similar to L_D, for other types of long-wave dissipation. Thus in the atmospheric context friction takes on a nonlinear (quadratic) form $D_i = -\alpha\mathbf{v}|\mathbf{v}|$ (in the Navier–Stokes equation), due to the turbulent Ekman boundary layer (see Ref. [86]). The inverse of α has the sense of some external scale. Here the forcing magnitude plays a secondary role (it would only determine the transition time to a statistically stationary regime), and one should use the standard Reynolds number, the ratio of the inertial to frictional terms. This Reynolds number on the forcing scale is equal to $1/(l\alpha)$. If we set the outer scale by requiring Reynolds number to be one, we get

$$L_D \sim \alpha^{-1} = l\,\mathrm{Re}.$$

The Reynolds number in this quadratic friction case measures the ratio of the external and forcing scales. The external scale is set by physical processes responsible for the quadratic friction and is not sensitive to the energy flux produced by the source. A detailed analysis is provided in Ref. [87].

We return now to the linear friction case. The above estimates of the outer (arrest) scale have a major flaw, since they implicitly assume a constant energy flux over the energy interval. Yet both friction laws, linear (Ekman), or nonlinear (quadratic), would drive the energy flux to zero at small k.

Paper [11] studied the dependence of the energy peak on Reynolds number numerically, using a 256^2-grid with a linear friction law. Its authors observed a slower rate of increase, $O(\mathrm{Re}^{0.4})$, than theoretically predicted one, $\mathrm{Re}^{3/4}$.

Figure 6a shows the energy spectra obtained in our 512^2 numerical simulations for several λ (0.05, 0.03, 0.02 and 0.015). We kept the source power fixed in all experiments, as seen in Fig. 6b for energy fluxes, defined by

$$\Pi_\varepsilon(k) = -\sum_{k'=0}^{k} T_{\mathbf{k}'} \tag{28}$$

(it equals to the sum of transfers from k through ∞, as the transfer integrated over all wave numbers is zero). The energy flux measures the cumulative transfer of energy inside $[0, k]$ across its upper bound k. A negative flux means an upscale transfer, as seen in Fig. 6b for interval $[0, k_f]$. The flux varies along this range due to friction. Also, decreasing λ makes the shallow (plateau) region near k_f stretch further in the energy range.

If the source power were increased at a fixed friction, the friction would not be able to dissipate the augmented energy flux. The energy would condense at the lowest modes, and the system would lose universality.

Given the variable energy flux over k, one should not expect the outer scale to depend on a single quantity, the energy production ε, but rather on its fraction that reaches the low mode region. Indeed, all the plots of Fig. 6a have equal ε, so estimate (26), if true, would imply a difference of L_D between the largest and the smallest λ by a factor 6, whereas the observed factor is about 3. Also one could hardy expect a universal dependence of the outer scale on the control

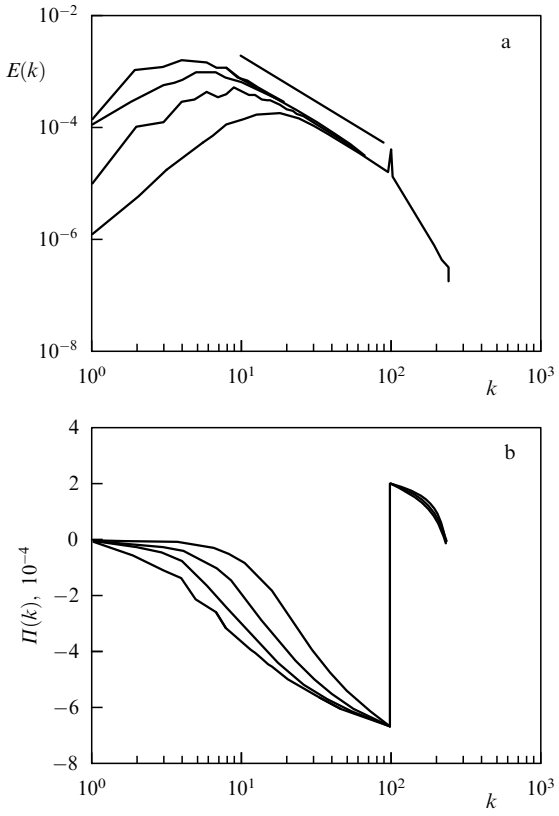

Figure 6. (a) Energy spectra and (b) spectral energy fluxes for different coefficients of the bottom friction, $\lambda = 0.05$, 0.03, 0.02, 0.015 and fixed source power. The straight line on the upper plot corresponds to a $-5/3$ slope.

(Reynolds) parameter. A special case of a linearly decaying flux in the range $0 \leqslant k \leqslant k_f$ yields $L_D \sim \mathrm{Re}_\lambda^{1/2}$, which does appear close to the numeric exponent 0.4 of Ref. [11].

Paper [11] claims a spectral slope close to $-5/3$ in the vicinity of k_f. The same appears in our Fig. 6a (here the straight line corresponds to a slope of $-5/3$). Similar intervals with a universal slope, insensitive to friction, appear in other papers (see, for instance, Ref. [64]). On the contrary hypofrictional dissipation [44] gives a nearly uniform flux, but the energy spectra deviate strongly from $k^{-5/3}$.

We have thus seen that bottom friction determines an outer scale for turbulent eddies. Early estimates of this scale, based on constant energy flux, do not agree with numerical experiments. Uniform linear friction destroys the inertial interval, but the energy flux still propagates upward. One could give another interpretation to the outer scale in terms of the characteristic turnover time

$$\left(k^2 \Pi(k)\right)^{-1/3}$$

for large eddies $1/k = L_D$. If it exceeds the friction time $1/\lambda$, large eddies will decay before completing the turnover 'cycle', so slower components of velocity should disappear.

Smith and Yakhot [27] argued that the bottom friction in the energy interval can give a -3 spectrum, through the balance of the nonlinear term and frictional dissipation in the Navier – Stokes equation. They assume scaling,

$$\Delta u = u_i(\mathbf{x} + \mathbf{i}r) - u_i(\mathbf{x}) \sim r^q \,,$$

and then balance λu_i against $\mathbf{u} \cdot \nabla u_i$, which implies $q = 1$ and

$$E(k) \sim k^{-2q-1} = k^{-3} \,.$$

However the velocity gradient over a distance r corresponds to the inverse turnover time. So the balance at hand simply sets a condition on the limiting size of large eddies. Motions satisfying such a balance should become extinct. The real balance involves the energy dissipation rate $\lambda E(k)$ and energy transfer $-\partial \Pi(k)/\partial k$ at k. It implies a link between the energy spectrum and energy flux, but does not control the shape of the spectrum.

4.3 Rhines scale

Rhines [8] pioneered the study of beta-plane 2D turbulence, and based his arguments on the subtle interplay between wave dynamics and turbulence. The turbulence is associated with the nonlinear Jacobian term $J(\psi, \zeta)$, while the (Rossby) waves arise from a linear operator,

$$[\psi, \beta y] = \beta \frac{\partial \psi}{\partial x}$$

so we look for a spectral (or physical) space, when both quantities are comparable. A parcel of wave-modes localized near wave number k_0 can be characterized by the phase-speed $c_p = \beta/(2k_0^2)$ with the factor 1/2 coming from the arbitrary orientation of wave crests. So one can measure the degree of nonlinearity by the variable

$$\epsilon = \frac{U}{c_p} = \frac{2k_0^2 U}{\beta} \,,$$

where U denotes the rms turbulent velocity. If $\epsilon < 1$, the nonlinear terms are negligible, and the dynamics are dominated by Rossby waves.

Since Rossby waves may propagate, turbulent energy will be radiated away, and Rhines argued that the upward energy cascade will be suppressed (more precisely, this occurs because interacting wave triplets require an auxiliary frequency synchrony besides matching wave vectors) at the wave number

$$k_\beta^{\mathrm{R}} = \left(\frac{\beta}{2U}\right)^{1/2} \,,$$

called the *Rhines scale* (the factor 2 in the denominator is unessential).

Rhines [8] made another observation concerning the energy spectra at small k. The frequency of turbulent motion, given by the formal dispersion $\omega = kU$, decreases with k, while the Rossby wave frequency $\beta(k_x/k^2)$ decreases at large k, or when k_x becomes small. The two tendencies could be reconciled when the energy flux takes on the North – South direction in the **k**-space. This means the formation of zonal (East – West) jets in the flow.

Numerical experiments at resolutions 64^2 (finite difference scheme) and 128^2 (pseudo-spectral method) in Ref. [8] confirmed Rhines' estimates and demonstrated the formation of a zonal structure in the presence of the beta-effect. Though the Rhines derivation was reproduced in many works, and laid the basis for the theory of the beta-plane turbulence, one should not take it literally. To begin with, phase-speed and the rms turbulent velocity have different transformation properties under time reversal. The true effect of the beta-plane is to

inhibit nonlinear transfers into the region where the beta-effect dominates, and the Rhines scale gives only one possible estimate of such a region.

There are other estimates, like that obtained by Holloway and Hendershott [88], who conducted a numerical study of the decaying turbulence on the beta-plane to verify their statistical closure model known as the test-field model. They found a strong anisotropy in the wave range

$$k \leqslant k_\beta^H = \frac{\beta}{Z}\,,$$

where Z denotes the rms vorticity. Their estimate gives a β-dependence different from that found by Rhines.

Paper [12] analyzed various scales associated with beta-plane turbulence, and gave a physical space picture of the beta-plane turbulence, which we shall briefly outline. We consider forced beta-plane turbulence with an isotropic source at sufficiently large k_f, and assume that the energy cascade to small k depends on a single parameter — the energy dissipation ε. Then the eddy turnover time can be estimated to be

$$\tau_t(k) = \varepsilon^{-1/3} k^{-2/3}\,,$$

and its reciprocal measures the rate of strain, or the turbulent eddy frequency. Equating this to the Rossby frequency gives the spectral borderline between waves and turbulence.

If we ignore the anisotropy of equation (25), and replace k_x in the numerator by k, we get the following expression for the transitional wave number

$$k_\beta = \left(\frac{\beta^3}{\varepsilon}\right)^{1/5}.$$

All three numbers, k_β^R, k_β^H, k_β are in general different, and Vallis and Maltrud explain their relationship. They estimate the rate of strain via

$$s(k) = \left[\int_{k_0}^{k} (k')^2 E(k')\,\mathrm{d}k'\right]^{1/2},$$

k_0 being the cut-off wave number for the energy containing eddies, and then use the standard 5/3-spectrum hypothesis to get τ_t and k_β with the coefficient $(3C_2/4)^{-1/2} \approx 0.46$ (assuming the Kolmogorov constant $C_2 = 6$).

If the energy is localized within a narrow spectral band, then $s(k)$ should coincide with the total enstrophy, and one obtains the external scale of Ref. [88]. The original Rhines' estimate corresponds to the choice

$$s(k) = k^3 E(k)\,.$$

For a power spectrum it differs from k_β by a numerical factor.

Equating $1/\tau_t$ to the Rossby frequency (25), one gets the following equation for the bounding curve of the cascade region

$$\begin{aligned} k_x &= \pm k_\beta \cos^{8/5}\theta\,,\\ k_y &= k_\beta \sin\theta \cos^{3/5}\theta\,, \end{aligned} \qquad (29)$$

in terms of polar angle θ of k (Fig. 7). This shows the characteristic anisotropy of the beta-plane turbulence.

Paper [12] verified these predictions in two ways. The first one exploits the so called EDQNM (Eddy-Damped-Quasi-Normal-Markovian) closure (we refer to Ref. [7] for an elementary exposition, and to Ref. [19] for a more complete description of the analytical statistical theories). Forcing and dissipation are not considered here, though this could be done in principle. Numerical simulations show the initially isotropic spectrum evolving into the characteristic dumbbell shape. The latter, however, doesn't remain fixed. Since statistical equilibria (in the absence of forcing dissipation) are defined by (isotropic) conserved integrals, the anisotropy would gradually disappear.

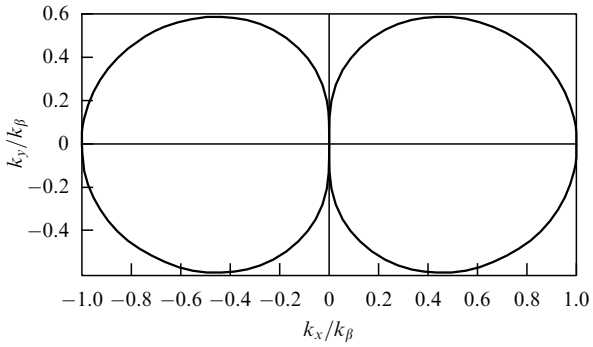

Figure 7. Bounding curve in the wave-number space of Eqn (29).

Let us remark that similar results hold for Rossby waves in the framework of the kinetic theory, as discussed in the review article by Reznik in Ref. [89].

EDQNM has advantages compared to those of direct numeric simulations, since it demonstrates the beta-effect in quasigeostrophic turbulence directly. The theory is formulated in the language of 2D energy, or enstrophy Fourier spectra. The energy density obeys the kinetic equation

$$\left(\partial_t + d(k) - \frac{\mathrm{i}\beta k_x}{k^2}\right) E_\mathbf{k}(t) = \mathrm{Re}\left\{T_\mathbf{k}(t)\right\} + F_\mathbf{k}(t)\,,$$

$$T_\mathbf{k} = \sum_{\mathbf{k}+\mathbf{p}+\mathbf{q}=\mathbf{0}} \theta_\mathbf{kpq} a_\mathbf{kpq} (E_\mathbf{p} E_\mathbf{q} - E_\mathbf{q} E_\mathbf{k})\,,$$

$$a_\mathbf{kpq} = \frac{2(\mathbf{p}\times\mathbf{q})^2}{k^2 p^2 q^2} (p^2 - q^2)(k^2 - p^2)\,,$$

where $d(k)$ denotes the linear dissipation operator and F_k the enstrophy source power. The transfer term $T_\mathbf{k}$ also involves the relaxation times $\theta_\mathbf{kpq}$ of triads $\mathbf{p}+\mathbf{q}+\mathbf{k}=\mathbf{0}$.

The latter, in the presence of the beta-effect, takes on the form [88]

$$\theta_\mathbf{kpq}^{-1} = \mathrm{i}(\omega_{-\mathbf{k}} + \omega_\mathbf{p} + \omega_\mathbf{q}) + \mu_{-\mathbf{k}} + \mu_\mathbf{p} + \mu_\mathbf{q}\,,$$

where $\omega_\mathbf{k}$ are the Rossby frequencies and

$$\mu_\mathbf{k} = a\left(\int_0^k l^2 E(l)\,\mathrm{d}l\right)^{1/2}$$

is the relaxation rate of the $\mathbf{k}$th mode [with coefficient $a = O(1)$], equal to the combined straining of large-scale eddies ($l \leqslant k$) on the $\mathbf{k}$th mode.

The straining rates μ and Rossby frequencies ω have a similar effect on the transfer term $\mathrm{Re}[T_\mathbf{k}(t)]$: the increase of either one lowers T, thus suppressing the nonlinear transfer. Thus the principal role of the beta-effect in the 2D turbulence

(from the EDQNM standpoint) is not the (Rossby) wave radiation, but the inhibition of nonlinear transfers, due to decoherence of the third moments, measured by $\theta_{\mathbf{kpq}}$.

The relation $|\omega_{\mathbf{k}}| = \mu_k$, or equivalently $k = k_\beta$ divides the k-space into two regions with different nonlinear interactions. In particular, the region of large anisotropy has inefficient interactions, because of short relaxation times. The same could be phrased in the language of triads: the dominant linear β-term in the PV evolution equation should impose an additional frequency synchrony on nonlinear interactions, and thus render them less efficient. Notice that f-plane (zero-beta) turbulence (purely 2D) is automatically synchronous, as all modes have zero frequency.

Vallis and Maltrud [12] carried out numerical simulations on a 256^2 lattice with isotropic forcing at $k_\mathrm{f} = 80$, and found that only broadly distributed friction could equilibrate such a system. If scale selective friction is turned on at small wave numbers, $k_c < k_\beta$, the energy will still accumulate at k_β and the system will not relax to equilibrium.

Wave number k_β is determined by the energy flux and remains fixed for a stationary source (e.g. a delta-correlated Gaussian [27, 44, 49]). If the long-wave dissipation is confined to small $k < k_\beta$, the energy will slip across the k_β-barrier, so it will no longer define the arrest scale [49]. Nevertheless the Rhines wave number k_β^R (or k_β^H — for the narrow-band spectra) can remain valid. It will decay with time, since the energy slips across k_β, increasing rms velocity and thus lowering k_β^R until reaching the dissipation range.

Thus we find that k_β and k_β^R have different meanings, but both express anisotropy and the departure from the 5/3-law, to be discussed below. Let us remark that in the forced turbulence case all three numbers, k_β^R, k_β and the wave number determined by bottom drag, should be related. It remains to be studied whether the Rhines scale k_β^R has the same meaning of the energy carrying scale in the presence of bottom friction.

Paper [12] presents the stationary two-dimensional spectrum for $k_\beta = 10$, with its characteristic ∞-shape. It becomes nearly isotropic for $k > k_\beta$. The wave-dominated ∞-regions have low energy density, typical of such experiments (e.g. Ref. [49]). So one should not consider k_β to separate 'waves and turbulence'.

Experiments [12] show k_β to approximately represent both the energy peak and the cut-off between the isotropic and anisotropic turbulence. In general, k_β should rather serve the latter role, as agreed by many authors.

We illustrate some features of the stationary beta-plane turbulence in Fig. 8. The simulation was performed on the

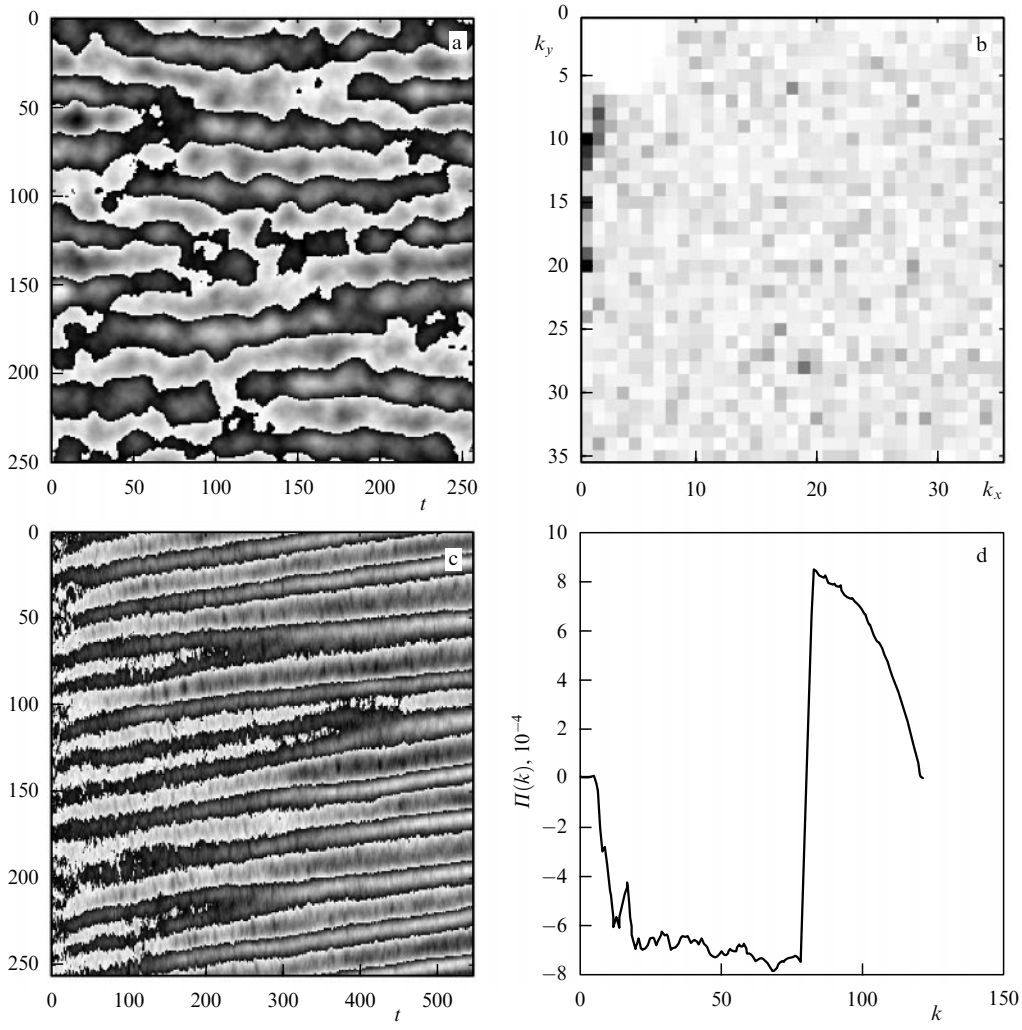

Figure 8. Two-dimensional turbulence on the beta-plane: (a) stream function at $t = 195$ (shading changes twice from black to white), (b) the corresponding compensated energy spectrum $k^{8/3}E(k_x, k_y)$, in the positive quadrant; (c) time evolution of zonally averaged zonal velocity field (double shading); and (d) spectral energy flux. Stabilization by bottom friction with $\lambda = 0.01$, integration time $t = 520$, $\beta = 60$, $k_\beta^\mathrm{R} \approx 18$, $k_\beta \approx 50$.

265^2 grid with forcing wave number $k \in [78, 82]$, friction coefficient $\lambda = 0.01$ and $\beta = 60$. It yielded stationary values $k_\beta^R \approx 18$, and $k_\beta \approx 50$. Figure 8a shows the stream-field at $t = 520$ (the shades change twice from black to white). One can see the large-scale organization of the systems in the form of zonal jets along the y-axis. The jet-structure slowly changes in time, and Fig. 8c reproduces the x-component of velocity averaged in the x-direction (zonal mean of zonal velocity) over the entire duration of the experiment.

The total mean kinetic energy remains nearly constant after $t = 120$, but its spectrum continues to evolve, as the formation of a zonal structure is a slow process. The westward jets (having negative velocities and white-color flanks) are broader than the eastward ones, and have stronger meanders. The jets are linearly stable according to Ref. [12], and all speculations about 'critical beta-plane stability criteria' for determining their width are redundant.

Figure 8b shows the compensated energy spectrum at $t = 520$, along the positive k-directions, multiplied by the theoretical $k^{5/3}$ and the factor k (to take into account the cylindrical divergence). It could be compared to the compensated isotropic spectrum. For better visualization the amplitudes of wave components $(0, 10)$ and $(1, 8)$ are reduced by factors of 4 and 2 respectively. The spectrum has a sharp fall-off in the upper left corner, which indicates nearly vanishing flux to small k. It attains its maximal value at the zonal wave vector $\mathbf{k} = (0, 10)$. The alternating zonal jets in physical space have a zero total (zonal) transport. The nonzonal spectral peak is located at $(1, 8)$ and has an amplitude lower than $(0, 10)$. Both wave-numbers are smaller than theoretical predictions, and k_β overestimates the outer (arrest) scale by a factor of 5.

Away from the maxima, the energy spectrum is practically isotropic, and has a slope close to $-5/3$. Figure 8d shows the angular average of the energy flux as a function of k, averaged over the last 10 units of time. The energy flux slowly decays with k to $k = 15$, which corresponds to k_β^R. The nonuniform flux is as above due to the bottom friction and falls sharply in the region of high energy density. The k_β^R-barrier is thus connected with the specific dissipation mechanism at low k. Clearly, for large drag coefficient λ, the energy flux will decay faster, and we reach a balance between the flux and dissipation at a higher k. As k_β is independent of the friction (as long as the friction is not too high on the forcing scale) we can raise λ, and thus bring k_β close to the energy peak.

The shape of the 2D spectrum [12] comes closer to the ∞-shape than in our Fig. 8b. To get a better measure of the stabilizing beta-effect, paper [12] suggests an energy peak wave number averaged over the angles $(-\pi/6, \pi 6)$ about the k_x-axis, called k_β^*. The jet wave number k_{jet} — the absolute spectral maximum, is always less than k_β^*, since the beta-effect becomes zero in the South–North direction, and allows uninhibited energy flux to low k. But the difference is marginal, more pronounced under special choices of the long-wave friction (see below). In our experiments (Fig. 8), the two quantities are close: $k_\beta^* \approx 12$, while $k_{\text{jet}} = 10$.

Paper [12] compares the computed values k_β^* and k_{jet} with theoretical predictions. The authors point out that theory overestimates these wave numbers, but comes close to them. They attribute the discrepancy to the bottom friction, and we have explained its role in determining such relations.

Paper [49] takes hypo-friction

$$D_i = \nu_i (-1)^{n+1} \Delta^{-n}$$

with $n = 5$, a space resolution 512^2, and a stationary source at $k \in [100, 105]$. It studies 3 cases: $\beta = 0$, and two others $k_\beta = 56$ and 158. Such a choice of friction makes the outer (arrest) wave number fall well below k_β in the two latter cases since long-wave dissipation resides at smaller wave numbers. The authors claim to obtain the $-5/3$ spectrum almost everywhere outside a narrow sector about k_y (our Fig. 8b shows similar behavior). The k_y-spectrum is much steeper with a slope reaching -5 (all spectra are averaged over small sectors of aperture $\pm\pi/12$ about the given direction).

The authors call it a Rhines spectrum, but this may be misleading. The relation

$$E(k) = c_1 \beta^2 k^{-5},$$

in the original work [8] marks the curve separating 'waves from turbulence', rather than the turbulent spectrum *per se*. Indeed, the equation

$$E(k)k = \frac{1}{2} U(k)^2,$$

yields the Rhines wave number k_β^R, and furthermore, relation $E(k) = c_1 \beta^2 k^{-5}$ has no spectral energy flux parameter. The observed slope -5 has no explanation. It could be due to a special form of the long range dissipation and angular averaging in Ref. [49].

The zonal jets of beta-plane turbulence could explain the underlying structure of the planetary atmospheres, like those of the Earth or Jupiter. So one is naturally led to studying turbulence in spherical geometry. Williams [90] did the first numerical simulation of 2D turbulence on a sphere, and found such a zonal structure. His computational region however was limited to 1/16 of the surface, due to the imposed symmetries, and he used a special spectral source. The spherical code of Ref. [66] didn't produce a clear zonal structure, most likely because of dissipation.

Next we mention a few recent works [42, 47, 91] devoted to the topic. The former studied forced turbulence without bottom friction (but with short-wave dissipation). The authors intentionally exclude long-wave dissipation. Such a system could eventually arrive at a statistical equilibrium, since it allows (small) direct energy cascade to the viscous range. But the authors note that the relaxation process to an equilibrium in the absence of long-wave dissipation is at present beyond the computational capability of modern tools.

Instead of stationary regimes, the paper studies the turbulent state after 1000 Jovian days. It looks for the dependence of the jet number on angular speed, with forcing at various spherical harmonics. In spherical geometry the Rhines argument would give the following estimate of the cut-off (spherical) wave-number

$$n_\beta^R (1 + n_\beta^R) = \frac{\Omega R}{U}, \tag{30}$$

where Ω is the rotation rate of the sphere, R the sphere radius, and U the rms velocity of vortex modes.

Model [47] has a spatial grid of 600×300 points, with truncation T199 (triangular truncation of higher spherical harmonics that leaves numbers $n \leqslant 199$). Figure 9 reproduced from Ref. [47] shows the dependence of the jet number on the rotation rate Ω. Only the relatively high wave number $n_f = 79$ shows a monotonic dependence of the jet number on Ω. When

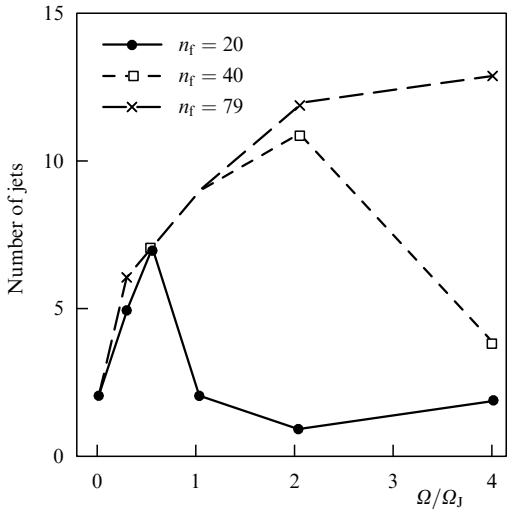

Figure 9. Jet number as a function of the rotation rate for non-stationary turbulent flow of the sphere after 1000 Jovian days [47].

the forcing number is smaller, e.g. $n_f = 20$ or $n_f = 40$, the dependence becomes irregular.

For a small forcing wave number and a high rotation rate Ω one gets only high latitude jets, and a circumpolar vortex bounded by a strong eastern current. The lower latitudes carry only wave-like undulations. In this case the jet comes close to the integral scale of the whole system.

Cho and Polvani studied decaying turbulence on a sphere for a shallow water system. We shall talk about additional effects in this system later on, and here focus only on the rotational effects. The paper exploits a triangular spherical truncation scheme T170 (on a 512×256 grid). The decaying turbulence is characterized by the energy centroid

$$\bar{n}(t) = \frac{\sum_n nE(n,t)}{\sum_n E(n,t)} ,$$

where n is the number of the spherical harmonic. The centroid gives the outer (arrest) scale of the inverse cascade due to the beta-effect (rotation).

All rapid rotation experiments yielded $\bar{n} < n_\beta^R$, where the latter quantity is defined for the equatorial value of β. Hence, it was concluded that the Rhines scale makes a poor prediction of the jet-number (as could be expected from the beta-plane geometry, the exact correspondence between these quantities does not necessarily exist). As Ω increases, the initial phase shows steepening of the spectral slope, which can be attributed to the termination of the inverse cascade. At larger times this tendency weakens. For small Rossby numbers, the turbulence evolves into a pair of anticyclonic polar vortices, as predicted in the earlier work [92] (cf. Ref. [47]).

Paper [91] studies both decaying and forced turbulence in a system with bottom friction. To some extent, it extends the planar analysis of Ref. [12] to the spherical case, and utilizes the T85 truncation (on a 256×128 grid) with forcing at $n_f = 55$. The 2D energy spectra, in both the decaying turbulence and the stationary forced turbulence, look similar to those in the planar case. Namely, the energy condenses in spherical modes with zonal wave numbers m close to 0. The difference appears at high latitudes, where jets weaken and broaden. This agrees with the decrease of β at high latitudes. The jets of decaying turbulence are less stable and robust than in the forced case. Also, the quasistationary spherical jets cannot move along a meridian, as their planar counterparts (with periodic boundary conditions), since $\beta = 0$ at the poles.

Paper [91] makes a difference between the full rms velocity and the rms vortex velocity obtained by subtracting the zonal mean. Fig. 10 shows the dependence of rms velocity on the mean wave number $[n(n+1)]_{CM}^{1/2}$ defined as the ratio of the mean zonal enstrophy to the mean zonal energy. Qualitatively, they follow from Eqn (30) with $n_\beta^R(1 + n_\beta^R)$ substituted for the squared wave number.

An important conclusion of Ref. [91] came from the analysis of spectral fluxes. The sustaining mechanism for jets was found to be the straining of small (forcing) scale vortices by the jets. Moreover, the intermediate scales practically disappear from the interaction after time averaging. The energy of vortex modes (defined by subtracting the zonal mean from the total field) peaks at the Rhines scale. However, large vortices do not interact with the zonal mean on average. These results, on the one hand, indicate nonlocal interactions to be typical of 2D turbulence; secondly, they separate the Rhines scale and the jet scale. The dynamics sustaining zonal jets have little relation to the Rhines-scale structures, identified with maximal vortex activity.

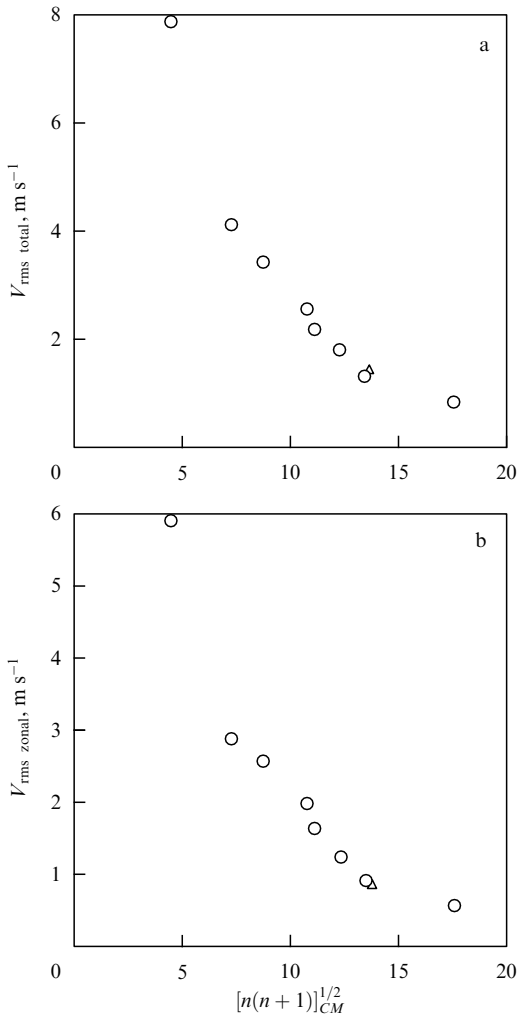

Figure 10. Dependence of rms velocity (a) and rms zonal velocity (b) on the mean wave number in numeric simulations [91]. The mean wave number squared is defined as the mean enstrophy over mean energy.

We reiterate the main points of this section:

• There are several theoretical estimates of the separation scale between small-scale isotropic eddies and the large-scale motions influenced by the beta-effect. The wave number k_β seems to be the best candidate for the boundary between isotropic and anisotropic turbulence although it tends to overestimate this boundary. The Rhines scale should fall in between k_β and the spectral peak wave number. The latter accounts for the basic zonal structure — the (East to West) jets on the beta-plane. All such estimates are, however, qualitative, as one should not expect a single parameter to describe the transition from anisotropic to isotropic turbulent regions. The original Rhines formulation was most often used in this context, but its ambiguity lies in the meaning of rms velocity fluctuations.

• The turbulent energy does not propagate up into the range of 'degenerate' Rossby waves, but condenses in the South – North direction in the Fourier space. Zonal jets are sustained mainly through the direct (non-local) interactions of small (forcing size) scales, and involve no Rossby waves.

• Long-wave dissipation brings more uncertainty (in the stationary state) because it can produce its own outer (arrest) scale. It is not clear whether the original Rhines number, or its cousins, could serve as a universal estimate of the outer scale in the presence of such dissipation.

4.4 Finite Rossby – Obukhov radius

In the previous section we talked about geostrophic turbulence on the beta plane, or sphere, in the limit of an infinite Rossby – Obukhov radius. A finite radius entails a new effect. The PV equation with a finite Rossby – Obukhov radius is often called the equivalent barotropic PV. It also appears in plasma physics under the name Hasegawa – Mima equation, and describes drift waves.

In this section we exclude Rossby waves by assuming a constant Coriolis parameter (the *f*-plane approximation). As is well known, a localized PV density in an equivalent barotropic fluid gives a localized velocity distribution, since the Laplacian in the relation between the vorticity and stream function is replaced with the Helmholtz operator,

$$\Delta\psi - \frac{1}{L_0^2}\,\psi = \omega_q\,.$$

So Green's function $G(\mathbf{r},\mathbf{r}_0)$ [for $\omega_q = \omega_0\delta(|\mathbf{r}-\mathbf{r}_0|)$] changes from the infinite range, log-potential one to the finite range (exponentially decaying) Bessel – MacDonald function

$$G(\mathbf{r},\mathbf{r}_0) = -\frac{1}{2\pi}\,\omega_0 K_0\left(\frac{\mathbf{r}-\mathbf{r}_0}{L_0}\right).$$

Thus one could expect inhibition of large-scale structures above L_0. Though a finite Rossby – Obukhov radius could suppress the inverse cascade, which, however, will not necessarily be stopped completely.

Indeed, in the limit

$$k \ll \frac{2\pi}{L_0} = k_{\mathrm{RO}}$$

the PV is approximated by

$$\omega_q = -\frac{\psi}{L_0^2}\,,$$

and PV evolution takes on the form

$$-L_0^{-2}\partial_t\psi + [\psi,\Delta\psi] = D + F\,, \tag{31}$$

conserving (in the absence of forcing – dissipation) the integrals

$$K = \int \psi\Delta\psi\,\mathrm{d}x\,\mathrm{d}y\,,$$

$$P = \int \psi^2\,\mathrm{d}x\,\mathrm{d}y$$

— the kinetic and potential energies. They can be regarded as limiting values for the total energy and enstrophy, conserved in the entire system. We note that the principal terms of the energy and enstrophy become proportional in the limit $k \to 0$, and turn into the 'potential energy', while the higher order terms in the small parameter $(kL_0)^2$ give the 'kinetic energy'.

According to Ref. [93] the two integrals K, P define two cascade regions: the upscale cascade of the potential energy, and the downscale one for the kinetic energy. The former has a spectral slope $-11/3$; the latter, -5. Paper [93] refers to an earlier work by Iroshnikov, who obtained these laws. Such spectral laws are much steeper than the standard 2D-turbulence and can be attributed to the drop in the cascade efficiency.

The large-scale turbulence driven by (31) evolves on a slow time scale tL_0^2/L^2, where L is the characteristic size of large eddies that could be identified with the outer (integral) scale of the system, $L = 2\pi$. So after energy penetrates into the upscale range, the dynamics slows down. Numerical experiments on decaying turbulence with the initial spectrum in the upper range $k \ll k_{\mathrm{RO}}$ [93] yielded spectra steeper than -5, as in the 2D decay case, which gave spectral slopes steeper than the theoretical slope -3. They also show that the PV dynamics driven by the complete QGS system are identical to the reduced equation (31).

Paper [94] considers turbulence forced within the wave-number band $47 < k < 50$, for

$$k_{\mathrm{RO}} = \frac{2\pi}{L_0} = 0, 10, 20, 40\,,$$

on a 256^2 grid, with standard hyperviscosity at high k, but without long-wave dissipation. The forcing scale is put below the Rossby radius, and one is interested in the energy transfer across the k_{RO}-barrier. Of course, such a system could not equilibrate without infrared dissipation.

The inverse cascade spectra, averaged over a sufficiently long time, depend on k_{RO} and steepen with k_{RO} from $-5/3$ to $-11/3$. The slow cascade process at $k < k_{\mathrm{RO}}$ leads to energy accumulation at low modes and to the formation of regularly spaced vortex structures – 'vortex crystallization', according to the terminology of Ref. [94]. Accordingly, the PV structure functions show oscillations as functions of the separation distance r.

The authors of Ref. [94] stress that the vortex lattice does not remain fixed. As energy continues to accumulate in the low modes, the quasi-periods of the vortex lattice grows. The authors attribute the growth process to vortex merging, but provide little evidence. They also don't address the interaction of strong vortices with the background field. Indeed, the source cannot directly contribute to large vortices, but only to

the small-scale background, and one needs a proper transfer mechanism to explain the growth of large structures.

The finite Rossby radius cannot arrest the inverse cascade without a dissipative sink. The simple linear drag becomes less efficient here, as the Ekman friction affects the relative vorticity rather than the PV. Our preliminary simulations show that the energy can go well above the Rossby – Obukhov radius and reach higher levels than for $k_{\mathrm{RO}} = 0$, all other parameters being equal. Here we see inefficient 'large scale friction' competing against inefficient nonlinearity, and the problem of equilibration of the inverse cascade by bottom drag remains open.

4.5 Shallow water turbulence

Rotating shallow water allows for surface (inertia-gravity) waves and raises the problem of vortex dynamics, in the presence of wave modes. This model is important for geophysical applications and is often discussed in the context of the so-called 'slow manifold'. The latter means a slowly evolving part of the coupled wave-vortex system, which should yield a nearly quasigeostrophic equilibrium for vortex modes. The shallow water system always emits fast gravity waves, so the problem could be also phrased in terms of the effect of gravity waves on the slow evolution of vortex modes.

Another issue studied in connection with shallow water is related to the Rossby – Obukhov radius. It could have some bearing on the wave generation, but is usually studied in the context of the equivalent barotropic model without waves (preceding section).

The study of the shallow water turbulence by itself could not solve the slow manifold problem, but it allows one to address some basic issues of wave-vortex interactions.

Rapid rotation decouples the wave and vortex modes, so one could expect that stirring only the slow part of the system (via a 'balanced source') should produce turbulence close to two-dimensional turbulence. This does happen to some extent, but gravity waves are still generated in the vicinity of intense vortex structures and can modify the dynamics of such structures.

If the Rossby and Froude numbers are small (the latter refers to the ratio of typical velocities to the speed of a 'surface wave'), the separation into the slow and fast modes could be implemented by a linear (gravity wave) operator (e.g. Ref. [95]). This operator has two types of eigenmodes — zero frequency, geostrophically balanced modes, and non-zero inertia-gravity modes. To take into account nonlinearity, one has to specify a proper nonlinear splitting.

The commonly used procedure exploits the gradient wind balance, and leads to the so-called balance equations (see e.g. Ref. [96]). All fields are decomposed into a vortical (balanced) component (labeled with subscript v), and a small (in Rossby – Froude numbers) unbalanced residual. The gradient-wind balance equation is obtained from the Navier – Stokes equations by applying the divergence operator and retaining the zeroth and first order parts in small Rossby number,

$$g\nabla^2 h_v = f\nabla^2\psi_v + 2J(\partial_x\psi_v, \partial_y\psi_v)\,.$$

The first term in the r.h.s. corresponds to the geostrophic balance; the second gives a quadratic correction (proportional to Ro). But the gradient wind balance can be considered for any value of Ro; in particular, for large Rossby numbers it corresponds to the so-called cyclostrophic balance.

The gradient wind equation gives the balanced component of the height-function in terms of the balanced stream-field ψ_v, but the definition of ψ_v requires additional assumptions. Paper [97] imposes them through the potential vorticity of the vortex mode

$$\omega_q = \nabla^2\psi_v - \frac{f}{H_0}\,h_v\,.$$

Thus the unbalanced residual would have zero geostrophic PV; this is a justified assumption as long as the residual remains small during the evolution, which, however, can be tested only by solving the system.

Two relations (gradient wind and the PV condition) allow one to recover the fields ψ_v and h_v from PV. The residual is merely the difference between the complete solution and the balanced one. The source of mass and momentum are then chosen to stir only the balanced mode.

Paper [97] integrates shallow water on a 256^2 grid with the source at wave numbers 7 – 9. Linear friction is confined to the first 6 wave numbers, and the Rossby – Obukhov radius exceeds the forcing scale by a factor of 2. The inverse cascade range is not resolved here, so the main focus of the paper is the direct enstrophy cascade.

The paper considers regimes with different Rossby and Froude numbers (the former being measured by the ratio of the rms vorticity to the Coriolis parameter), varying them within the range from 0.1 to 1. One example is a stationary regime with a Rossby number of 0.45 and a Froude number of 0.25. Here the vortex mode develops a spectral slope -3.3 (the initial one was somewhat steeper, -3.8), consistent with standard 2D turbulence. The vortex modes dominate the spectrum in the low wave-number range. But the gravity wave spectra decay more slowly than the vortex ones, and become dominant at large wave numbers. They have no power law approximation.

For physical space, paper [97] reports active zones of wave generation (large divergence) on the periphery of strong vortices. Thus wave-modes are stirred by the large scale vortex components, and their spectra are sensitive to the enstrophy resolution.

The paper shows that the vortical modes of shallow water share many characteristics of 2D turbulence. For instance, the direct (enstrophy) cascade, as in 2D turbulence, is dominated by elongated triads. If the Rossby number exceeds 0.2, the spectral slope of inertia-gravity waves becomes much shallower than the slope of vortex modes, and starts to dominate at large k.

The paper takes Rossby and Froude numbers close to the atmospheric values, and claims that the transition from the -3 slope to a gentler one roughly corresponds to the 500 km scale in the atmosphere. Thus mesoscale motions dominated by gravity waves could arise in the absence of small scale forcing.

A complete study of decaying shallow water turbulence was conducted in paper [98]. It studied the evolution of the initially balanced spectrum. To get the balanced initial conditions, it uses balance relations, whereby the velocity field is represented as the sum of the vortex field and a small potential field

$$\mathbf{v} = \mathrm{rot}\,\psi\mathbf{e}_z + \epsilon\nabla\chi\,,$$

with $\epsilon \ll 1$. This expansion is substituted into the shallow water equations, and all terms of order higher than $\epsilon \mathrm{Ro}$ are dropped. Given the spectrum of the vortex component ψ, one can compute the spectra of the velocity potential χ and surface elevation h with the help of balanced equations, and use them as the initial conditions. The shallow water equations are then integrated on a spatial grid of 200^2, or with a higher resolution of 500^2. The initial spectrum is centered at the wave number $k_0 = 14$. The numerical simulations [98] cover the widest range of the Rossby and Froude parameters in the shallow water system to date.

One particular aspect of the study is the effect of a finite Rossby–Obukhov radius on the turbulent cascade, controlled by the dimensionless Burgers number

$$B = \frac{\mathrm{Ro}^2}{Fr^2} = \frac{L_0^2}{L^2},$$

where L is the typical linear scale, and L_0 the Rossby–Obukhov radius.

A small value of B means large initial vortices, compared to L_0, and weak inverse cascade. The authors study the kinetic energy centroid k_K as a function of the Burgers number after 1000 eddy turnover periods. This relation shows that for small values of B it deviates moderately from the initial k_0. As the Burgers number is increased, the centroid k_K moves down and stabilizes at some value. This happens as the Rossby–Obukhov radius comes close to the box size when B approximately equals 200, and for higher values of B the evolution of turbulence is determined by (non-universal) large scale geometry.

Another important parameter is the vorticity kurtosis, which measures the intermittency of the system. Paper [98] shows the time evolution of kurtosis for 3 experiments. The first experiment has an initial vortex scale several times as large as the Rossby-Obukhov radius. The second one takes it to be of order $L_0/2$ and the third one, $L_0/5$. The first case maintains kurtosis close to the Gaussian value 3, as in the initial state. In the second experiment the intense vortex formation stops at time $t = 200$, when the typical vortex size approaches the Rossby–Obukhov radius. After this the inverse cascade becomes inefficient and the kurtosis saturates. In the third experiment, the typical vortex size does not reach the Rossby–Obukhov radius even at $t = 1000$, and the kurtosis continues growing.

The paper notes that the evolution of turbulence leads to the growth of asymmetry between cyclonic (positive) and anticyclonic (negative) vorticity. The skewness (measure of asymmetry) of the vorticity field, initially zero, becomes negative in a long run. The asymmetry depends on the Froude number and appears at the early stages of experiments. Cyclones look less regular than anticyclones, and grow more slowly. The paper doesn't offer a convincing explanation of such behavior, but points out that cyclones have a lower thickness and, therefore, a smaller local Rossby–Obukhov radius, as well as a smaller zone of influence.

The problem of asymmetry between cyclones and anticyclones was also studied in Ref. [99]. It showed that the merging of anticyclones leads to axi-symmetrization and strengthening of the combined structure, whereas merged cyclones remain elongated and dissipate energy in the direct (enstrophy) cascade. These results agree with the conclusions of Ref. [98]. In this regard we should remark that quasigeostrophy maintains complete symmetry between cyclones and anticyclones, since the surface elevation appears through a linearized (symmetric) approximation:

$$\frac{1}{H} = \frac{1}{H_0}\left(1 - \frac{h}{H_0}\right).$$

The equations for shallow water make no such approximations and treat the surface nonlinearly. So the dynamics of cyclones and anticyclones need not be similar.

The analysis of Ref. [98] shows that unbalanced fields grow with Rossby and Froude numbers, but remain small on average for small Rossby numbers. Like Ref. [97] this paper finds large coherent vortex structures to be surrounded by gravity wave fronts (bores). Bores stretch radially from vortex centers; they are formed during the merging processes of cyclones and anticyclones.

The unbalanced motions in the simulations of Refs [97, 98] remain small, since the sources can stir only balanced modes, and strong small-scale dissipation prevents energy accumulation at high k. The situation changes in conservative systems. In that case fast modes are always generated by the slow ones, but there is no direct feedback of waves to vorticity (generation of gravity waves by vorticity at small Froude number bears analogy to generation of sound by turbulence). The slow leak of vortex energy to waves can be studied adiabatically and modeled by slow evolution of the basic parameters of vortex modes. Such 'super-slow' evolution can be interpreted as a higher level 'slow manifold'.

Of course, the real dynamics and their adiabatic approximation can diverge at large time, as demonstrated in Ref. [100] by a specific example. As wave modes accumulate sufficient energy, they can become dynamically independent, rather than enslaved to 'balanced vortex modes', and this can lead to a gradual departure from the slow manifold.

Paper [42] (mentioned in the preceding section) studied the effect of finite Rossby–Obukhov radius on turbulence decay for shallow water on a rotating sphere. It shows that large circumpolar vortices are replaced by groups of small vortices of Rossby–Obukhov size. The zonal jet structure disappears and turns into a spiral structure. These results can also be attributed to the reduced efficiency of nonlinear interactions for large vortices.

5. Geostrophic turbulence

5.1 Quasigeostrophic potential vorticity in stratified fluids

So far our discussion of various geophysical factors (the beta-effect, topography, finite Rossby–Obukhov radius) has been confined to barotropic fluids. Real systems are stratified, so a latitudinally varying heat flux renders isothermal surfaces of potential temperature in the atmosphere (or potential density in the ocean) inclined to the horizontal plane (isobaric surfaces). Such an inclination implies the presence of a potential energy that can be released into baroclinic motions. Stratification means that the potential temperature or density are functions of the vertical coordinate. The standard textbooks (e.g. Refs [5, 7]) show that stratified (baroclinic) fluids conserve the quasigeostrophic potential vorticity PV in the absence of forcing and dissipation,

$$D_t \omega_q = 0. \tag{32}$$

As above we denote $D_t = \partial_t + (\mathbf{v}\nabla)$ (this takes into account the horizontal advection by a geostrophic velocity field), and

$$\omega_q = \Delta\psi + f^2\partial_z\left(\frac{1}{N^2}\,\partial_z\psi\right) + f$$

is the quasigeostrophic PV in a stratified fluid defined in terms of the horizontal Laplacian Δ and the Brunt – Väisälä (buoyancy) frequency $N(z)$. The latter depends on the vertical stratification,

$$N^2(z) = -g\,\frac{\partial_z\,\rho_s(z)}{\rho_0}$$

for the ocean and

$$N^2(z) = g\,\frac{\partial_z\theta_s(z)}{\theta_0}$$

for the atmosphere, where ρ_0 and θ_0 are the reference potential density and temperature. Thus a quasigeostrophic PV, compared to the case of barotropic fluid, has an additional z-dependent term. But the quasigeostrophic motion of the stratified fluid is still horizontal (in layers) and, therefore, determined by a single stream function of three space coordinates and time.

From the basic hydrostatic and geostrophic balances one gets the thermal wind relations

$$\partial_z v_x = -\frac{g}{f}\,\partial_y\,\frac{\theta}{\theta_s}\,, \qquad \partial_z v_y = \frac{g}{f}\,\partial_x\,\frac{\theta}{\theta_s},$$

where θ means the departure of potential temperature from its basic (mean) profile θ_s. For the ocean, the ratio of potential temperatures should be replaced by the ratio of two densities (with negative sign). By virtue of the thermal wind balance the horizontal gradient of potential temperature is proportional to the vertical wind shear. In particular, the meridional temperature contrast gives rise to a vertical shear along the x-axis.

The conserved dynamics of quasigeostrophic PV (32) imply conservation of the total energy

$$E = -\frac{1}{2}\int\psi\omega_q\,\mathrm{d}V = \frac{1}{2}\int\left(|\nabla\psi|^2 + \frac{N^2}{f^2}\,(\partial_z\psi)^2\right)\mathrm{d}V$$

and quasigeostrophic potential enstrophy

$$Z = \int\omega_q^2\,\mathrm{d}V\,.$$

Charney [101] has shown that two conserved integrals of motion allow one to adopt the two-dimensional theory to the quasigeostrophic turbulence, assuming an isotropic distribution of energy in 3D space with a stretched vertical coordinate $z' = zN/f$ (for constant Brunt-Väisälä frequency). The isotropization hypothesis for geostrophic turbulence was tested in Ref. [102] by means of a simplified Test Field Model. It considered the decaying turbulence and showed that at large wave numbers (greater than the energy peak) a turbulent flow becomes almost isotropic. This process however, proceeds at a slow pace, due to the k^{-3} energy spectrum. Indeed, the rate of strain at wave number k,

$$\left(\int_0^k E(p)p^2\,\mathrm{d}p\right)^{1/2},$$

should grow logarithmically slowly with k for a k^{-3} energy spectrum. At the low k end, the 3D isotropic distribution transforms into a two-dimensional one.

Charney's 3D isotropization assumes a degree of homogeneity in the vertical direction, while the real atmosphere and ocean have only limited vertical extent. Besides we use the 2D advection in Eqn (32) and 3D elliptic operator in the definition of ω_q. So to show the equivalence of the quasigeostrophic and the 2D turbulence, one needs to compare the triad structure in both cases.

Paper [103] does it for $N = \text{const}$, and notes that a non-constant Brunt – Väisälä would not allow such isomorphism. The numerical simulations of Ref. [103] verify Charney's hypothesis in a model with horizontal resolution 128×128 and 6 vertical modes. The vertical modes are solutions of the Sturm – Liouville problem

$$\frac{\partial}{\partial z}\left[\frac{f^2}{N^2}\,\frac{\partial}{\partial z}\,F_m(z)\right] = -\lambda_m^2 F_m(z)$$

with rigid lids on the top and bottom of the fluid layer. The $m = 0$ mode $F_0(z) = 1$ is *barotropic*, while the rest are *baroclinic*,

$$F_m(z) = \sqrt{2}\cos\left(\frac{m\pi z}{H}\right), \qquad \lambda_m^2 = \left(\frac{m\pi f}{NH}\right)^2.$$

where H is the depth of the layer.

Assuming an external shear profile $\mathbf{U} = (U(z), 0)$ to be fixed by the balance of the heat flux and dissipation in (32) via the thermal wind relation, one can study the stability problem (we shall describe it below in more detail for the two-layer fluid). Such a flow is known to be unstable to baroclinic perturbations (see e.g. Ref. [5]). Such instability evolves into the turbulence studied in Ref. [103]. Here the vertical velocity profile $U(z)$ is assumed to have only the first (most unstable) baroclinic mode. Stationary states can exist due to the bottom friction, which augments the r.h.s. of (32) with $-\lambda\nabla^2\psi|_{z=0}$. The external flow can be accounted for by adding $-\mathbf{U}\nabla\omega_q$ term on the r.h.s. of Eqn (32), or expanding all the fields in the mean and perturbation.

The statement of problem in Ref. [103] differs from that of standard 2D turbulence, as the forcing scale here is not fixed. The Rossby radius of the first mode, λ_1^{-1}, gives the principal instability scale, so the energy input is confined to the vicinity of $k = \lambda_1$.

The energy pumping in Ref. [103] is clearly anisotropic in 3D, as it involves the first baroclinic mode. But the energy spectra at large 3D wave numbers

$$K = (k^2 + \lambda_m^2)^{1/2}$$

are equal (in the constant Brunt – Väisällä frequency case). That means 3D-isotropization in the modal representation, with the spectral density depending on K only.

The energy peaks of the fixed vertical modes, as functions of horizontal k, have different positions, but the peaks of the barotropic and the first baroclinic modes coincide. The horizontal wave-number of the energy peak is close to the Rhines scale k_β^{R} of the barotropic mode.

Experiments with variable (exponential) Brunt – Väisällä frequency lose universality. The energy spectra are no more functions of the 3D wave-number, though different vertical numbers m have the same horizontal slope in k. However,

decaying turbulence with 3D isotropic initial conditions and a variable Brunt–Väisällä frequency profile restores the isotropic spectra and universal relations. The authors suggest that the tendency to 3D isotropization in general depends on the isotropy of the source.

Paper [103] also considers the energy budget for different modes. It shows that nonlinear energy transfer for the barotropic mode is positive at small horizontal wave numbers, like in the inverse cascade of 2D turbulence. This transfer is largely balanced by the bottom friction, whereas the baroclinic instability plays a minor role. For baroclinic modes the nonlinear energy transfer is negative in the low k range, and one gets the direct cascade to high k.

The energy balance of the first baroclinic mode is sustained by generation and nonlinear transfer. An interesting effect of the bottom friction is the positive contribution to the balances of baroclinic modes at small wave numbers, due to the coupling of baroclinic modes to the barotropic one at the lower boundary. We shall come back to spectral fluxes in the next section on multi-layer models. Here we only state the principal conclusion: a multimode stratified fluid can produce an inverse energy cascade only through its barotropic mode.

Paper [104] compares the decay regimes of 2D turbulence and quasigeostrophic (3D) turbulence (with homogeneous vertical structure). Their gross features (enstrophy slope, enstrophy decay rate, as function of a time, etc.) look qualitatively similar, but differ in details. As in the 2D decay turbulence long lived vortices appear in the 3D quasigeostrophic case [105]. A recent paper [106] conducted a statistical analysis of geostrophic vortices, and showed that after the initial transient the vortex statistics become self-similar, and agree with the scaling based on constant energy, vorticity extrema and the ratio of vertical to horizontal vortex sizes (cf. Refs [70, 72]).

The dynamic study of quasigeostrophic turbulence is much more laborious compared to the 2D case, due to 3D integration. Only a few papers have made such attempts. Most results of geophysical significance were obtained by means of multi-layer (typically two-layer) models, which we shall now describe.

5.2 Multi-layer models

The main source of atmospheric energy comes from the solar radiation that creates the temperature contrast between the poles and the equator. The horizontal gradient makes the isotherms of the potential temperature inclined and causes baroclinic instability, which releases the available potential energy. The observational data, however, show that the maximum kinetic energy of nonstationary atmospheric vortices and the maximal heat flux correspond to zonal wave-numbers 4–7, in contrast to the Earth's baroclinic instability modes, which correspond to wave numbers 12–15 [107]; see Fig. 11 reproduced from Ref. [108]. Hence the basic problem is as follows: what are processes responsible for the observed maximum, and how can they explain its seasonal variations, as well as its variations between the northern and southern hemispheres?

The ocean currents gain part of their energy from the wind stress at the surface. The source scale here is comparable to that of the basin. The wind stress gives rise to vertical shear, proportional, via the thermal wind relation, to the meridional gradient of the temperature. So the baroclinic instability is still responsible for the energy flux. The classical problem of oceanography is the Antarctic Circumpolar Current in the Southern Ocean — a jet flow whose meridional extent is far lower than the wind stress scale [109].

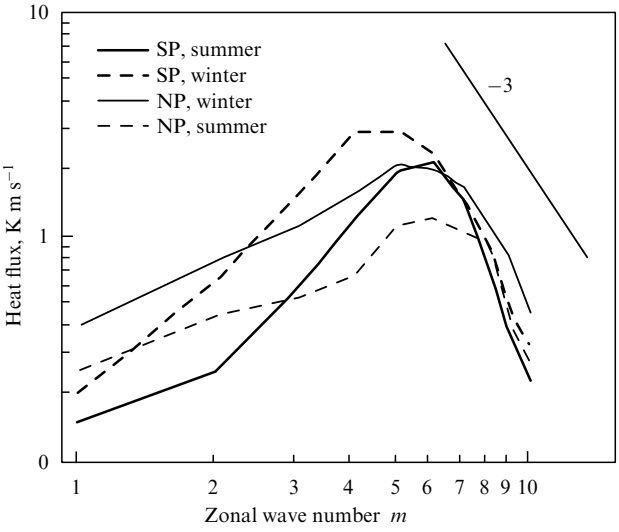

Figure 11. Meridional heat flux as a function of the zonal wave number for the Earth's atmosphere [108].

The physics of such localization is only part of the problem. Another important point comes from the relatively small inner Rossby radius of the ocean — 40–50 km, compared to 800–1000 km for the atmosphere. This radius characterizes the energy release scale for baroclinic modes, and its small value does not allow it to be resolved in any general circulation model. The subgrid turbulence must be parametrized in terms of the resolved fields (or mean fields in the simplest models). Thus one needs an effective parametrization for turbulent fluxes of heat, potential vorticity and momentum, which by itself is a big unresolved problem that we leave aside in this review.

The basic tool for such problems, used in many works, are multi-layer (often two-layer) models. They are most efficient from the computational standpoint, if one has to compute the important statistics and parameters.

Quasigeostrophic equations for PV in a two-layer fluid of equal thickness and with a rigid lid (the latter is equivalent to the infinite outer Rossby–Obukhov radius) have the following form (see Ref. [5] for more detail):

$$\partial_t q_i + J(\psi_i, q_i) = F_i\,, \tag{33}$$

where $i = 1, 2$ labels the layer: 1 — upper, 2 — lower. The potential vorticity in each layer is computed via

$$q_i = \Delta\psi_i + f + \frac{1}{2}\,k_{\mathrm{R}}^2(\psi_j - \psi_i)\,, \qquad j = 3 - i\,,$$

where $k_{\mathrm{R}} = 2(f^2/(g'H_0))^{1/2}$ measures the inverse of the internal Rossby radius ($g' = g\Delta\rho/\rho$ the reduced gravity acceleration, $\Delta\rho$ the density drop between two layers), and F_i designate the forcing-dissipation in two layers. These terms look different for the atmospheric and oceanic models. In the ocean the surface wind stress provides the source. It enters the model through the meridional gradient of the tangential wind stress on the upper layer; the long wave dissipation consists of the Ekman bottom friction on the lower layer, and one uses hyperviscosity for the short-wave energy sink,

$$F_1 = -\partial_y\tau + D_{1u}\,, \qquad F_2 = -\lambda\Delta\psi_2 + D_{2u}\,.$$

The second terms in both expressions mean hyperviscosity, which we will not specify.

For atmospheric models solar radiation provides the source, while dissipation is due to both bottom friction and radiative cooling. For continuously stratified models the heat source is proportional to the vertical derivative of the heat flux [5]. This gives two heat sources of equal amplitude and opposite sign, in two layers. The temperature in the two-layer system is proportional to the difference of two stream-fields, and the radiative cooling amounts to relaxation of the temperature. This yields the following sources in the upper and lower layers:

$$F_1 = \varkappa_T\left(\frac{\psi_1-\psi_2}{2}-\tau_e(y)\right)+D_{1u}\,,$$

$$F_2 = -\varkappa_T\left(\frac{\psi_1-\psi_2}{2}-\tau_e(y)\right)-\lambda\Delta\psi_2+D_{2u}\,,$$

and the quantity $\varkappa_T\tau_e(y)$ denotes the meridional profile of the source.

Unlike the previous case we could find a stationary solution, which balances the heat source, radiative cooling and Ekman friction. In the absence of Ekman friction and short-wave dissipation, the stationary meridional temperature profile is proportional to τ_e. This fixes only the difference between two stream functions, but not the stream functions themselves. One can add Ekman friction and neglect short-wave dissipation (making use of the large disparity between the forcing and viscous scales). This implies $\Delta\psi_2=0$, i.e. a uniform flow in the lower layer, whose velocity must be zero in the absence of momentum sources in the lower layer.

Given such a stationary state, we can consider solutions for the two-layer system in the form of the sum of the reference (mean) flow and its perturbation due to instabilities. In the oceanic case the upper layer source can be balanced only through non-stationary and nonlinear effects, so we have no stationary reference flow.

Salmon [110, 111] outlined the general scheme of the two-layer turbulence (see Ref. [7] for elementary exposition). One replaces layer stream-functions ψ_1, ψ_2 with $\psi=(\psi_1+\psi_2)/2$ and $\tau=(\psi_1-\psi_2)/2$, — *barotropic and baroclinic stream functions* (they correspond to the barotropic and first baroclinic modes of multi-mode systems). The derivation of corresponding equations for barotropic and baroclinic stream functions follows easily from Eqns (33).

The total mean energy per unit mass is given by

$$E=\frac{1}{2S}\int(\nabla\psi\cdot\nabla\psi+\nabla\tau\cdot\nabla\tau+k_{\mathrm R}^2\tau^2)\,\mathrm{d}x\,\mathrm{d}y\,,$$

where S is the area covered by the flow. This energy consists of the barotropic kinetic, baroclinic kinetic and baroclinic potential energies.

In the absence of forcing-dissipation the total energy is conserved. Moreover, the potential enstrophies of each layer are also conserved. We denote the total barotropic energy of the Fourier mode $\mathbf{k}$, as $U_{\mathbf k}$, and total baroclinic energy as $T_{\mathbf k}$. The analysis [111] of triad interactions for $\mathbf{p}$, $\mathbf{q}$, $\mathbf{k}$ $(\mathbf{k}+\mathbf{p}+\mathbf{q}=0)$ gives two kinds of triplets: barotropic $(\psi_{\mathbf k},\psi_{\mathbf p},\psi_{\mathbf q})$, and mixed baroclinic $(\psi_{\mathbf k},\tau_{\mathbf p},\tau_{\mathbf q})$.

In the first case we have conservation of the energy and enstrophy as in the 2D case,

$$\dot U_{\mathbf k}+\dot U_{\mathbf p}+\dot U_{\mathbf q}=0\,,\qquad k^2\dot U_{\mathbf k}+p^2\dot U_{\mathbf p}+q^2\dot U_{\mathbf q}=0\,.$$

So one should expect similar relations and the existence of inverse energy and direct enstrophy cascades for the barotropic mode. For the mixed type of interaction, the conservation of energy and enstrophy implies

$$\dot U_{\mathbf k}+\dot T_{\mathbf p}+\dot T_{\mathbf q}=0\,,$$
$$k^2\dot U_{\mathbf k}+(p^2+k_{\mathrm R}^2)\dot T_{\mathbf p}+(q^2+k_{\mathrm R}^2)\dot T_{\mathbf q}=0\,.$$

Far below Rossby-scale wave number $k_{\mathrm R}$ the energy exchange should involve two baroclinic modes, with small influx to the barotropic mode. In this limit, energy conservation also implies enstrophy conservation, and direct cascade to large wave numbers is not prohibited. The barotropic components becomes involved in interactions in the vicinity of the wave-number $k_{\mathrm R}$. Salmon concludes that the energy and enstrophy transfer follow the scheme presented in Fig. 12 (redrawn from Refs [7, 111]).

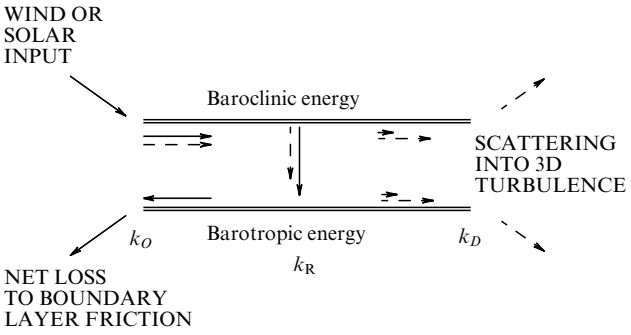

Figure 12. Schematic view of energy (solid) and potential enstrophy (dashed) fluxes in the baroclinic turbulent flow [110, 111].

The numerics of Ref. [111] are carried out on a 32×32 grid and agree with simulations of the Markovian model of turbulence. Here $k_{\mathrm R}=8$, and the maximum kinetic energy falls in the wave-numbers 3–4. The spectral slope for large k is close to -3. Higher resolution simulations appear in papers [112, 113] (three-layer models), and [13–15, 114–117] (two-layer ones). Below we describe the results that take into account the beta-effect.

Paper [112] was motivated by the problem of the Antarctic Circumpolar Current. It uses a finite-difference scheme. The domain of integration is periodic in the zonal direction, and has a rigid latitudinal boundary (where the proper boundary conditions require special consideration [118]). It uses quadratic bottom friction and linear friction between the layers. The grid resolution varies from 38.5 to 9.8 km, and the domain of integration covers 2000 km zonally and 1000 km along the meridian. The surface stress obeys a $\sin(\pi y/L_y)$-law. The channel regime corresponds to a meandering jet, whose localization across the channel is far less than the localization of the wind stress. The PV field has a frontal structure with irregular, nonstationary vortices.

A substantial part of the paper deals with mean balances, which we shall not discuss, as we are primarily interested in spectral characteristics. Spectral density of the velocity fluctuations on the channel axis has a broad range where the spectral slope is close to -3, and the meridional component v' has a much higher amplitude than the zonal u'. The -3 range covers both the radius-of-deformation wave-number and the maximal instability range. It does not extend, however, to small wave-numbers, where the bulk of the energy resides.

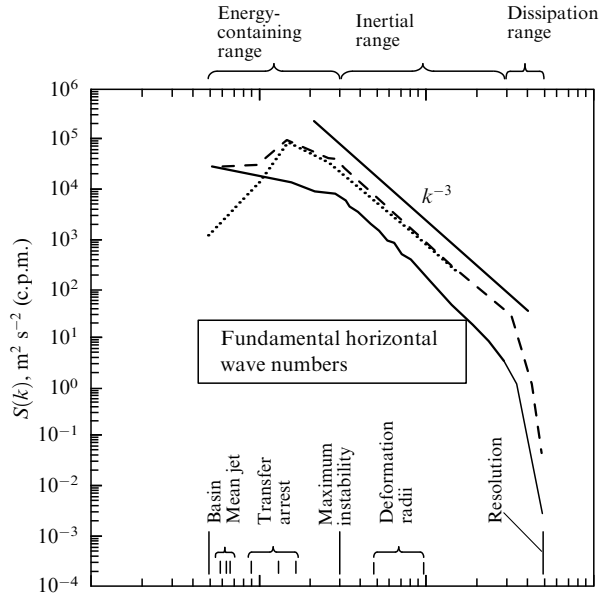

Figure 13. Spectra of the axial velocity components in the upper layer of a 3-layer fluid and scale ratio [112]. Spectrum of the zonal component (thick solid line) is less in absolute value than the meridional spectrum (dotted line). The total spectrum of the kinetic energy (dashed line) almost coincides with the meridional spectrum. The spectra are obtained by averaging 720 instantaneous snapshots.

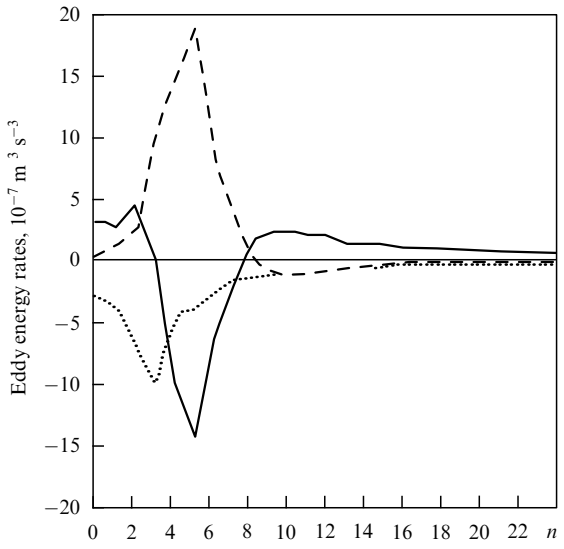

Figure 14. Vortex energy budget in numerical experiments [112]. Energy production shown in dashed line is balanced by nonlinear transfer (solid), and dissipation (dotted). The energy is transferred from the source region in both directions, to large and small wave-numbers.

The spectral maximum sits close to $(2\pi)^{-1}\beta^{1/2}\left(u'^2\right)^{-1/4}$, i.e. to the Rhines scale [8]. This scale changes by a factor of 2 from the lower to the upper layer. The jet wave-number (determined by the exponential fall of the velocity) is smaller than the spectral peak; we observed a similar feature for the beta-plane turbulence.

Figure 13 shows spectra for various components of velocity, as well as the scales of the problem [112]. The frequency spectrum computed in Ref. [112] also exhibits a -3 region, which confirms the Taylor hypothesis of frozen turbulence. The corresponding frequency interval, however, is shorter than the -3 region of k-spectra and belongs to the short-wave range.

The energy spectra in the zonal wave number look similar to the velocity spectra on the axis of the channel. The kinetic energy spectrum has a -3 region, but the potential energy drops as k^{-4} there. The spectrum of the total energy has an intermediate shape. Finally, the energy budget on Fig. 14 (follows Fig. 21 of Ref. [112]) indicates that the energy is gained from the mean flow on intermediate scales and transferred away from there through nonlinear interactions between vortices both to large and small wave-numbers.

The energy dissipation is comparable with the nonlinear transfer over a wide range of wave-numbers n, so the problem of the dissipation-free inertial interval remains open even in the -3 region. The maximal dissipation has smaller values of k than energy generation and coincides with the energy peak. We stress that this budget concerns the total energy, made of the barotropic and baroclinic components. It says little about Salmon's scenario, but we have already discussed other results [103] that confirm his picture.

Paper [13] studied the jet-structure in the atmospheric conditions in detail. It used a pseudo-spectral code with $N = 64$ or 128, in each direction and each layer. The heat source gives a uniform flow of velocity U_0 in the upper layer, and the stream-function has a period $2\pi/L$, $L = 15, 20, 30$ in units $1/k_{\mathrm{R}}$. Most experiments do not consider temperature relaxation. The transition time to a stable-jet state depends on forcing-dissipation. The author notes that the global characteristics of the flow (such as the total energy or heat-flux) are settled rapidly, over several dozens of time units $1/(U_0 k_{\mathrm{R}})$. The organization of jets, however, requires substantially longer (higher order) periods.

The paper presents stream-field realization, PV and the time averaged zonal velocity component; they clearly visualize the jet-structure in both layers. The dependence of the wave number k_J, equal to the jet number over channel width L, on the Rhines $k_\beta^{\mathrm{R}} = \sqrt{\beta/2U}$ of Ref. [13], is shown in Fig. 15. The rms velocity is determined via the total vortex kinetic energy $U = \sqrt{2E}$. The *vortices* of Ref. [13] are any departures from the base flow, including zonal jets.

The three dependencies on the figure differ by the bottom friction coefficient and β. The thick line has $\lambda = 0.05$ and $\beta = 0.1-0.5$ in dimensionless units (determined via k_{R} and U_0). The other solid line has $\lambda = 0.15$ and $\beta = 0.2-0.5$, while the dashed line corresponds to a fixed $\beta = 0.25$, and variable friction $\lambda = 0.015-0.4$. The jets weaken considerably as the friction grows. We should also remark that variable friction has an effect similar to that of variable β. Both parameters can significantly modify the energy of the flow. The last figure clearly demonstrates that a relation exists between the jet-number and the wave number k_β^{R}, thus bottom friction affects the flow in a given range of parameters through the rms velocity.

The total kinetic energy E includes both the barotropic and baroclinic contributions, and this contradicts, to some extent, the argument of Rhines. However, the barotropic energy in all experiments [13] far exceeded the baroclinic energy.

Paper [13] gives maps of the zonal component of 'vortical velocity', as a function of time and meridional coordinate (similar to Fig. 8c). The position and width of jets vary with time, but their number remains fixed. The maxima of vortex

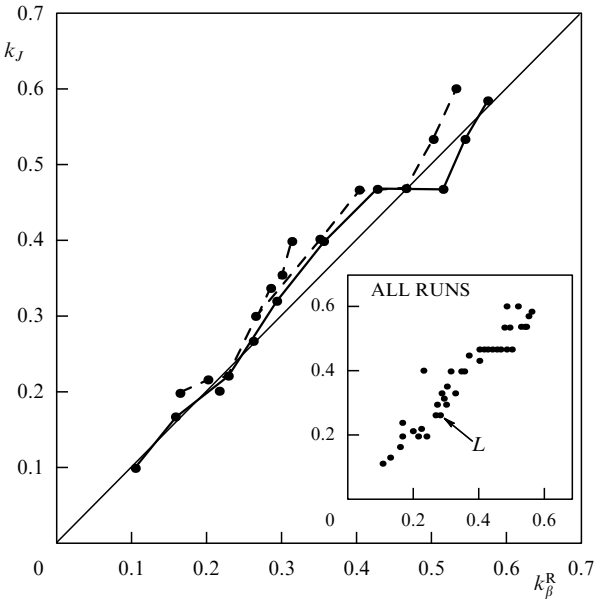

Figure 15. Dependence of the experimentally measured wave number k_J, obtained as the jet number divided by L, on the Rhines number $k_\beta^R = (\beta/(2U))^{1/2}$ [13]. Rms velocity is defined by the total boundary condition energy (including the zonal mean component of jets).

activity lie in between jets, therefore energy-carrying eddies are close to but somewhat smaller than the jet-scale.

We mention two important conclusions of Ref. [13]. It points out that any attempts to produce stationary regimes without bottom friction failed, allegedly because of the absence of a long-wave sink for the barotropic mode. This stresses once again the leading role of long-wave dissipation in stabilizing flows and forming jets.

The second remark concerns the characteristics of the inverse cascade of kinetic energy. The author observes that the region of energy generation moves dynamically to larger scales with increasing heat influx (or diminishing dissipation, or β). The distance between the kinetic energy peak and the energy generation peak is smaller than these numbers. Hence one has the energy flux to large scales, but no inertial interval with a self-similar spectrum. This apparently takes place for the total energy budget. The kinetic energy at large scale is indeed dominated by the barotropic mode, but the kinetic energy source is baroclinic. According to Salmon, the transfer of the baroclinic mode into barotropic proceeds in the vicinity of the Rossby radius.

The Earth's atmosphere poses a problem of low frequency variability. There are indications that such variability could appear even in the absence of zonal heat contrast, being an internal characteristic of the system. In this case it must be related to some characteristics of the quasi-two-dimensional turbulence. Paper [115] tackles this problem for a two-layer quasigeostrophic model. It takes a jet in the upper layer rather than uniform flow as the base flow, and uses a somewhat lower resolution (31 in both directions) than [13] does. It finds that k_β^R gives a good estimate of the energy peak wave number of vortex modes, and also for the maximal low-frequency variability. The dynamics of these waves are not related to the inverse energy cascade: the nonlinear transfer is small, and the wave amplitude is determined by the balance between generation (via mean flow) and dissipation.

As in the preceding paper, the conclusion in Ref. [115] is drawn for the total energy, hence the result is incomplete (the inverse cascade exists only for the barotropic mode). Unlike the preceding paper, however, the vortex mode is measured by its departure from zonally and temporally averaged flow. The paper shows that the transfer term becomes zero near the maximal production wave-number. The transfer is positive for smaller k and negative at the highest energy production region, since this energy is transported to other wave-numbers. The energy peak and the maximum production peak are nearly identical, which agrees with the earlier work [112].

Though all authors agree that Rhines scales corresponds to the maximal vortex energy in quasigeostrophic turbulence, such a result by itself has little predictive power, as long as one has no independent estimate of the rms velocity. There is no direct analogy here with barotropic turbulence on the beta-plane, since we are dealing with spectra in zonal wave numbers, and the energy flux is caused by instabilities of the global anisotropic zonal flow.

Held and Larichev [14, 15] used an idealized picture of quasigeostrophic turbulence in two-layer systems to estimate the rms velocities and turbulent diffusion coefficient for PV. Their argumentation is as follows. Let the source be such that in the absence of vortices it generates a shear

$$U = \frac{U_1 - U_2}{2} > 0$$

between the upper and the lower layers (subscripts 1, 2). Then we get the mean PV gradients in the upper and lower layers

$$\beta \pm Uk_R^2 = Uk_R^2(\zeta^{-1} \pm 1)\,,$$

where $\zeta = Uk_R^2/\beta$ is a dimensionless parameter. The condition of linear instability for such flow is $\zeta > 1$ (see Ref. [5]).

We assume that the flow is mostly barotropic on scales greater than the deformation radius $1/k_R$ (this condition holds in experiments [13]), and that the inverse cascade is arrested at some wave number k_0. If the spectral slope for $k > k_0$ is sufficiently steep, the bulk of energy is confined to the vicinity of k_0. The resulting large scale barotropic field should carry over baroclinic PV. We can estimate the baroclinic PV to be

$$q' = k_0^{-1}(Uk_R^2)$$

and its flux to be

$$\overline{v'q'} \approx -D(Uk_R^2)\,,$$

where $D = V/k_0$ is the diffusion coefficient and V the barotropic rms velocity. Hence, the rate of energy production per unit mass is

$$\epsilon = -\frac{U_1\overline{v_1'q_1'} + U_2\overline{v_2'q_2'}}{2} \approx Vk_0^{-1}(Uk_R)^2\,.$$

The baroclinic vortex energy is generated at the wave number k_0 (where the barotropic energy resides), then transferred to small scales through the cascade process, and converted to barotropic energy in the vicinity of k_R. The cascade is halted at k_R, as all larger k are barotropic (2D), so only enstrophy is allowed to cascade down.

The authors argue that the energy flux into the barotropic mode should be equilibrated by the production of baroclinic energy, hence

$$\epsilon \approx V^3 k_0$$

(one could dispute this claim, as it neglects the contribution of energy dissipation at small wave-numbers). This yields an estimate

$$V \approx \frac{U k_R}{k_0},$$

so the barotropic rms velocity far exceeds the vertical shear.

Another key assumption of Ref. [15] is the equality $k_0 = k_\beta^R$, which implies

$$\frac{V}{U} \approx \zeta, \quad k_0 \approx \frac{k_R}{\zeta}, \quad D = \frac{U\zeta^2}{k_R}.$$

The second of these predictions is supported by the numerical results of Ref. [13] (in Fig. 18), that exhibits a nearly linear dependence of the energy peak number on β.

The premises and estimates of the Held – Larichev theory were tested in numerical simulations with a model described in Ref. [14]. The domain of integration L was chosen so that

$$\frac{2\pi}{k_R} = \frac{L}{50},$$

is 50 times the smallest wave number. The bottom friction coefficient is taken as

$$\lambda = 0.16 U k_R$$

and varies according to the forcing amplitude U. The paper computes spectra of the squared barotropic component of the meridional velocity and the energy production rate ϵ, as functions of k. The maxima of the two spectra are well correlated with k_β^R, whose definition involves the meridional barotropic velocity. The energy and its production rate grow with ζ much faster than the predicted ζ^2 law (and come close to ζ^4). There are noticeable departures from the relation $k_0/k_R = \zeta$.

The authors attribute these departures to oversimplified barotropic dynamics, though we believe that there might be other reasons. Indeed, their arguments completely ignore the bottom friction. It tends, as we already observed, to suppress the upscale energy flux (in this case barotropic kinetic energy), hence it should change their estimates (the possible dependence of the turbulent statistics on the bottom friction is mentioned in Ref. [15]). Held and Larichev also claim that the development of a reliable theory for vortex amplitudes could be untenable because of a strong positive feedback between vortex fluxes and their sizes.

We summarize the basic results of this section. Many specific features and problems in two-layer models are due to complicated transfer processes (with two interacting modes) and different forcing mechanisms. Such systems possess outer scales, a highly anisotropic structure, and excite the baroclinic modes as a result of baroclinic instability. One could expect isotropization at small scales $k > k_R$, but large scales should be dominated by zonal-type spectra. Scales of the highest energy production rate are close and dynamically coupled to scales of the maximal kinetic energy; in this respect the qualitative picture of Held and Larichev grasps the essence of the process.

The Rhines scale in most cases gives reasonably good estimates of the vortex energy peak and the jet number of the flow, though different authors use different rms velocities. Nobody has so far studied two-layer geostrophic turbulence and its nonlinear transfer structure as comprehensively as quasi-2D turbulence in barotropic fluids on the beta plane [12] or on a sphere [91]. The main goal of such study is to determine whether the balance of two cascade processes — barotropic upscale transfer and baroclinic downscale transfer — could explain the structure of quasigeostrophic turbulence and its energy carrying scales.

6. Observational data and laboratory experiments

6.1 Observational data

The GASP experiment (Global Atmospheric Sampling Program) has conducted detailed measurements of the horizontal velocity spectra in the upper troposphere and lower stratosphere on scales ranging from 3000 km to several km. The results were reported in papers [119, 120]. They gave $k^{-5/3}$ spectra in the mesoscale range $10^{-5} - 10^{-3}$ rad/m, whereas in the range of small wave numbers $k < 10^{-5}$ rad/m the spectra had a slope of -3, see Fig. 16. More recent work [121] takes a lower altitude, and obtains spectra with the same slope $-5/3$ in the $10^{-5} - 10^{-3}$ range, but of somewhat lower amplitude. The slope steepens to $-9/4$ in the range $10^{-3} - 10^{-2}$ rad/m, and then flattens at even larger wave-numbers.

Paper [31] analyses commercial aircraft data, the MOZAIC database, confirming the $-5/3$ spectrum at small scales, and -3 at larger scales, consistent with the previous observations.

Paper [122] analyzes the TOGA COARE (Tropical Ocean Global Atmospheric Coupled Ocean-Atmosphere Response Experiment) data, which refer to the range from 1 km to 1000 km. The entire data set has a spectrum with a slope close to $-5/3$, but for subsets of the data the slope varies between $-5/3$ and -2. This work found no -3 slope (it corresponds to larger scales).

There have been several attempts to explain the observational results within the conventional paradigm of 2D-turbulence. The main difficulty results from the reversal of two spectral branches. The traditional interpretation of the -3 and $-5/3$ slopes, based on the inertial intervals of 2D turbulence, traces back to Refs [123, 124], see also Ref. [121]. Lilly suggested that the $5/3$ spectrum is due to the inverse energy cascade from the mesoscale convective source. Convective motions in the stratified atmosphere give rise to gravity waves and stratified turbulence. The latter should be almost two-dimensional (notice that the quasigeostrophic approximation is no longer valid at such scales, and rotation has negligible effect).

Stratified turbulence and the problem of the mesoscale spectra were discussed in two recent survey articles [125] and [126]. We forego the details but just point out that numerical experiments with narrow band forcing do show a tendency to quasi-two-dimensionalization. Spectral fluxes at small (horizontal) wave-numbers k become negative (inverse cascade), but the spectral slopes deviate strongly from $-5/3$, and the spectral energy peak comes close to the forcing scale. Papers

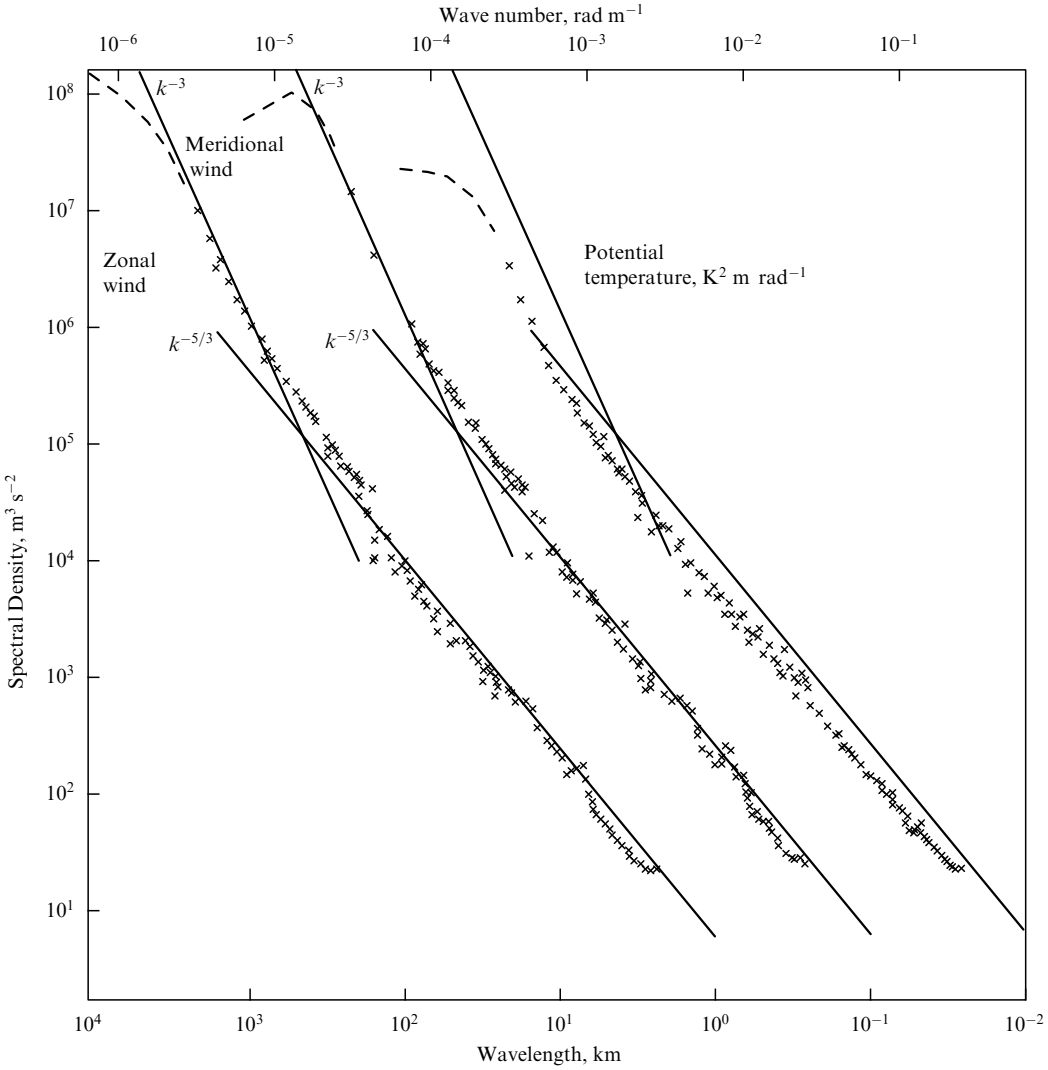

Figure 16. Spectra of the wind and potential temperature variance from GASP data [120]. The meridional wind and potential temperature spectra are shifted by one and two decades to the right.

that consider broad band forcing and take into account the physics of convective processes report spectra close to $-5/3$ ([127]).

Paper [120] suggests that the source of mesoscale turbulence could be the breakup of internal gravity waves.

The conventional -3 spectrum appears in the direct (enstrophy) range when the forcing scale exceeds the inner Rossby radius. Paper [128] points out that -3 and $-5/3$ branches of the spectrum can coexist if the system has two sources at large and small scales, even without energy and enstrophy sinks at intermediate scales. Maltrud and Vallis have obtained such a spectrum numerically [41].

A different viewpoint is presented in Ref. [27]. Its authors claim that a -3 spectrum could be explained in the framework of the inverse cascade damped by the bottom friction, but, as we mentioned earlier, these arguments are flawed.

All observational spectra, however, have serious flaws, as one computes them indirectly from the observed frequency spectra. So their slopes alone do not qualify such processes as 2D turbulence. In particular, to identify the $-5/3$ slope with the 'inverse cascade', one would need the energy fluxes, and hence, space realizations of the velocity field, or at least its third order structure function.

Besides, the two-dimensionality of the system, approximately valid at the lower end of the $5/3$-range (about 500 km), is completely lost at the upper end (kilometers to tens of kilometers). As for the large scales, a spectral slope of -3 does agree with the discussion of geostrophic turbulence in the previous section. Indeed, spectral slopes of the kinetic energy in Refs [15] (its Fig. 1) and [112] (Fig. 13 here) come close to this value.

The comparative analysis of Ref. [31] reaffirms such conclusions. This paper uses reanalysis of the experimental data to compute the structure functions. It takes advantage of the relations between longitudinal and transverse structure functions, which differ for 2D and 3D turbulence. The author concludes that the interval of large separations (-3 range) better agrees with two-dimensional dynamics than a smaller range does. Hence, the $k^{-5/3}$ spectrum should not be attributed to 2D-turbulence.

The paper also computes the third order structure function. These functions are reliably measured in the range 30 – 300 km and prove to be positive. Positivity indicates the presence of an inverse energy cascade, or at least of a significant two-dimensional contribution. Thus the $-5/3$ range should not also be attributed to purely 3D turbulence.

Stratified turbulence offers the best choice for describing the mesoscale atmospheric motions, but the persistence of a $-5/3$ slope for over 2 decades remains an open issue.

An important complement to observational data comes from spectral reanalysis of the data of weather forecasting centers. Paper [129] gives such spectra for February 1993, based on ECMWF data (European Centre for Medium-Range Forecasts); for January 1989, based on NMC (National Meteorological Center); and for January 1979, based on FGGE-3b experimental data. They show the spectral slope (of vertically integrated energy spectrum) in the range of spherical harmonics $10-30$ to be close to -3 for all three data sets.

For $n > 30$ the spectra diverge, due to the different spatial resolution in the three experiments. The spectral energy flux is positive for $n < 10$ and turns negative in the range $n = 10-30$, which means that such a range (of spectral slope -3) does not belong to the inverse cascade. The data were filtered by the T60 scheme and contained no wave numbers of the above $-5/3$ interval.

The analysis [130] for 14 winter seasons and 15 summer seasons of ECMWF data gave slopes $-(2.5-2.6)$ for the vertically averaged energy spectra in the range $n = 10-40$. Even in view of possible variability such a slope still differs substantially from the -3 of the preceding work. The authors didn't find the $-5/3$ range for large n.

They also find spectral fluxes for the energy and enstrophy. The energy flux is positive for $n = 3-10$, in the range of planetary waves, and negative in the synoptic range $10-40$. This once again would rather link the -3 range to the direct cascade. The authors point out that nonlocal interactions of planetary waves play a role in the enstrophy transfer, whereas more local interactions in the synoptic range are largely responsible for the energy transfer to large scales.

A simplified view of the large scale atmospheric motion as two-dimensional turbulence does not account for the vertical structure. The vertically averaged spectra sum the contributions of the barotropic and baroclinic modes, and even this fact taken alone could bring about an uncertainty of slopes. The aircraft data would rather be related to the energy spectra at the flight altitude than characterize the atmosphere as a whole.

6.2 Laboratory experiments

There are few laboratory experiments on 2D turbulence. The early works surveyed in Ref. [131] are mostly qualitative. The recent ones are discussed in Ref. [21].

Here we shall briefly review the quantitative results and describe the laboratory techniques reproducing 2D fluid motion. One way, most natural from the geophysical standpoint, requires a rapidly rotating homogeneous fluid, with small Rossby number. Such fluid should move as a whole in Taylor columns, according to the Taylor–Proudman theorem. The stirring source may be arbitrary, but, as long as the Rossby number is small, the 3D effects will be confined to a thin Proudman–Stewartson layer, with the bulk remaining two-dimensional. The fluid can be stirred by a combination of sources and sinks [83, 132]. Weak ageostrophic currents created by sources and sinks and enhanced by the Coriolis force would grow into strong geostrophic vortex motion. Its instabilities, in turn, would give rise to complex vortex patterns associated with 2D turbulence.

A rotating fluid in a cylindrical channel can be heated on one side and cooled on the other, as in the experiments by Hide and Mason [133]. This can represent the stirring mechanism of the global circulation. Heating creates inclined isopicnal surfaces, and the resulting baroclinic instability for a sufficiently strong temperature contrast can stir turbulent motions.

For conducting fluids a strong vertical magnetic field would have the same effect as rotation has. The vortex motion could then be excited by electric currents produced by a system of electrodes of alternating polarity [84]. The resulting regular vortex lattice could lose stability past the critical current value and would create a two-dimensional flow with a complex spatial-temporal pattern.

The simplest means of 'two-dimensionalization' is using a thin layer of fluid. If typical horizontal scales of motion are much larger than the thickness, and the motions are slow compared to the speed of surface waves, the vertical velocities remain small, and the motion is quasi-two-dimensional. Such flows are typically generated by magneto-hydrodynamic (MHD) sources.

A weak electrolytic fluid is poured into a container over a checkerboard array of magnets of opposite polarity. The electric current through such a fluid would create vortex motion, generated by the Ampere force (see, for instance, Ref. [82]). As the current through the electrolyte is increased, the primary flow becomes unstable. The tracer plot of Fig. 17 gives an example of the complicated spatial organization of the flow in such experiments.

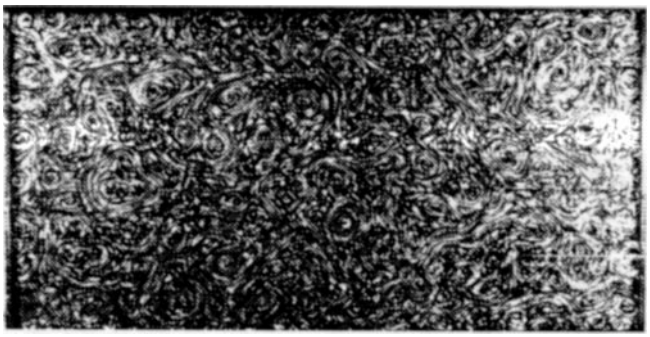

Figure 17. Streak photograph of an MDH induced flow in a thin layer. The magnetic configuration corresponds to a lattice of 8×8 elliptical vortices of $2:1$ eccentricity. The resulting non-stationary flow is due to instability of the basic flow.

Let us remark that all experimental quasi-2D systems have bottom friction. For a rotating fluid it manifests itself via the formation of an Ekman boundary layer at the bottom of the tank. For MHD experiments in electro-conducting fluids the friction is due to the Hartmann boundary layer. Finally, experiments with thin fluid layers create a quasi-Poiseuille vertical profile, hence

$$\nu \partial_{zz}\mathbf{u} \sim -\lambda \mathbf{u}\,,$$

where $\lambda = \nu\varkappa/H_0^2$ with parameter $\varkappa = O(1)$. Clearly, in this case we are dealing with a parametrization that grasps the essence of bottom influence on dissipation.

Another type of experiment involves soap films between two wires under the force of gravity. Such flows are clearly quasi-two-dimensional, as the film thickness is only several microns, and the surrounding air subjects such flows to frictional dissipation. Assuming friction to be proportional

to the flow velocity, we come to the same quasi-two-dimensional setup as above.

Papers [136 – 143] run experiments with decaying turbulence, while [30, 84, 144 – 151] do the same for forced turbulence.

Paper [136] exploits a technique of MHD generation. A strong electric current runs through the fluid during a short period, after which the decay of the flow is studied. The horizontal size of a single magnet is 8×5 mm^2, the layer thickness $H_0 = 3$ mm. The apparatus has 14×13 magnets, which can create the same number of vortices. The flow is visualized with tracer particles, and velocities are measured by correlating subsequent video-snapshots. The space resolution of the measured velocity is 32×32 grid points, which can be tracked over time.

The initial state with 100 vortices gives the following relation between energy and enstrophy:

$$\frac{\Omega}{E} \approx t^{-0.44 \pm 0.06},$$

after a few seconds. This law departs from the Batchelor theory [4] that predicts enstrophy decaying as t^{-2}, but is close to the numerical results of Ref. [70]. However, according to Ref. [70], the area occupied by vortices should decrease with time, whereas experiments [136] show them densely filling the entire region. The authors conclude that decay turbulence does not follow either of the two scenarios.

The departure from theoretical predictions is hardly surprising, as the assumptions of either theory do not hold in the experiment. Thus energy is conserved in the theory, but decays exponentially in experiments with time constant 2.3 s. The latter comes close to the bottom friction time,

$$\frac{1}{2\lambda} \approx \frac{H_0^2}{4\nu},$$

of about 2.2 s.

The paper does not examine the relative role of nonlinear terms responsible for the transfer, compared to that of dissipation. So one couldn't say to what extent it reproduces the turbulent regime, or a viscous decay process (which combines standard viscosity and bottom friction). Here the geometry and physical size makes standard viscosity comparable to the bottom friction at the forcing scale: the estimated viscous time $(2\nu k_f^2)^{-1}$ gives 1.6 s, close to but somewhat lower than the friction time. Since the forcing scale components decay rapidly, the flow should be largely controlled by dissipation.

The kurtosis in Ref. [136] remained close to the initial value 3 (as expected for Gaussian fields) over the entire evolution. This differs markedly from the numeric experiments with decaying turbulence, where the typical vorticity kurtosis may exceed several dozens, after attaining maximal enstrophy dissipation, which signals the appearance of strong vortices on an otherwise (statistically) uniform background.

Experiments [138] also deal with the decay laws and vortex statistics of 2D turbulence, and are similar to the experiments in Ref. [136]. Ref. [138] claims that the improved methodology (using a two-layer fluid with a small density drop between the layers) and a different interpretation of the results yield complete agreement with theoretical results of Ref. [70]. This refers to the decay laws for the number of vortices, their separation and their mean size. A new interpretation requires a change of variables in the vorticity equation,

$$\zeta^* = \zeta \exp(\lambda t)$$

and a time change to

$$t^* = \lambda^{-1}\left(1 - \exp(-\lambda t)\right).$$

The new variables eliminate the friction term and change the infinite time range into a finite interval. The viscosity coefficient would now grow exponentially

$$\partial_t \zeta^* + [\psi^*, \zeta^*] = \nu^* \Delta \zeta^*, \qquad \nu^* = \nu \exp(\lambda t).$$

The authors of Ref. [138] suggest that the change of viscosity is not essential, so one could regard the flow as a standard 2D flow. Then one should compare the theoretical predictions with experimental data in new variables. As the Reynolds number is close to that of Ref. [136], the new interpretation maintains the relation between nonlinear transfers and dissipation, but changes the time dependence.

Let us point out, however, that the decay laws of two-dimensional turbulence are sensitive to the short-wave dissipation. The decay laws of Ref. [70] are derived for a special hyperviscous case, and differ significantly from the laws observed for standard viscosity. For this reason any agreement of the results of Refs [138] and [70] should not be considered universal.

Another uncertainty stems from the procedure of separation of experimental flows into the background and vortices. Unlike numerical turbulence, where local vorticity extrema can exceed rms several times, the experiments show a marginal difference.

Paper [139] considers the 2D turbulence in a soap film between two vertical wires. The wires are 180 cm long, 5 cm apart. They start at the bottom of a reservoir of soap mixture, leaking through a 0.02 cm wide slit. The flow velocity in the film could vary from 20 cm s^{-1} to 4 m s^{-1}. Two methods were used to measure velocity: homodyne photon correlation spectroscopy and fiber anemometry. We shall discuss the results obtained with the latter technique.

The turbulence is stirred by a horizontal comb of 3(1) mm grid separation, and the flow is measured 4(1) cm downstream from the grid. Taylor's hypothesis allows one to convert the frequency spectra of vertical and horizontal velocity into spatial (Fourier) spectra. Both spectra are nearly identical in the frequency range 100 to 1000 Hz (meaning isotropy), and have slopes of -3.3 (-3.6). This frequency range corresponds to scales of 2 – 0.2 cm (for 2 m s^{-1} velocity).

In the frequency range 20 – 100 Hz the isotropy is broken, but the spectra become shallower, with a slope of approximately -2. The authors interpret the high frequency spectra as enstrophy cascade. Since turbulence in such experiments evolves downstream, one can expect the integral scale (the flow velocity over the frequency of spectral peak) to grow linearly along the flow, as in Batchelor turbulence [4], where the vortex sizes grow linearly in time.

The latter was indeed shown in paper [140]. The experimental setup is similar to that of the preceding work, but the velocity field is measured with the two-component laser Doppler velocimeter at different downstream locations. The spectral slopes of the high frequency part (where the signal level exceeds the noise) are approximately -3.3. The linear growth of the integral scale downstream, however, goes along with a decreased in the kinetic energy density, due to the air

friction. The authors show that lowering the air pressure could yield a substantial reduction of the dissipation, but the spectral shape and the integral scale law do not change.

Soap films are not strictly two-dimensional systems, since their thickness can change. Thus experiments [141] estimate the change of thickness to be such that the mean divergence makes up 10–20% of the mean vorticity. These experiments use a setup similar to that of two preceding works: a 120 cm long channel with 6 cm distance between wires, and a mean flow velocity of 1.05 m s^{-1}. The turbulent velocity fluctuations were measured by the digital video-imaging system that resolves 60×60 grid points on a 1.5 cm $\times$ 1.5 cm square of the film. The paper shows that the change of thickness is correlated with the vorticity of the flow (a shallow water type behavior), but the surface tension introduces some specific features.

The authors of [141] measured the laws of decay of thickness fluctuations, divergence squared and enstrophy downstream. The latter two quantities have the same decay rate, which goes faster than the energy decay. Since the energy decay here is due to the air friction, one could not associate it with any known decay theory.

The relatively high divergence makes soap film experiments less valuable from the standpoint of two-dimensional turbulence. Nevertheless, one can expect many qualitative characteristics to be maintained by such a system. The paper studies second order structure functions of vorticity and longitudinal velocity, as well as the 3rd order structure functions

$$S_{v\zeta\zeta} = \left\langle \delta v_L (\delta\zeta)^2 \right\rangle .$$

The latter obeys an exact relation in the enstrophy interval,

$$\left\langle \delta v_L (\delta\zeta)^2 \right\rangle = -2\eta r ,$$

obtained similarly to (9). The measured structure function $S_{v\zeta\zeta}$ does have a range (about a decade long) where the theoretical relation holds (over the scale range from fractions of mm to 1 cm). The measurements were taken 5 cm downstream, and the grid had 2.7 mm combs spaced 3 mm apart.

The second order structure function of vorticity had a slope of 0.4, consistent with the energy slope steeper than -3 for the other soap experiments. But the velocity structure function had a slope of 1.6, which should give an energy spectral slope of -2.6. The reason for such a wide gap may be the limited enstrophy interval.

Another work [142], which ran similar experiments (wire length 120 cm, distance 6.2 cm, mean velocity 1.8 m s^{-1} with laser Doppler velocimetry), also reported a slope of 1.6 for the second structure function in the enstrophy interval. The velocity measurements show a spectral range with a slope of -3.3, which also agrees with the previous results. The measured third order structure function gave negative values for small separation, as one could expect in the enstrophy range, but as r grows, it becomes positive, in agreement with the 3/2 law for the 2D turbulence. This suggests an inverse energy cascade.

The paper raises the question of verifying the relation between the second and third structure functions for 2D turbulence [a consequence of (7)]. This question can be answered only qualitatively, since one studies the decaying system and needs estimates of time derivatives (let alone the outer dissipation).

Paper [143] also discussed the structure function $S_{v\zeta\zeta}$. It showed the experimentally measured ratio $S_{v\zeta\zeta}/r$ to have a plateau region, and thus confirmed the preceding work. The paper also measures the PDF of $S_{v\zeta\zeta}$, and finds a large departure from the Gaussian distribution. The measurements were conducted with two fiber anemometers, and the experimental setup was similar to those in other experiments.

The numerical work [152] models turbulent experiments on soap films. It studies a 2D flow behind a grid with cylindrical combs, and finds a value of -3.7 for the spectral slope and a slope of 2 for the second structure function of longitudinal velocities, which gradually becomes 1.6 as the separation r grows. The structure functions of vorticity have slopes close to their order n for $n = 2, 4$.

If turbulence evolves in the absence of forcing and dissipation, one can apply the methods of statistical mechanics (cf. Refs [7, 153, 154]), which predict a functional dependence between the (mean) stream-field and vorticity. Paper [137] made an attempt to check the prediction of the statistical theories, using the experimental apparatus of Ref. [136]. The authors conclude that the real evolution does not follow the prescriptions of either statistical theory, nor 'selective dissipation', nor 'minimum enstrophy'. However, the paper does not examine the relation between the energy dissipation and energy transfer, so strictly speaking one cannot claim the system to be in a turbulent state.

Paper [155] observes that the evolution driven by viscous dissipation alone can look similar to the evolution of 2D turbulence flow, since it is also accompanied by a growth of vortex size.

We now turn to forced turbulence. Paper [84] carried out measurements in thin layers of mercury in an external magnetic field. Vortex motion was created by 36 electrodes of alternating polarity at the bottom of the tank. The velocity field was measured at 11 points along a line. Hence, the author detects only one-dimensional spectra of the transverse velocity, but argues that spectral slopes of the 1D spectra should be close to the wave number spectra (assuming isotropic velocities). These spectra contain an interval of nearly $-5/3$ slope, but it does not extend beyond half a decade. The paper also discussed how the spectrum varies with the level of supercriticality. It showed that the energy transfer to large scale is limited by the bottom drag, and the energy peak scale grows higher with increasing Reynolds number.

The turbulence is stirred at the wave vector $(6, 6)$ (a sine decomposition is used, so wave numbers characterize the numbers of vortices along each coordinate), and a Reynolds number $\mathrm{Re}_\lambda \approx 20$ drives the energy peak to the system size. Unfortunately, the data on the $k_{\max}$ dependence of the Reynolds number are incomplete, and involve only one-dimensional spectra.

Paper [144] studies turbulent motion that results from the baroclinic instability of the frontal upwelling. The motion is produced by the surface stress applied to a two-layer fluid in a cylindrical rotating vessel. Because of special techniques of stirring, turbulence is most likely quasigeostrophic. The paper does not discuss the vertical penetration of stirring and whether it creates a quasi-two-dimensional flow. The velocities were recovered by streak photographs of tracers on the fluid surface, where the resolution was from 1 cm to 90 cm (outer diameter). The paper applies several techniques to process the streak photographs to get velocity spectra. The first one attempts to recover spectral slopes from the particle

dispersion. It overestimates slopes and gives a value below -2.5.

The second one computes two-dimensional Fourier spectra for velocities interpolated on a regular grid. The third method computes a one dimensional Fourier transform of the correlation function for longitudinal velocity. The second and third methods give consistent results. For the 2D Fourier transform one interpolates the velocity field on a regular 32×32 grid. The main results of the paper are the $-5/3$ spectrum for small k, and the slope -5.5 for large wave numbers. The spatial resolution, however, is too limited to draw broad conclusions.

Paper [145] applies the source-and-sink stirring mechanism for stratified rotating flow. The alternating sources and sinks are placed on a ring of inner diameter 563 mm, suspended horizontally inside the fluid layer, 445 mm deep. The rotating fluid experiments use 8 pairs of sources and sinks, with diameter 4 mm. The authors measure velocity, using the DigImage tracking system, which allows up to 2000 particles to be followed in a given horizontal cross-section with frequency 6.25 Hz.

The paper studies the evolution of turbulence from the rest state, and claims that the Rossby radius based on the total fluid depth should halt the inverse energy cascade, provided the initial vortex scale is below the Rossby radius. As vortices grow to the Rossby scale, they also extend vertically, so one observes the effective barotropization of the large-scale flow. But this also brings in the bottom friction. The latter could also favor the arrest of the inverse cascade at the Rossby scale. This could serve as a possible explanation for the absence of transfer beyond the Rossby scale, which one could expect based on geostrophic turbulence theory.

The forced turbulence of Refs [146, 147] is stirred by the baroclinic instability in the cylindrical channel and the cylindrical tank respectively. The fluid is cooled at the outer wall and heated from inside. The inclined bottom in both cases models the beta-effect. The energy spectra are computed for the horizontal cross-section of velocity. The results of both works show that the energy peak may exceed the Rhines scale in the case of a negative beta-slope or coincide with it for positive beta-slope. The short-wave component decays more steeply than k^{-3}, and there are some indications of the $-5/3$ slope at large scales, which, however, are larger than the Rhines scale.

The Rossby deformation radius is small in all cases, and falls within the limits of resolution. Hence, one could expect a $k^{-5/3}$ spectrum all way until the Rhines scale, but this was not observed. Again, we have to note the limited spectral resolution: 6 for the maximal radial wave-number, and 15 for azimuthal one. In such a case one can discuss spectral slopes only qualitatively.

Papers [148] and [30] give by far the most complete measured characteristics of the forced quasi-2D turbulence in the inverse cascade range. Paper [30] considers a turbulent flow stirred by the MHD method in a thin layer of weak electrolyte. The system has a size 15×15 cm, and a forcing scale of 15 mm (determined by the size of magnets). The electric current has constant amplitude, but random phases, unlike other MHD experiments, where the current was kept steady. The velocity field is estimated on a 64×64 grid. The paper considers two cases. In the first case the thin fluid layer (5.5 mm) creates large bottom friction, so the experimental wave-number spectrum in suppressed at large scales. The spectrum contains an interval of $-5/3$ slope, but its extent, being the largest for all known measurements, is nevertheless shorter than a decade.

The second experiment deals with a deeper fluid layer, so bottom friction cannot arrest the inverse cascade to large scales. This implies, however, that the observed spectra strongly depend on the system size and geometry.

Figure 18 gives simultaneous views of the energy spectrum and spectral energy flux. Their comparison shows a region of spectral slope close to $-5/3$, where the spectral flux goes practically to zero. This decay is caused by the bottom friction and confirms the numerical results [11]. In both cases the $-5/3$ spectrum extends further into the infrared region than could be expected from the nonuniform energy flux. The measured flux [30] never remains uniform and decays monotonically to 0 as $k \to 0$.

Experimental work [30] not only includes spectral measurements but also analyses structure functions of different orders for the longitudinal and transverse velocity components. The Kolmogorov turbulence in the inertial interval should obey the law

$$\langle \delta v^p \rangle \sim \varepsilon^{p/3} r^{p/3} .$$

The even structure functions of the transverse component measured in Ref. [30] have a power dependence on the separation distance only within a narrow range, because of the suppression of the inverse cascade.

It turns out that the theory of extended self-similarity (ESS) can give better predictions:

$$\left\langle |\delta v_l|^p \right\rangle \sim \left\langle |\delta v_l|^s \right\rangle^{\zeta_p/\zeta_s} .$$

One expects the relative exponent ζ_p/ζ_s to be scale independent in situations where absolute exponents are not.

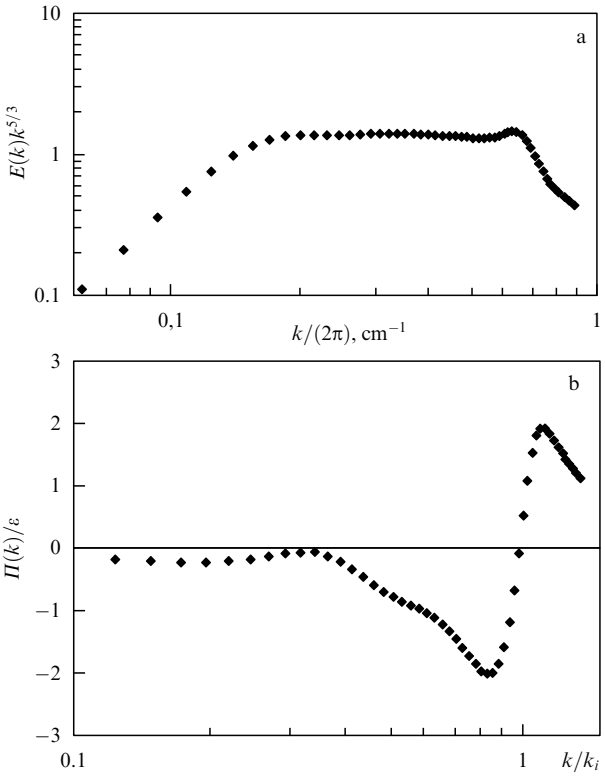

Figure 18. Energy spectrum of stationary quasi-two-dimensional flow (a), and its energy flux (b) from the MHD experiments in a thin layer [30].

As we have already mentioned, Ref. [33] shows the third moment $\langle \delta v^3 \rangle$ to play the foremost role here; in particular, the relative exponents ζ_p/ζ_3 for even low order moments remain constant over a broad range of scales.

Laboratory experiments [30] demonstrate a similar feature. Furthermore, the relative exponents for the longitudinal structure functions are close to the Kolmogorov values up to $p = 12$, while the normalized even functions remain nearly Gaussian. This work didn't measure the relative exponents of the transverse velocities, but found the even function to be also close to Gaussian values.

All this implies that intermittency is practically absent in an inverse cascade, and velocity fields have Gaussian statistics (cf. Ref. [27]). Paper [30], however, points out small departures from Gaussianity, in particular, a weak but detectable asymmetry of the PDF for the transverse velocity increments. Without it, there would be no inverse cascade.

The authors of Ref. [30] also consider the distribution of vortex sizes, most of which belong to the forcing scale, with a handful spread in the inertial interval. Vortex merging is rare, and the principal mechanism of energy transfer to large scales is aggregation (clustering) of like-sign vortices. This process is observed at the initial stage of numerical experiments.

Paper [149] studies 3 realizations of MHD induced quasi-2D flows. The forcing scale is 1/8 of the system size, the magnetic field is weaker than in the previous experiments, but the electric current is stronger, 1, 3, and 9 A. The supercriticality defined as the ratio of the Reynolds number to its critical value (associated with the loss of stability) corresponds here to 9, 30 and 90. The velocity field is reconstructed via digital processing of streak photographs. Each picture contains roughly 15000 tracks, and the velocity field is recovered on a 256×128 grid. The energy spectra and fluxes based on the realizations show the arrest of the cascade at large scales — both the spectral density and flux go to 0 as $k \to 0$. Once again we see the effect of bottom friction. But the $-5/3$ region is absent here, as the supercriticality remains relatively low.

The experiments in Ref. [150] dealt with the energy spectra and statistics of vorticity in the enstrophy interval. They used the same experimental setup as in Ref. [30], but changed the distribution of magnets. The square region was divided into diagonal sectors, filled with randomly distributed magnets of like polarity, and opposite sectors had like polarities.

Thus the forcing has the scale of the entire system. The velocities are reconstructed on a 64×64 grid, as in [30], and have a spatial resolution of 2.5 mm. The authors estimate the error to be several percent for velocity and about 10% for vorticity. The electric current consists of pulses of changing polarity with zero mean.

The energy spectra based on 200 realizations contain a -3 interval, shown in Fig. 19, which is shorter than a decade. The vorticity flatness comes close to the Gaussian value 3, which means the absence of vortex structures. The inset to Fig. 19 shows the measured enstrophy flux, which is highly intermittent and attains its maximum far away from the forcing scale.

The flux is everywhere positive, which implies a direct cascade of enstrophy to large wave numbers. But its nonuniform shape precludes the presence of an inertial enstrophy interval. To compute η the authors average the flux over the interval between the forcing scale and the maximal wave number. This yields an estimate of the Batchelor – Kraichnan constant $C \approx 1.4 \pm 0.3$, close to that reported in Ref. [48]. The

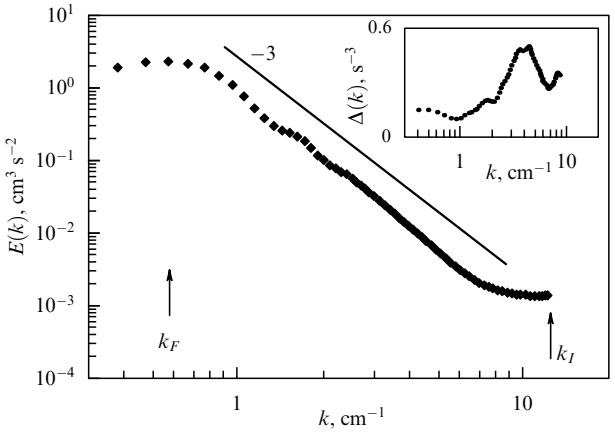

Figure 19. Energy spectra of the stationary quasi-two-dimensional flow in the enstrophy range. The inset shows enstrophy flux [150].

latter study computes the enstrophy cascade (nearly constant), and the agreement between the two results seems somewhat surprising.

Paper [150] reports the measured PDF of the vorticity difference for several separations, corresponding to the k^{-3} range. It has non-Gaussian tails. It also reports the experimental data for the even structure functions of vorticity $\langle \delta\zeta^p \rangle$ with $p = 2, 4, 6, 8, 10$. Although they change with distance, the corresponding exponents are small (between -0.05 and 0.15), close to zero within experimental error. The logarithmic correction (which appears at $p = 2$ for the same reason as for the velocity structure functions) cannot be reliably verified.

The constant values of structure functions mean that the corrections for intermittency should be small in the cascade range, in agreement with Ref. [32], which finds intermittency to be weak in the enstrophy interval. But the non-uniform enstrophy flux in Ref. [150] does not allow the results of the paper to be regarded as universal.

As we mentioned earlier, high space resolution (like 4096^2 in Refs [48, 60]) with hyperviscosity yields spectra close to -3 in the enstrophy interval. But neither property refers to experiments [150]. The authors do not give the power spectrum of the source. Its slope could also affect the energy slope.

Experiment [151] with soap films places the grid either vertically or at some angle to the vertical, as shown schematically in Fig. 20. The authors use, as in Ref. [140], a two-component laser Doppler velocimeter to measure velocity. The power spectrum of horizontal velocity, A in Fig. 20a, is measured between two combs that stir the flow. This spectrum has a short $-5/3$ interval, and its maximum corresponds to the wavelength λ related to the largest scale structures. As the measuring window is displaced downflow, the spectrum is transformed to that of decaying turbulence. The $-5/3$ interval disappears, and only -3 remains.

The energy peak moves to smaller k, and its amplitude decreases due to friction. The power spectra of vertical velocity on Fig. 20b show the tendency of changes in what could be called the forcing scale (on the borderline between different slopes), as the measurement point is displaced from the comb.

We thus see that modern laboratory techniques make possible quantitative studies of spectral and other characteristics of quasi-2D turbulent flows. Some experimental results

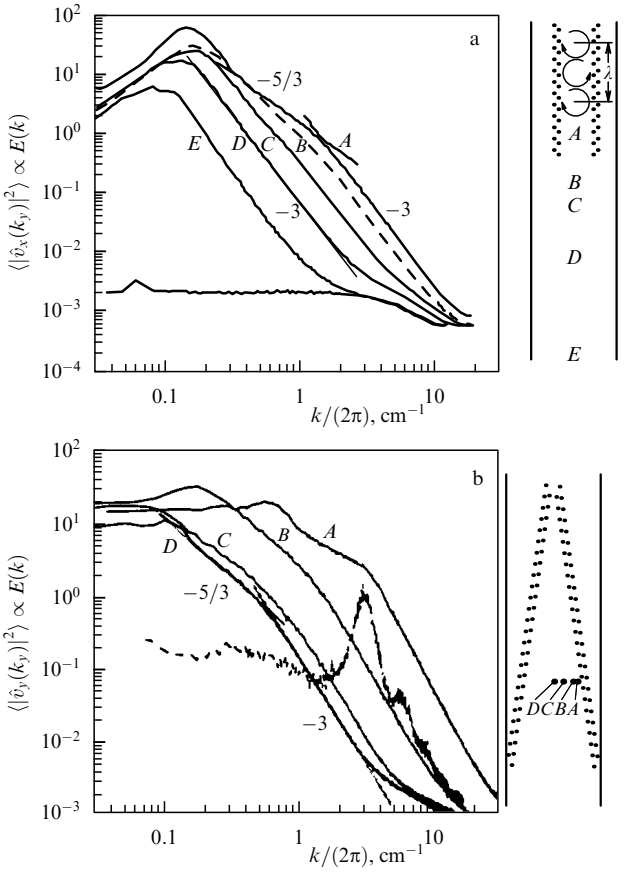

Figure 20. (a) Power spectra of the horizontal velocity. The lower curve shows the noise level. The film width is 8 cm, the combs are 2.5 cm apart, and the coordinates relative to the ends of combs are 5, −5, −10, −20, −40 cm. (b) Power spectra of the vertical velocity. The dashed curve shows the spectrum due to a single comb tooth, 2 cm down the flow. The distance between combs is 2 cm on top, 7 cm at the bottom [151].

show good agreement with the theory. This primarily concerns spectral slopes, the signs of (energy, enstrophy) spectral fluxes, and the role of bottom friction. Despite all this, they are far from providing test tools for verifying theoretical predictions. No experiment has so far managed to reproduce constant spectral fluxes of energy and enstrophy.

This is largely due to a limited spatial resolution. Even the latest experiments yielded the minimal (maximal) scale and the forcing scale differing by only one order of magnitude. Experimental flows are often far away from the idealized numerical experiments and have additional features hard to analyze.

In particular, experiments with MHD-driven thin layers of weak electrolyte are two-dimensional only in the sense that the velocity is nearly horizontal. But the velocity can change with depth (being zero at the bottom), and its vertical profile is a complicated function of 3 space coordinates and time. The latter means that the bottom friction $\nu\partial^2\mathbf{v}/\partial z^2$ in nonstationary flows can be parametrized by the Rayleigh friction only in a qualitative sense (the profile does not relax to a Poiseuille state). Meanwhile, it is bottom friction that provides the energy sink in Ref. [30] and the enstrophy sink in Ref. [150], where the most extensive measurements are presented. Such friction is not used in numerical studies.

7. Conclusions

Even strictly two-dimensional turbulence, though additional dissipation at both spectral ends (viscous at the ultraviolet end and frictional at the infrared end) frequently makes its two-dimensionality imperfect, departs from the conventional cascade theory based on the notion of inertial intervals (for energy and enstrophy). The main reason for this in the short-wave part of the spectrum is the nonlocality of interactions, with at least one leg of a typical triad sitting at the forcing scale. Such systems retain memory of the source (and/or outer parameters and processes) at small scales, and strictly speaking, invalidate the idea of the inertial interval, because the spectral fluxes depend on both local and external characteristics.

Sufficient spectral resolution could bring system to the ideal (theoretical) state, and produce slopes close to -3 for sufficiently large k. This happens since the small scale vorticity behaves as a passive tracer driven by the large (forcing scale) eddies (the enstrophy flux is determined by such large eddies).

The energy spectrum in the energy interval is typically close to $k^{-5/3}$, but this spectrum also exhibits deviations from the standard phenomenology due to large-scale dissipation. The classical $-5/3$ slope could be restored by artificial means — careful tuning of the long wave dissipation [62], which would eliminate the backscatter.

The natural dissipation via Ekman (bottom) drag could give spectra close to $-5/3$ over a limited range, but energy spectral flux would still decay within the $-5/3$ range. On the contrary, scale selective friction at small k could produce a nearly uniform spectral flux (well into the infrared region), but the resulting spectra would strongly deviate from the ideal $-5/3$ law (to a slope of -3, reported in Ref. [44]).

Such systems typically develop strong coherent vortices, whose growth can modify the 2D turbulent dynamics and spectra. Localized vortices also appear in the $-5/3$ case, but remain mostly at the forcing scale. Also, the $-5/3$ turbulent field was found to be almost Gaussian in recent experiments.

Strictly two-dimensional turbulence is of only limited use for geophysical applications, since bottom friction, the beta-effect, and vertical stratification can modify it significantly. Bottom friction reduces the energy flux to large scales, and thus sets the outer scale for the 2D turbulence.

The beta-effect separates small scale isotropic turbulence from highly anisotropic jet-structures, oriented in the zonal direction and controlled by the Rhines scale. The conventional view of the Rhines scale as separating isotropic turbulence from Rossby waves is however flawed, since waves are absent from the spectral region predicted by qualitative arguments of Rhines.

The Rhines scale arrests the inverse cascade in decay turbulence [54], but in stationary (forced) turbulence this can be achieved only by infrared dissipation. The same applies to the Rossby – Obukhov radius. It halts the inverse cascade of decay turbulence [54], but the stationary case also requires dissipation. In barotropic problems, the large-scale dissipation comes through the bottom friction. But its role in organizing the outer scales in the presence of the beta-effect and at a finite Rossby – Obukhov radius has not been explored.

The situation becomes increasingly complicated for simple layered baroclinic models. The energy source here comes from the baroclinic instability, and on scales larger

than or equal to the inner Rossby radius (800 – 1000 km for the atmosphere and 40 – 50 km for the ocean). The energy transfer via barotropic and baroclinic modes proceeds in opposite directions. Most papers observed the energy peak above the Rossby scale, which agrees well with the Rhines scale.

The problem of rms vorticity and its dependence on the source lies at the heart of the Rhines theory, but we have no conclusive answer at the moment. We believe such estimates should include the bottom drag and radiative cooling to provide for the proper energy sink. Otherwise (i.e. in a dissipation-free system) one should not expect a reliable outer scale.

Laboratory experiments on two-dimensional turbulence are few in number and have limited spatial resolution. But recent progress in the video-imaging technology gives hope of achieving higher resolution.

This work was sponsored by the GTP program at NCAR. The authors thank J Herring and V Gryanik for stimulating discussions, valuable comments and references to literature. We are especially indebted to F V Dolzhanskiĭ, who stimulated our interest in the topic. The first author was supported by RFBR grants (99-05-64350, 99-05-64351) and an NRC COBASE grant.

References

1. Kraichnan R H *Phys. Fluids* **10** 1417 (1967)
2. Kraichnan R H *J. Fluid Mech.* **47** 525 (1971)
3. Leith C E *Phys. Fluids* **11** 671 (1968)
4. Batchelor G K *Phys. Fluids Suppl. II* **12** 233 (1969)
5. Pedlosky J *Geophysical Fluid Dynamics* 2nd ed. (New York: Springer-Verlag, 1979) [Translated into Russian (Moscow: Mir, 1984)]
6. Monin A S *Theoretical Geophysical Fluid Dynamics* (Dordrecht: Kluwer Academic Publishers, 1990)
7. Salmon R *Lectures on Geophysical Fluid Dynamics* (New York: Oxford University Press, 1998)
8. Rhines P B *J. Fluid Mech.* **69** 417 (1975)
9. Lilly D K *Geophys. Fluid Dyn.* **3** 289 (1972)
10. Manin D Yu *Izv. Akad. Nauk SSSR Fiz. Atmos. Okeana* **26** 579 (1990)
11. Danilov S D, Dolzhanskiĭ F V *Izv. Ross. Akad. Nauk Fiz. Atmos. Okeana* **34** (3) 293 (1998)
12. Vallis G K, Maltrud M E *J. Phys. Oceanogr.* **23** 1346 (1993)
13. Panetta R L *J. Atmos. Sci.* **50** 2073 (1993)
14. Larichev V D, Held I M *J. Phys. Oceanogr.* **25** 2285 (1995)
15. Held I M, Larichev V D *J. Atmos. Sci.* **53** 946 (1996)
16. Monin A S, Mirabel' A P *Usp. Mekh.* **2** (3) 47 (1979)
17. Rhines P B *Ann. Rev. Fluid Mech.* **11** 401 (1979)
18. Mirabel' A P, Monin A S *Izv. Akad. Nauk SSSR Fiz. Atmos. Okeana* **16** 1011 (1980)
19. Lesieur M *Turbulence in Fluids* 3d ed. (Dordrecht: Kluwer Acad. Publ., 1997)
20. Vallis G K, in *Nonlinear Phenomena in Atmospheric and Oceanic Sciences* (The IMA Volumes in Mathematics and Its Applications, Vol. 40, Eds G F Carnevale, R T Pierrehumbert) (New York: Springer-Verlag, 1992)
21. 2D *Turbulence. A Tentative Dictionary* (NATO ASI Series. Ser. B: Physics, Vol. 341, Eds P Tabeling, O Cardoso) (New York: Plenum Press, 1997)
22. Monin A S, Ozmidov R V *Okeanskaya Turbulentnost'* (Turbulence in the Ocean) (Leningrad: Gidrometeoizdat, 1981) [Translated into English (Dordrecht: D. Reidel Publ. Co., 1985)]
23. Fjørtoft R *Tellus* **5** 225 (1953)
24. Novikov E L *Izv. Akad. Nauk SSSR Fiz. Atmos. Okeana* **14** 668 (1978)
25. Oetzel K G, Vallis G K *Phys. Fluids* **9** 2991 (1997)
26. Smith L M, Yakhot V *Phys. Rev. Lett.* **71** 352 (1993)
27. Smith L M, Yakhot V *J. Fluid Mech.* **274** 115 (1994)
28. Orszag S A *J. Fluid Mech.* **41** 363 (1970)
29. Holloway G *Ann. Rev. Fluid Mech.* **18** 91 (1986)
30. Paret J, Tabeling P *Phys. Fluids* **10** 3126 (1998)
31. Lindborg E *J. Fluid Mech.* **388** 259 (1999)
32. Babiano A, Dubrulle B, Frick P *Phys. Rev. E* **52** 3719 (1995)
33. Babiano A, Dubrulle B, Frick P *Phys. Rev. E* **55** 2693 (1997)
34. Landau L D, Lifshitz E M *Fluid Mechanics* (Oxford: Pergamon Press, 1959)
35. Frisch U *Turbulence*: *The Legacy of A N Kolmogorov* (Cambridge: Cambridge University Press, 1995)
36. Kolmogorov A N *Dokl. Akad. Nauk SSSR* **32** 19 (1941)
37. Kolmogorov A N *Dokl. Akad. Nauk SSSR* **30** 299 (1941)
38. Babiano A, Basdevant C, Sadourny R *J. Atmos. Sci.* **42** 941 (1985)
39. Lilly D K *Phys. Fluids Suppl. II* **12** 240 (1969)
40. Lilly D K *J. Fluid Mech.* **45** 395 (1971)
41. Maltrud M E, Vallis G K *J. Fluid Mech.* **228** 321 (1991)
42. Cho J Y-K, Polvani L M *Phys. Fluids* **8** 1531 (1996)
43. Maltrud M E, Vallis G K *Phys. Fluids A* **5** 1760 (1993)
44. Borue V *Phys. Rev. Lett.* **72** 1475 (1994)
45. Kukharkin N N *J. Sci. Comput.* **10** 409 (1995)
46. Chekhlov A et al. *Phys. Fluids* **6** 2548 (1994)
47. Nozawa T, Yoden S *Phys. Fluids* **9** 2081 (1997)
48. Borue V *Phys. Rev. Lett.* **71** 3967 (1993)
49. Chekhlov A et al. *Physica D* **98** 321 (1996)
50. Chasnov R J *Phys. Fluids* **9** 171 (1997)
51. Legras B, Santangelo P, Benzi R *Europhys. Lett.* **5** 37 (1988)
52. Ohkitani K *Phys. Fluids A* **3** 1598 (1991)
53. Ohkitani K *Phys. Fluids A* **2** 1529 (1990)
54. McWilliams J C *J. Fluid Mech.* **146** 21 (1984)
55. Herring J, McWilliams J *J. Fluid Mech.* **153** 229 (1985)
56. McWilliams J C *Phys. Fluids A* **2** 547 (1990)
57. Lesieur M, Herring J R *J. Fluid Mech.* **161** 77 (1985)
58. Dubrulle B, Nazarenko S *Physica D* **110** 123 (1997)
59. Gotoh T *Phys. Rev. E* **57** 2984 (1998)
60. Lindborg E, Avelius K *Phys. Fluids* **12** 945 (2000)
61. Frish U, Sulem P L *Phys. Fluids* **8** 1921 (1984)
62. Sukoriansky S, Galperin B, Chekhlov A *Fhys. Fluids* **11** 3043 (1999)
63. Yakhot V *Phys. Rev. E* **60** 5544 (1999)
64. Boffetta G, Celani A, Vergassola M *Phys. Rev. E* **61** R29 (2000)
65. Fornberg B *J. Comput. Phys.* **25** 1 (1977)
66. Basdevant C et al. *J. Atmos. Sci.* **38** 2305 (1981)
67. Santangelo P, Benzi R, Legras B *Phys. Fluids A* **1** 1027 (1989)
68. Benzi R, Patarnello S, Santangelo P *J. Phys. A* **21** 1221 (1988)
69. McWilliams J C *J. Fluid Mech.* **219** 361 (1990)
70. Carnevale G F et al. *Phys. Rev. Lett.* **66** 2735 (1991)
71. Benzi R et al. *Phys. Fluids A* **4** 1036 (1992)
72. Weiss J B, McWilliams J C *Phys. Fluids A* **5** 608 (1993)
73. Matthaeus W H et al. *Phys. Rev. Lett.* **66** 2731 (1991)
74. Matthaeus W H et al. *Physica D* **51** 531 (1991)
75. Carnevale G F et al. *Phys. Fluids A* **4** 1314 (1992)
76. Dritschel D G *Phys. Fluids A* **5** 984 (1993)
77. Legras B, Dritschel D *J. Comput. Phys.* **104** 287 (1993)
78. Mariotti A, Legras B, Dritschel D G *Phys. Fluids* **6** 3954 (1994)
79. Bartello P, Warn T *J. Fluid Mech.* **326** 357 (1996)
80. Chasnov J R, Herring J R (in press)
81. Dolzhansky F V *Izv. Ross. Akad. Nauk Fiz. Atmos. Okeana* **35** (2) 163 (1999) [*Izv., Atm. Oceanic Phys.* **35** 147 (1999)]
82. Dolzhanskiĭ F V, Krymov V A, Manin D Yu *Usp. Fiz. Nauk* **160** (7) 1 (1990) [*Sov. Phys. Usp.* **33** 495 (1990)]
83. Colin de Verdiere A *Geophys. Astrophys. Fluid Dyn.* **15** 213 (1980)
84. Sommeria J *J. Fluid Mech.* **170** 139 (1986)
85. Hopfinger E J, Griffiths R W, Mory M *J. Mech. Theor. Appl.* (Numéro Special) **2** 21 (1983)
86. Dolzhanskii F V, Manin D Yu *Geophys. Astrophys. Fluid Dyn.* **72** 93 (1993)
87. Danilov S D, Dolzhanskii F V, Krymov V A *Chaos* **4** (2) 299 (1994)
88. Holloway G, Hendershott M *J. Fluid Mech.* **82** 747 (1977)
89. Kamenkovich V M, Koshlyakov M N, Monin A S *Sinopticheskie Vikhri v Okeane* (Synoptic Eddies in the Ocean) (Leningrad: Gidrometeoizdat, 1982) [Translated into English (Dordtrecht: D. Reidel Publ. Co., 1986)]
90. Williams G P *J. Atmos. Sci.* **35** 1399 (1978)
91. Huang H-P, Robinson W A *J. Atmos. Sci.* **55** 611 (1998)
92. Yoden S, Yamada M *J. Atmos. Sci.* **50** 631 (1993)

93. Larichev V D, McWilliams J C *Phys. Fluids A* **3** 938 (1991)
94. Kukharkin N, Orszag S A, Yakhot V *Phys. Rev. Lett.* **75** 2486 (1995)
95. Farge M, Sadorny R *J. Fluid Mech.* **206** 433 (1989)
96. McWilliams J C *Phys. Fluids* **10** 3178 (1998)
97. Yuan L, Hamilton K *J. Fluid Mech.* **280** 369 (1994)
98. Polvani L M et al. *Chaos* **4** (2) 177 (1994)
99. Arai M, Yamagata T *Chaos* **4** 163 (1994)
100. Ford R *Phys. Fluids* **6** 3694 (1993)
101. Charney J G *J. Atmos. Sci.* **28** 1087 (1971)
102. Herring J R *J. Atmos. Sci.* **37** 969 (1980)
103. Hua B L, Haidvogel D B *J. Atmos. Sci.* **43** 2923 (1986)
104. McWilliams J C, Weiss J B *Chaos* **4** 305 (1994)
105. McWilliams J C *J. Fluid Mech.* **219** 387 (1990)
106. McWilliams J C, Weiss J B, Yavneh I *J. Fluid Mech.* **401** 1 (1999)
107. Gall R *J. Atmos. Sci.* **33** 349 (1976)
108. Randel W, Held I *J. Atmos. Sci.* **48** 688 (1991)
109. Olbers D, Wolf J-O, Völker C *J. Phys. Oceanogr.* **30** 1645 (2000)
110. Salmon R *Geophys. Astrophys. Fluid Dyn.* **10** 25 (1978)
111. Salmon R *Geophys. Astrophys. Fluid Dyn.* **15** 167 (1980)
112. McWilliams J C, Chow H S *J. Phys. Oceanogr.* **11** 921 (1981)
113. Held I M, O'Brien E *J. Atmos. Sci.* **49** 1861 (1992)
114. Haidvogel D B, Held I M *J. Atmos. Sci.* **37** 2644 (1980)
115. Whitaker J S, Barsilon A *J. Atmos. Sci.* **52** 491 (1995)
116. Lee S *J. Atmos. Sci.* **54** 1726 (1997)
117. Pavan V, Held I M *J. Atmos. Sci.* **53** 1262 (1996)
118. McWillliams J C *Dyn. Atmos. Oceans* **1** 427 (1977)
119. Nastrom G D, Gage K S *J. Atmos. Sci.* **42** 950 (1985)
120. Gage K S, Nastrom G D *J. Atmos. Sci.* **43** 729 (1986)
121. Högström U, Smedman A-S, Bergström H *J. Atmos. Sci.* **56** 959 (1999)
122. Wikle C K, Milliff R F, Large W G *J. Atmos. Res.* **56** 2222 (1999)
123. Larsen M F, Kellet M C, Gage K S *J. Atmos. Sci.* **39** 1035 (1982)
124. Lilly D K *J. Atmos. Sci.* **40** 749 (1983)
125. Lilly D K et al. *Theor. Comput. Fluid Dyn.* **11** 139 (1998)
126. Herring J R *Fluid Dyn. Res.* **24** 363 (1999)
127. Vallis G K, Shutts G J, Gray M E B *Quart. J. R. Met. Soc.* **12** 1621 (1996)
128. Lilly D K *J. Atmos. Sci.* **46** 2026 (1989)
129. Koshyk J N, Boer G J *J. Atmos. Sci.* **52** 965 (1995)
130. Straus D M, Ditlevsen P *Tellus* **51A** 749 (1999)
131. Tritton D J, in *Turbulence and Predictability in Geophysical Fluid Dynamics and Climate Dynamics* (Proc. of the School of Physics "Enrico Fermi", Course 88, Eds M Ghil, R Benzi, G Parisi) (Amsterdam: North-Holland, 1985) p. 172
132. Hide R *J. Fluid Mech.* **32** 737 (1968)
133. Hide R, Mason P J *Adv. Phys.* **24** 47 (1975)
134. Couder Y, Chomaz J M, Rabaud M *Physica D* **37** 384 (1989)
135. Charib M, Derango P *Physica D* **37** 406 (1989)
136. Cardoso O, Marteau D, Tabeling P *Phys. Rev. E* **49** 454 (1994)
137. Marteau D, Cardoso O, Tabeling P *Phys. Rev. E* **51** 5124 (1995)
138. Hansen A E, Marteau D, Tabeling P *Phys. Rev. E* **58** 7261 (1998)
139. Kellay H, Wu X L, Goldburg W I *Phys. Rev. Lett.* **74** 3975 (1995)
140. Martin B K, Wu X L, Goldburg W I *Phys. Rev. Lett.* **80** 3964 (1998)
141. Rivera M, Vorobieff P, Recke R E *Phys. Rev. Lett.* **81** 1417 (1998)
142. Belmonte A et al. *Phys. Fluids* **11** 1196 (1999)
143. Kellay H, Bruneau C H, Wu X L *Phys. Rev. Lett.* **84** 1696 (2000)
144. Narimousa S, Maxworthy T, Spedding G R *J. Fluid Mech.* **223** 113 (1991)
145. Linden P F, Boubnov B M, Dalziel S B *J. Fluid Mech.* **298** 81 (1995)
146. Bastin M E, Read P L *J. Fluid Mech.* **339** 173 (1997)
147. Bastin M E, Read P L *Phys. Fluids* **10** 374 (1998)
148. Paret J, Tabeling P *Phys. Rev. Lett.* **79** 4162 (1997)
149. Danilov S D, Dovzhenko V A, Krymov V A *Izv. Ross. Akad. Nauk Fiz. Atmos. Okeana* **36** 284 (2000) [*Izv., Atm. Oceanic Phys.* **36** 261 (2000)]
150. Paret J, Jullien M-C, Tabeling P *Phys. Rev. Lett.* **83** 3418 (1999)
151. Rutgers M A *Phys. Rev. Lett.* **81** 2244 (1998)
152. Bruneau C H, Greffier O, Kellay H *Phys. Rev. E* **60** 1162 (1999)
153. Salmon R, Holloway G, Hendershott M *J. Fluid Mech.* **75** 691 (1976)
154. Rober R, Sommeria J *J. Fluid Mech.* **229** 291 (1991)
155. Van de Konijenberg J A, Flór J D, Van Heijst G J F *Phys. Fluids* **10** 595 (1998)
156. Cardoso O et al. *Phys. Fluids* **8** 209 (1996)